Nonlinear Flows with Entropy Generation

By

Muhammad Waleed Ahmed Khan

Department of Mathematics
Quaid-I-Azam University
Islamabad, Pakistan
2020

Nonlinear Flows with Entropy Generation

By

Muhammad Waleed Ahmed Khan

Supervised By

Prof. Dr. Tasawar Hayat

Department of Mathematics
Quaid-I-Azam University
Islamabad, Pakistan
2020

Nonlinear Flows with Entropy Generation

By

Muhammad Waleed Ahmed Khan

A THESIS SUBMITTED IN THE PARTIAL FULFILLMENT OF THE REQUIREMENT FOR

THE DEGREE OF

DOCTOR OF PHILOSOPHY

IN

MATHEMATICS

Supervised By

Prof. Dr. Tasawar Hayat
Department of Mathematics
Quaid-I-Azam University
Islamabad, Pakistan
2020

Author's Declaration

I, _Muhammad Waleed Ahmed Khan_, hereby state that my PhD thesis titled _Nonlinear flows with entropy generation_ is my own work and has not been submitted previously by me for taking any degree from Quaid-I-Azam University Islamabad, Pakistan or anywhere else in country/world.

At any time, if my statement is found to be incorrect even after my graduation the university has the right to withdraw my PhD degree.

Name of student: Muhammad Waleed Ahmed Khan

Dated: 22/07 /2020

Plagiarism Undertaking

I solemnly declare that research work presented in the thesis titled "*Nonlinear flows with entropy generation*" is solely my research work with no significant contribution from any other person. Small contribution/help wherever taken has been duly acknowledged and that complete thesis has been written by me.

I understand the zero-tolerance policy of the HEC and Quaid-I-Azam University towards plagiarism. Therefore, I as an Author of the above titled thesis declare that no portion of my thesis has been plagiarized and any material used as reference is properly referred/cited.

I undertake that if I am found guilty of any formal plagiarism in the above titled thesis even afterward of PhD degree, the University reserves the rights to withdraw/revoke my PhD degree and that HEC and the University has the right to publish my name on the HEC/University Website on which names of students are placed who submitted plagiarized thesis.

Student/Author Signature

Name: Muhammad Waleed Ahmed Khan
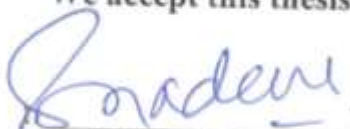
Nonlinear Flows with Entropy Generation

By

Muhammad Waleed Ahmed Khan

CERTIFICATE

A THESIS SUBMITTED IN THE PARTIAL FULFILLMENT OF THE
REQUIREMENTS FOR THE DEGREE OF THE DOCTOR OF
PHILOSOPHY

We accept this thesis as conforming to the required standard

_____
Prof. Dr. Sohail Nadeem
(Chairman)

2. _____
Prof. Dr. Tasawar Hayat
(Supervisor)

3. _____
Dr. Saleem Asghar
(External Examiner)

4. _____
Dr. Nasir Ali
(External Examiner)

Department of Mathematics,
COMSATS University
Park Road Chak Shahzad,
Islamabad.

Department of Mathematics & Statistics
Faculty of Basic & Applied Sciences,
International Islamic University, Islamabad.

Department of Mathematics
Quaid-I-Azam University
Islamabad, Pakistan
2020

Certificate of Approval

This is to certify that the research work presented in this thesis entitled _Nonlinear flows with entropy generation_ was conducted by _Mr. Muhammad Waleed Ahmed Khan_ under the kind supervision of _Prof. Dr. Tasawar Hayat_. No part of this thesis has been submitted anywhere else for any other degree. This thesis is submitted to the Department of Mathematics, Quaid-I-Azam University, Islamabad in partial fulfillment of the requirements for the degree of Doctor of Philosophy in field of Mathematics from Department of Mathematics, Quaid-I-Azam University, Islamabad, Pakistan.

Student Name: **Muhammad Waleed Ahmed Khan**

Signature: _____

External committee:

a) **External Examiner 1**:   Signature: _Saleem Asghar_

Name: **Dr. Saleem Asghar**

Designation: Professor

Office Address: Department of Mathematics, COMSATS University Park Road Chak Shahzad, Islamabad.

b) **External Examiner 2**:   Signature: _____

Name: **Dr. Nasir Ali**

Designation: Associate Professor

Office Address: Department of Mathematics & Statistics, Faculty of Basic & Applied Sciences, International Islamic University, Islamabad

c) **Internal Examiner**   Signature: _____

Name: **Prof. Dr. Tasawar Hayat**

Designation: Professor

Office Address: Department of Mathematics, QAU Islamabad.

Supervisor Name: Signature: _____

Prof. Dr. Tasawar Hayat

Name of Dean/ HOD   Signature: _____

Prof. Dr. Sohail Nadeem

Dedicated

to

my fiancée

Dr. Sidra Shams

Acknowledgment

First and foremost, I start my acknowledgment to say Thanks to Almighty Allah for giving me strength, wisdom, confidence and perseverance to continue my studies. Without His sufficient grace and mercy, I would not have been able to complete this work. After Almighty Allah I say thanks to the Holy Prophet Hazrat Muhammad (Peace be upon Him) Who emphasized the importance of knowledge by saying " Learn the knowledge from cradle to grave". I say thanks from the deepness of heart to my great teacher and kind supervisor Professor Dr. Tasawar Hayat for his advice, guidance and the numerus opportunities he has provided me. Additionally, I would also like to thank all my teachers who taught and bring me able to overcome all the challenges. particularly Professor Dr M. Ayub, Professor Dr. Tasawar Hayat, Professor Dr. Sohail Nadeem (Chairman), Professor Dr. Masood Khan, Professor Dr. Tariq Shah, Professor Dr. Asif Ali, and Dr. Khalid Saifullah. I am extremely grateful for the continued support of my parents, brothers and sisters, whose prayers are source of my every achievement. Without support of my parents and brothers I wouldn't be in the position I find myself now. I must also say thanks to my senior lab fellows, Dr. Muhammad Farooq, Dr. Waqas, Dr. Shahid Farooq, Dr Sajid Qayyum, for the excellent guidance and helped during the initial and final stages of my studies, my batchmates Dr. M. Ijaz Khan, Dr. Sumaira Qayyum, my fellows

Preface

Major interest in this thesis is to analyze entropy generation in hydrodynamic and magnetohydrodynamic flows of viscous and non-Newtonian fluids. Especially the non-Newtonian fluids have pivotal role in many industrial and technological processes such as extrusion of polymers, glass industries, medical equipment, automotive engines, power engineering, oil and food processing industries, aircraft engines, car brake systems, atomizers, turbine engineering and rotational air cleaners etc. In all such processes the flow of fluids, drag forces and transfer of heat is of paramount importance. The rheological characteristics of all the non-Newtonian fluids cannot be determined by a single fundamental equation. Therefore, several models for the study of such fluids have been proposed. In addition, the entropy of system, by second thermodynamics law, consistently increases. Entropy literally measures disorderliness in any system. It is generated by the irreversibility in a process. In all the real-world applications we always need to increase the efficiency of machines by decreasing the irreversibilities in the system. Thus more stress is given here to entropy optimization and Bejan number. Bejan number is employed to determine measure of ratio of thermal irreversibilities to total irreversibilities. Previous information witness that little attention is given to entropy generation in flow of non-Newtonian liquids. We will model problems for flow by stretching sheet and rotating disk. Results of pertinent involved parameters will be shown through graphical interpretations. Skin friction and Nusselt numbers will be discussed. Tabulated values will be used for comparative study of present analysis with previous literatures in limiting cases. This thesis consists of nine chapters Chapter wise detail is given as follows:

Chapter one is about some basic definitions and a brief literature survey which provides background and motivation of the present research work. Further, solution procedure is discussed in detail.

Chapter two is about nonlinear radiative mixed convective flow with entropy generation minimization rate and heat generation/absorption. A variable thicked stretchable sheet is taken as a source of fluid motion. Heat stretched sheet has nonlinear velocity. Velocity and temperature with respect to different parameters are examined. Entropy generation and Bejan number are sketched and discussed. These contents are published in **Physica B: Condensed Matter 538 (2018) 95–103**.

Chapter three is the extension of chapter two for numerical solution development of power law

fluid flow. Flow subject to magnetohydrodynamics (MHD), viscous dissipation and convective conditions is addressed. Solution for governing nonlinear equations is obtained through ND solve technique. Entropy and Bejan numbers are discussed. The obtained results are summarized in the conclusion section. The material of this chapter is accepted for publication in **Computer Methods and Programs in Biomedicine https://doi.org/10.1016/j.cmpb.2019.105262.**

Chapter four generalizes analysis of chapter three. It analyzes the entropy optimization of nonlinear thermal radiative nanofluid flow by a thin needle. Water is taken as a base-fluid having different types of nanomaterials. The resulting ordinary differential equations for the current flow problem are tackled through Shooting technique. Entropy optimization is explored in terms of temperature and velocity gradient. Effects of velocity and temperature through pertinent parameters are shown graphically. The obtained results are concluded in the last section. The contents of this chapter are published in **Physica B: Condensed Matter 34 (2018) 113–119**.

Chapter five reveals the characteristics of entropy optimization in Sisko fluid flow with source/sink and nonlinear radiative heat flux. A rotating stretchable disk is considered as a source of motion for the fluid particles. Fluid characteristics are studied with nonlinear mixed convection, viscous dissipation and Brownian motion. Entropy is computed and shown graphically. Materials of this chapter are published in **Journal of the Brazilian Society of Mechanical Sciences and Engineering (2018) 40:373 https://doi.org/10.1007/s40430-018-1288-0**

Chapter six is the extension of chapter five. This chapter is about the entropy production in MHD nanofluid flow caused by a rotating disk having variable thickness. Nanofluid flow is studied in presence of Brownian motion and thermophoresis mechanisms. The source for flow is nonlinear stretching of the disk. The obtained problems are transformed through suitable transformations and solved by homotopy analysis method. Convergent solutions are developed Entropy is calculated as a function of velocity and temperature. Graphical results are obtained and discussed. Contents of this chapter are submitted for publication in **Physica A**.

In chapter seven we study the dissipative convective flow of hybrid nanomaterials caused by stretchable disk with entropy optimization. Hybrid nanomaterials are used to increase the thermal properties of the material. Convective conditions are implemented on the disk. Skin friction, heat

transfer, entropy minimization and Bejan number are analyzed for engineering interest. Content of this chapter are published in **Materials [Research Express](#) 6(8) April 2019. Doi.10.1088/2053-1591/ab1b88.**

In chapter eight, the concept of hybrid nanoparticles flow by a rotating disk is generalized in the presence of MHD and mixed convection. Heat properties are discussed with Joule heating and viscous dissipation. Governing equations are tackled through ND solve technique. Velocity, temperature, heat transfer rate, skin friction, entropy and Bejan number are numerically discussed. Results of this chapters are submitted for publication in **Journal of Molecular liquids**.

Chapter nine is about entropy optimization for non-Newtonian fluid flow with Arrhenius activation energy and binary chemical reaction. Here we analyze the radiative mixed convective flow of Casson nanofluid over a stretching sheet. Heat transfer is with nonlinear thermal radiation, viscous dissipation and heat generation/absorption. Total entropy is calculated. Velocity is studied with uniform magnetic field and nonlinear mixed convection. Brownian motion and thermophoresis are considered. Governing equations are tackled by the built in ND solve technique. Results for velocity, temperature, concentration, entropy and Bejan number are presented. Material of this chapter is published in **Physica A: Statistical Mechanics and its Applications, 538, (2020), Article 122806.**

Contents

2

Chapter 1. Background and fundamental expressions

Introduction

Recently much interest is seen in viscous and non-Newtonian fluids. Non-Newtonian materials are those materials in which shear stress and deformation rate are nonlinearly proportional to each other. Presently these liquids have many applications in biochemical, cosmetic and pharmaceutical industries such as paints production, syrups, cleansers, gases, oils and deodorizers etc. Other examples of such fluids are custards, starch suspensions, shampoo, toothpaste, salt solutions and many molten polymers etc.

Initially Crane [1] started the work to examine viscous fluid flow over a stretching sheet. Several investigators [2-4] extended the work by considering mass transfer effects with different flow problems. Nadeem et al [5] studied characteristics of nanofluid taking water as a base fluid. Mukhopadhyay et al. [6] scrutinized effects of thermal radiation in flow generated by an exponentially stretching sheet. Characteristics of power law nanofluid by stretching surface with magnetic and slip effects is discussed by Zhang et al. [7]. Majeed et al. [8] scrutinized ferromagnetic fluid by a stretching plate. Flow with thermal nonlinear radiation over a stretchable surface is determined by Pal and Saha [9]. Weidman [10] formulated stagnation point flow towards an unsteady stretchable sheet.

Sisko [11] fluid model is significantly used due to its applications in prediction of both the characteristics of shear thickening and thinning fluids. Flow analysis of peristaltic Sisko fluid over convectively heated sheet is carried by Shaheen and Asjad [12]. Flow of Sisko fluid for the case of permeable stretching cylinder with Fourier heat conduction is explored by Malik et al. [13]

Flows over stretching surfaces with heat transfer have key role in controlling quality of the industrial products. These processes mainly depend on the stretching and cooling rates. Makinde [14] analyzed viscous fluid flow with slip and Newtonian heating effects. Hayat et al. [15] examined effects of viscous dissipation in flow of magnetic nanofluid. Many researchers examined different aspects of stretching surfaces for both the cases of viscous and non-Newtonian liquids. Three-dimensional viscoelastic fluid flow over a stretching surface is studied by Hayat et al. [16]. Abbas et al. [17] investigated the mixed convective stagnation-point flow of a Maxwell fluid towards a vertical stretching surface. Hayat et al. [18] examined MHD stagnation-point flow of a micropolar fluid causedvby a non-linear stretching sheet. Mushtaq et al. [19] numerically studied

rotating flow of nanofluids generated by an exponential stretching sheet. Hayat et al. [20] investigated flow of second grade fluid with Joule heating effect. They utilized Homotopy technique [21-30] to get the series solution for proposed problem. Nanomaterial depends upon thermophoresis and Brownian motion. It was clearly observed that velocity of fluid particles shows increasing behavior for higher viscoelastic parameter. Additionally, the velocity gradient has opposite behavior for larger magnetic and viscoelastic parameters while more heat transfer is observed for higher Reynolds number.

Modern fields of technology mainly depend on cooling effects for better efficiencies. The present sources for cooling processes are limited and insufficient for fulfilling industrial demands of such devices. Scientists are searching for more advanced methods of cooling due to their vast use in many technological processes. Keeping these applications in mind, air and liquid are considered the main available sources used for cooling purposes in many electronic devices. Cooling through air is the most common and convenient way but is not enough in modern era. It is having some deficiencies e.g. need of a large heat source/sink reservoir, it is less efficient, lower thermal conductivity etc. As compared to air cooling, liquid cooling is more efficient. However, it is also not as useful as needed because of its lower convective heat transfer properties. Researchers thus require some advanced methodologies with higher thermal conductance and advanced heat transfer abilities. Achieving higher thermal conductivity is the main objective of researches in modern cooling appliances. This is obtained by the conventional method of adding nanoparticles to the base fluids. Choi [31] utilized the nanomaterials taking water as a base-fluid to improve thermal characteristics of fluids and obtained better results. Such nanoparticles consisted of metals (Cu, Ag, Al, Au, etc.), nonmetals (CNT, etc.), metal oxides (CuO, ZnO, Al2O3, TiO2, etc.) and ceramics. These nanoparticles range from 1 to 100 nm in size [32-34]. It has been noted that thermal properties of the fluids have been increased by an appreciable amount of about 30% [35-40]. Hayat et al. [41] examined the viscoelastic nanofluid flow bounded by a stretched surface. Many nanomaterials comprising. copper, silver, aluminum, gold, silver oxide, copper oxide and aluminum oxide etc. with different types of base-fluids were tried for thermal conductivities enhancement by various scientists [42-46]. Sheikholeslami [47] computed the solution for MHD Al_2O_3-water nanofluid in a porous space. Dogonchi and Ganji [48] analyzed radiative MHD flow subject to Cattaneo-Christov heat flux.

Power law fluid flows along with natural convection have been thoroughly studied by many

researchers [49-53]. In these studies, heat and mass transfer rates play better role in the above industrial processes. Further the design has been precisely modified by calculating entropy generation since it reduces energy loses in manufacturing processes. Entropy is mainly generated by the irreversibilities in the system under consideration, that is why a proper knowledge of parameters related to such irreversibilities is crucial for finding best operating conditions. Bejan [54] has characterized impressive engineering designs whenever heat transfer or insulation of thermal energy were needed involving minimization of entropy production. Khan et al. [55] calculated entropy generation in flow of Williamson nanofluid with the effects of Joule heating and chemical reaction. Hayat et al. [56] examined entropy generation with thermo-diffusion impact on unsteady dissipative flow. Sheikholeslami et al. [57] numerically investigated Al2O3 water nanofluid flow with magnetic effects and thermal transport in a semi-annulus enclosure. Study of entropy generation with heat and mass transfer in mixed electro-kinetically and forced flow through a slit microchannel is examined by Matin and Waqar [58]. Escandon et al. [59] studied entropy optimization in electro-osmotic flows of non-Newtonian liquids inside a microchannel.

Moreover, importance of permeable media in various industrial applications and thermal transport situations cannot be denied. Wood, sandstone, limestone and outflow of water in river beds are common examples of naturally existing porous medium. Porous medium has been characterized by utilizing Darcy law in case of viscous fluids. This situation can be further clarified by reviewing the previous literature in this regard [60-62].

Activation energy is considered as the least energy needed for stimulating particles and make their transport possible in chemical reactions. In fact it is regarded as a thermal barrier between two states of energy. Any chemical process just starts when this level is achieved. In a chemical process the atoms or molecules have an amount of energy which exceeds this limit of activation energy. Molecules with enough energy more than the activation energy can pass the energy barrier. This energy can be considered as the height of the barrier. Few research articles for activation energy with chemical reaction can be seen in the studies [63-67].

Previous literature reveals that study of cooling efficiency of nanoparticles is mainly dependent upon first law of thermodynamics. Since it is a fact that conversion of heat into same amount of useful work is impossible. Efficiency of the system is evaluated by determining amount of useful work. Amount of lost energy due to irreversibility effects is determined by second law of

thermodynamics. Therefore the rate of entropy generation is an important tool to determine such irreversibilities in energy processes.

Mass Conservation expression

Here mass in any isolated system can neither be created nor destroyed.

Mathematically

$$\frac{\partial \rho_f}{\partial t} + \nabla \cdot (\rho_f \boldsymbol{V}) = 0. \tag{1.1}$$

For incompressible fluids

$$\nabla \cdot \boldsymbol{V} = 0, \tag{1.2}$$

or

$$\frac{\partial u}{\partial x} + \frac{\partial v}{\partial y} + \frac{\partial w}{\partial z} = 0. \tag{1.3}$$

In cylindrical form

$$\frac{1}{r}\frac{\partial u}{\partial r}(rv_r) + \frac{\partial v_\theta}{\partial \theta} + \frac{\partial v_x}{\partial x} = 0. \tag{1.4}$$

Momentum Conservation law

According to this law total momentum of the colliding particles in an isolated system, before and after the collision remain conserved. Mathematically one has

$$\rho_f a_i = \nabla p + div\boldsymbol{S} + \rho_f \boldsymbol{B},$$

$$\tag{1.5}$$

where ρ_f denotes the fluid density, $\boldsymbol{S}$ the extra stress tensor and $\boldsymbol{B}$ the body force.

Energy conservation expression

According to this law, energy can neither be created nor be destroyed in a thermodynamic system but can only be transformed from one form to another. Like potential energy is converted into kinetic energy, electrical into mechanical energy, light into chemical energy and chemical into heat energy etc.

$$(\rho c_p)_f \frac{dT}{dt} = \tau.L - divq - divq_r. \tag{1.6}$$

Here c_p is the specific heat capacity, q heat flux and q_r radiative heat flux.

Law of Conservation of concentration

According to this law the total concentration of the fluid particles in an isolated system remains conserved. Mathematically it is derived from Fick's law.

$$\frac{dC}{dt} = -\nabla.j, \tag{1.7}$$

with

$$j = -D\nabla C. \tag{1.8}$$

Expression. (1.7) takes the form

$$\frac{dC}{dt} = D\nabla^2 C. \tag{1.9}$$

Entropy

Entropy in physical sense is a measure of disorderliness in a system and its surrounding. Basically heat transfer is one of the main sources for entropy production because with heat transfer some additional movements also occur e.g. internal movement of molecule, internal molecular vibration, friction, kinetic energy and spin moment etc. which result in losing of heat thus we are unable to transform heat fully into useful work. These additional factors create disturbance inside the system and its surroundings.

It is also observed that such energy losses cannot be re-obtained so system can't come to its original position without some extra work done on it. Therefore entropy is considered as the measure of irreversibilities.

In all real-life processes, some sort of macroscopic as well as microscopic loss occur. This is because, every thermodynamic process is an irreversible process.

In such process, a system generates finite amount of entropy σ of their own due to either some known or unknown cause.

Irreversibilities of the system are given by the entropy generation rate. These terms in the entropy generation rate are mainly due to thermal irreversibilities, fluid friction irreversibilities and magnetic irreversibilities etc.

Bejan number

To find the ratio of thermal irreversibilities to total irreversibilities in a system, a term known as Bejan number is used. This term shows either heat transfer irreversibilities dominates or other irreversibilities are more dominant. Bejan number is given by

$$Be = \frac{Entropy\ generated\ due\ to\ heat\ transfer}{Total\ entropy\ generated} \tag{1.10}$$

Homotopy analysis method

One of the most convenient tools to solve system of nonlinear differential equations is through homotopy analysis method. The concept of homotopy is used in this method. Two functions *f(x)* and *g(x)* are said to be homotopic if one can be transformed into another function. This idea was first utilized by Liao [68] in 1992. This method is used due to its applications for solving nonlinear differential equations. Some advantages for this method are as follows.

- It is independent of small/large parameter.

- Convergence is guaranteed.

- A great choice of linear operators and base function is available.

Series solution for different nonlinear problems are developed using this technique.

A nonlinear equation of the form

$$N[u(x)] = 0. \tag{1.11}$$

Homotopic equation is given as

$$(1 - q)L[u(x, q) - u_0(n, q)] = q\hbar N[u(x, q)] \tag{1.12}$$

where $\hbar \neq 0$ and $0 \leq q \leq 1$.

For $q = 0$ the above-mentioned condition is known as zeroth order deformation expression. For the values of q ranging from 0 to 1, the solution $u(x, q)$ approaches from initial guess $u_0(x)$ to the ultimate solution $u(x)$

The solution can be obtained using some appropriate softwares e.g. maple and Mathematica. When the variables, initial guess and corresponding linear operators are selected in appropriate manner, series will converge for $q = 1$.

$$u(x, q) - u(x) = 0 \tag{1.13}$$

$$u(x, 1) - u(x) = 0 \tag{1.14}$$

By Taylor series one has

$$u(x, q) = u_0(x) + \sum_{m=1}^{\infty} u_m(x) q^m, \tag{1.15}$$

$$u_m(x) = \frac{1}{m!} \frac{\partial u(x, q)}{\partial q^m}, \tag{1.16}$$

$$L[u_m(x) - \chi_m u_{m-1}(x)] = \hbar R u_{m-1}(x), \tag{1.17}$$

$$R_m u_{m-1}(x) = \frac{1}{(m-1)!} \frac{\partial^{m-1} u(x, q)}{\partial q^{m-1}}, \tag{1.18}$$

$$\chi_m = \begin{cases} 0, m \leq 1 \\ 1, m > 1 \end{cases}, \tag{1.19}$$

$$u(x) = u_0(x) + \sum_{m=1}^{\infty} u_m(x). \tag{1.20}$$

Chapter 2

Nonlinear radiative mixed convective flow with heat source and entropy generation

Introduction

Entropy generation in thermally radiative nonlinear mixed convective flow over a variable thicked surface is discussed. Entropy expression in terms of velocity and temperature is analyzed. Stretching of sheet is the main cause for the motion of flow analysis. Equation for entropy optimization is examined. Convergent solutions for the deformed systems are determined. Graphical solutions for velocity profile, temperature gradient and concentration are discussed. Total entropy is studied with nonlinear mixed convection and radiative heat flux. The obtained results are concluded in the final remarks.

Formulation

Here steady, $2D$ mixed convective flow of viscous liquid towards a variable thicked surface is analyzed. Magnetic field B acts in transverse direction to sheet. Small Reynolds number implies no induced magnetic field. Heat source/sink and nonlinear thermal radiation effects are analyzed. Furthermore the impact of nonlinear mixed convection and simple chemical reaction are examined. Sheet lies parallel to x -axis with stretching velocity $U_w = U_0(x + b)^n$ (see Fig. 2.1). Here T_w is wall temperature while T_∞ being ambient temperature. The relevant flow problems are:
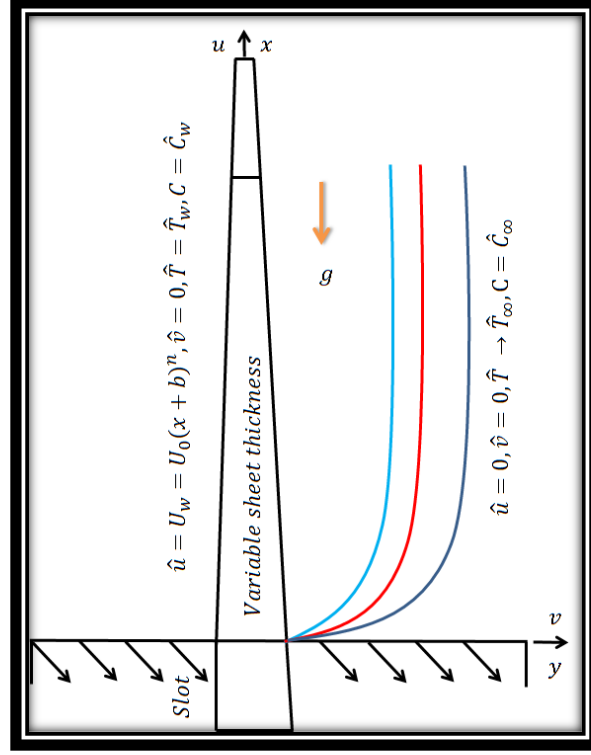
Fig. 2.1. Flow geometry.

$$\frac{\partial \hat{u}}{\partial x} + \frac{\partial \hat{v}}{\partial y} = 0, \tag{2.1}$$

$$\left.\begin{aligned}\hat{u}\frac{\partial u}{\partial x} + \hat{v}\frac{\partial u}{\partial y} &= v\frac{\partial^2 \hat{u}}{\partial y^2} + g(\lambda_1(T - T_\infty) + \lambda_2(T - T_\infty)^2) \\ &\quad + g(\lambda_3(C - C_\infty) + \lambda_4(C - C_\infty)^2),\end{aligned}\right\} \tag{2.2}$$

$$\left(\hat{u}\frac{\partial T}{\partial x} + \hat{v}\frac{\partial T}{\partial y}\right) = \frac{k}{\rho c_p}\frac{\partial^2 T}{\partial y^2} + \frac{1}{\rho c_p}\frac{\partial q_r}{\partial y} + \frac{Q}{\rho c_p}(T - T_\infty), \tag{2.3}$$

$$\hat{u}\frac{\partial C}{\partial x} + \hat{v}\frac{\partial C}{\partial y} = D\frac{\partial^2 C}{\partial y^2} - K(C - C_\infty), \tag{2.4}$$

$$\left.\begin{aligned}\hat{u} = U_w = U_0(x + b)^n, \hat{v} = 0, T_w, \; C = C_w \; \text{at } y = A_1(x + b)^{\frac{1-n}{2}}, \\ \hat{u} = 0, \hat{v} = 0, T = T_\infty, C = C_\infty \text{ at } y \to \infty,\end{aligned}\right\} \tag{2.5}$$

where $B = B_0(x + b)^{\frac{n-1}{2}}$, $Q = Q_0(x + b)^{n-1}$, $K = K_1(x + b)^{n-1}$.

Here $\hat{u}, \hat{v}$ indicate velocity components, v kinematic viscosity, g gravitational acceleration, λ_1 and λ_2 linear and nonlinear coefficients of thermal expansion, λ_3 and λ_4 linear and nonlinear coefficients of solutal expansion, T temperature, T_∞ ambient temperature, C concentration, C_∞ ambient concentration, k thermal conductivity, q_r radiative heat flux, ρ density, c_p specific heat, Q coefficient of heat source/sink, D diffusion coefficient, K chemical reaction rate, U_w stretching velocity, b dimensional constant, A_1 small variable regarding surface is sufficient thin and n power

law index.

Considering the following transformations

$$\eta = \sqrt{\frac{(n+1)U_0(x+b)^{n-1}}{2\nu}}\, y, \quad \psi = \sqrt{\frac{2\nu U_0(x+b)^{n+1}}{n+1}}\, F(\eta),$$

$$\hat{u} = U_0(x+b)^n F'(\eta), \hat{v} = -\sqrt{\frac{(n+1)\nu U_0(x+b)^{n-1}}{2}}\left(F(\eta) + \eta\frac{n-1}{n+1}F'(\eta)\right), \quad \text{(2.6)}$$

$$\Theta(\eta) = \frac{T-T_\infty}{T_w-T_\infty}, \quad \Phi = \frac{C-C_\infty}{C_w-C_\infty}$$

Incompressibility condition is trivially justified while the other expressions are

$$F''' + FF'' - \left(\frac{2}{n+1}\right)F'^2 - \left(\frac{2}{n+1}\right)HaF' + \frac{2\alpha_1}{n+1}(\Theta + \beta_t\Theta^2)$$
$$+\frac{2\alpha_1 N^*}{n+1}(\Phi + \beta_c\Phi^2) = 0 \qquad \qquad \text{(2.7)}$$

$$\Theta'' + \frac{4}{3}R_d\left(\Theta(\theta_w - 1) + 1\right)^2[3\Theta'^2(\theta_w - 1) + (\Theta(\theta_w - 1) + 1)\Theta'']$$
$$+ Pr\, F\,\Theta' + \left(\frac{2}{n+1}\right)Pr\,\delta\,\Theta = 0 \qquad \qquad \text{(2.8)}$$

$$\Phi'' + 2Sc\,Re\,F\,\Phi' - \left(\frac{2}{n+1}\right)Sc\beta_1\Phi = 0, \qquad \qquad \text{(2.9)}$$

$$F(\alpha) = \alpha\left(\frac{1-n}{1+n}\right), F'(\alpha) = 0, F'(\infty) = 0,$$
$$\Theta(\alpha) = 1, \Theta(\infty) = 0, \qquad \qquad \text{(2.10)}$$
$$\Phi(\alpha) = 1, \Phi(\infty) = 0,$$

where $\alpha(= A_1\sqrt{\frac{(n+1)U_0}{2\nu}})$ is the sheet thickness.

Applying the following transformations

$$F(\eta) = f(\eta - \alpha) = f(\xi),$$
$$\Theta(\eta) = \theta(\eta - \alpha) = \theta(\xi), \qquad \qquad \text{(2.11)}$$
$$\Phi(\eta) = \phi(\eta - \alpha) = \phi(\xi).$$

Equations $(2.7 - 2.10)$ lead to

$$f''' + ff'' - \left(\frac{2}{n+1}\right)f'^2 - \left(\frac{2}{n+1}\right)Haf' + \frac{2\alpha_1}{n+1}(\theta + \beta_t\theta^2)$$
$$+\frac{2\alpha_1 N^*}{n+1}(\phi + \beta_c\phi^2) = 0 \qquad \qquad \text{(2.12)}$$

$$\theta'' + \frac{4}{3}R_d(\theta(\theta_w - 1) + 1)^2[3\theta'^2(\theta_w - 1) + (\theta(\theta_w - 1) + 1)\theta'']$$
$$+ Pr\, F\,\theta' + \left(\frac{2}{n+1}\right)Pr\,\delta\,\theta = 0 \qquad \qquad \text{(2.13)}$$

$$\phi'' + 2Sc\,Re\,f\,\phi' - \left(\frac{2}{n+1}\right)Sc\beta_1\phi = 0, \qquad \qquad \text{(2.14)}$$

14

$$f(0) = \alpha \left(\frac{1-n}{1+n}\right), f'(0) = 1, f'(\infty) = 0,$$
$$\theta(0) = 1, \theta(\infty) = 0,$$
$$\phi(0) = 1, \phi(\infty) = 0. \tag{2.15}$$

Here $Ha \left(= \frac{\sigma B_0^2}{\rho U_0}\right)$ shows the Hartman number, $Pr \left(= \frac{\rho c_p \nu}{k}\right)$ Prandtl number, $\delta \left(= \frac{Q_0}{\rho c_p U_0}\right)$ heat

generation parameter, $\alpha_1 \left(= \frac{g\lambda_1 (T_w - T_\infty)}{U_0^2 (x+b)^{2n-1}}\right)$ linear mixed convection parameter, $\beta_t \left(= \frac{g\lambda_2 (T_w - T_\infty)^2}{U_0^2 (x+b)^{2n-1}}\right)$

nonlinear mixed convection for temperature, $N^* \left(= \frac{(C_w - C_\infty)\lambda_3}{(T_w - T_\infty)\lambda_1}\right)$ the ratio of concentration to

thermal buoyancy forces, $\theta_w \left(= \frac{T_w}{T_\infty}\right)$ temperature ratio parameter, $R_d \left(= \frac{4\sigma^* T_\infty^3}{kk^*}\right)$ radiation

parameter, $Sc \left(= \frac{\nu}{D}\right)$ Schmidt number, $Re \left(= \frac{U_w (x+b)}{\nu}\right)$ Reynolds number, $\beta_1 \left(= \frac{K_1}{U_0}\right)$ chemical

reaction parameter and $\beta_c \left(= \frac{(C_w - C_\infty)^2 \lambda_4}{(T_w - T_\infty)}\right)$ nonlinear mixed convection variable for concentration.

Quantities of interest

Surface drag force

Mathematically surface drag force is

$$\frac{1}{2} C_{fx} Re^{0.5} = \left(\frac{n+1}{2}\right)^{1/2} \tilde{f}'(0). \tag{2.16}$$

Heat transfer rate

Similarly heat transfer rate is

$$Nu_x Re^{-0.5} = -\left(\frac{n+1}{2}\right)\left(1 + \frac{4}{3}R_d(1 + (\theta_w - 1)\theta(0))^3\right)\theta'(0). \tag{2.17}$$

Mass transfer rate

Expression for Sherwood number is defined as

$$Sh_x Re^{-0.5} = -\phi'(0). \tag{2.18}$$

Expression for entropy generation

In dimensional form equation for entropy generation is given as

$$S_G = \frac{k}{T_\infty^2}\left(1 + \frac{16\sigma^* T^3}{3kk^*}\right)\left(\frac{\partial T}{\partial y}\right)^2 + \frac{\mu}{T_\infty}\left(\frac{\partial \hat{u}}{\partial y}\right)^2 + \frac{R^* D}{C_\infty}(\nabla C)^2 + \frac{R^* D}{T_\infty}(\nabla C \cdot \nabla T) + \frac{\sigma}{T_\infty}B^2(\hat{u}^2), \tag{2.19}$$

where

$$(\nabla C)^2 = \left(\frac{\partial C}{\partial x}, \frac{\partial C}{\partial y}\right) \cdot \left(\frac{\partial C}{\partial x}, \frac{\partial C}{\partial y}\right)$$
$$\nabla C \cdot \nabla T = \left(\frac{\partial C}{\partial x}, \frac{\partial C}{\partial y}\right) \cdot \left(\frac{\partial T}{\partial x}, \frac{\partial T}{\partial y}\right). \tag{2.20}$$

Above expressions after utilizing boundary layer approximations yield

$$S_G = \underbrace{\frac{k}{T_\infty^2}\left(1 + \frac{16\sigma^* T^3}{3kk^*}\right)\left(\frac{\partial T}{\partial y}\right)^2}_{\text{Thermal irreversibility}} + \underbrace{\frac{\mu}{T_\infty}\left(\frac{\partial \hat{u}}{\partial y}\right)^2}_{\text{Fluid friction irreversibility}}$$

$$\left.\begin{array}{c} \frac{R*D}{C_\infty}\left(\frac{\partial C}{\partial y}\right)^2 + \frac{R*D}{T_\infty}\left(\frac{\partial C}{\partial x}\frac{\partial T}{\partial x} + \frac{\partial C}{\partial y}\frac{\partial T}{\partial y}\right) \\ + \underbrace{\frac{\sigma}{T_\infty}B^2(\hat{u}^2)}_{\text{Joule dissipation irreversibility}} \end{array}\right\}. \tag{2.21}$$

Dimensionless entropy is defined as

$$\left.\begin{array}{c} N_G = \left(1 + \frac{4}{3}R_d[\theta(\theta_w - 1) + 1]^3\right)\left(\frac{n+1}{2}\right)\theta'^2\alpha_2 \\ + \left(\frac{n+1}{2}\right)\lambda_1^*\theta'\phi' + \left(\frac{n+1}{2}\right)\frac{\alpha_2^*}{\alpha_2}\lambda_1^*\phi'^2 \\ + \left(\frac{n+1}{2}\right)Brf''^2 + HaBrf'^2 \end{array}\right\}, \tag{2.22}$$

with

$$\left.\begin{array}{c} \alpha_2 = \frac{T_w - T_\infty}{T_w} = \frac{\Delta T}{T_w}, \alpha_2^* = \frac{C_w - C_\infty}{C_\infty}, \lambda_1^* = \frac{R^*D}{k}(C_w - C_\infty), \\ Br = \frac{\mu U_w^2}{k\Delta T}, N_G = \frac{T_\infty S_G \nu}{k\Delta T U_0 (x+b)^{n-1}}. \end{array}\right\} \tag{2.23}$$

Here α_2 denotes dimensionless temperature difference, λ_1^* dimensionless diffusion parameter, Br Brinkman number and $N_G\left(= \frac{T_\infty S_G \nu}{k\Delta T U_0 (x+b)^{n-1}}\right)$ entropy generation rate.

Bejan number (Be) has following definition

$$Be = \frac{\text{Entropy generated due to thermal irreversibilities}}{\text{Total entropy generation}}, \tag{2.24}$$

$$Be = \frac{\left(1 + \frac{4}{3}R_d[\theta(\theta_w - 1) + 1]^3\right)\left(\frac{n+1}{2}\right)\theta'^2\alpha_2}{\left.\begin{array}{c}\left(1 + \frac{4}{3}R_d[\theta(\theta_w - 1) + 1]^3\right)\left(\frac{n+1}{2}\right)\theta'^2\alpha_2 \\ + \left(\frac{n+1}{2}\right)\lambda_1^*\theta'\phi' + \left(\frac{n+1}{2}\right)\frac{\alpha_2^*}{\alpha_2}\lambda_1^*\phi'^2 \\ + \left(\frac{n+1}{2}\right)Brf''^2 + HaBrf'^2\end{array}\right\}}. \tag{2.25}$$

Heat transfer irreversibility is prominent when $Be \geq 0.5$. When $Be \leq 0.5$ the effect of viscous irreversibilities dominates. For $Be = 0.5$ both the effects are same.

Homotopy procedure

This procedure provides opportunity to choose initial approximations along with linear operators. Thus we consider

$$f_0(\xi) = \alpha\frac{1-n}{1+n} + 1 - exp(-\xi),$$
$$\left.\theta_0(\xi) = exp(-\xi),\right\}$$
$$\phi_0(\xi) = exp(-\xi),$$

(2.26)

$$L_f = f''' - f, L_\theta = \theta'' - \theta, L_\phi = \phi'' - \phi,$$

(2.27)

with

$$L_f\left[c_1 + c_2 e^\xi + c_3 e^{-\xi}\right] = 0,$$
$$\left.L_\theta\left[c_4 e^\xi + c_5 e^{-\xi}\right] = 0,\right\}$$
$$L_\phi\left[c_6 e^\xi + c_7 e^{-\xi}\right] = 0,$$

(2.28)

where c_i $(i = 1-7)$ denote the arbitrary constants.

Convergence analysis

Auxiliary parameters $\hbar_f$, $\hbar_\theta$ and $\hbar_\phi$ are chosen which provide us the choice to control the convergence of solutions for nonlinear equations. Fig. 2.2 shows the $\hbar$ -curves for momentum, heat and concentration equations at various orders of approximation. Suitable values of such parameters vary as $-1.5 \le \hbar_f \le -0.2$, $-1.3 \le \hbar_\theta \le -0.3$ and $-1.7 \le \hbar_\phi \le -0.3$. Table 2.1 displays the convergent series solutions of momentum, energy and concentration for the current flow situation. Table 2.1 indicates that $f''(0)$, $\theta'(0)$ and $\phi'(0)$ converge at 15th ,25th and 19th order of approximations respectively.

Table 2.1: Order of approximations when $\alpha_1 = 0.3$, $\beta_t = n = 0.5$, $\beta_c = 0.7$, Ha=0.7, $Pr = 1.9, R_d = 0.1, \theta_w = 0.3, N^* = 0.2, \delta = 0.5, Sc = 1.2, Re = 1.0$ and $\beta_1 = 0.5$.

Order of approximation	$f''(0)$	$-\theta'(0)$	$-\phi'(0)$
1	0.1610	0.8295	1.55556
11	0.2859	0.5038	1.26243
15	0.2857	0.5233	1.25899
19	0.2857	0.5341	1.25894
25	0.2857	0.5350	1.25894
30	0.2857	0.5350	1.25894
35	0.2857	0.5350	1.25894
40	0.2857	0.5350	1.25894
50	0.2857	0.5350	1.25894

Discussion

Impacts of various dimensionless parameters on MHD viscous fluid flow over a variable thicked sheet is discussed in this section. Figs. $(2.3 - 2.20)$ are portrayed for results of velocity $f'(\xi)$, temperature $\theta(\xi)$, concentration $\phi(\xi)$, skin friction $Cu_{fx}Re^{(0.5)}$ heat transfer rate $Nu_x Re^{(-0.5)}$ and Sherwood number $Sh_x Re^{(-0.5)}$. Effect of wall thickness on velocity profile and temperature gradient are exhibited in Figs. $2.3a$ and $2.3b$. Velocity profile due to wall thickness variable is given in Fig. $2.3a$. For increasing values of wall thickness parameter, less disturbance is created in the fluid by stretching of sheet. Hence velocity decreases. Effect of sheet thickness variable on temperature is given in Fig. $2.3b$. Here $\theta(\xi)$ decreases for wall thickness parameter. The reason is that less heat is transported to system and thus temperature decays. Impact of (α_1) mixed convection parameter on velocity profile is shown via Fig. 2.2. Velocity profile enhances for larger values of (α_1). Fig. 2.4 shows that the higher thermal buoyancy force is the reason to increase velocity profile. Behavior of heat generation parameter on temperature is sketched via Fig. 2.5. More heat is observed by introducing heat generation factor. So temperature increases. Fig. 2.6 shows the behavior of mixed convection parameter due to temperature (β_t). It tells that velocity

show increasing behavior for β_t. Fig. 2.7 shows the influence of magnetic parameter on the velocity. Since this parameter is about Lorentz force so enhancement in values of Ha resist the fluid motion which reduces the velocity. Behavior of magnetic parameter Ha on $\tilde{\theta}(\xi)$ is revealed in Fig. 2.8. Here temperature profile increases for larger Ha. Because Lorentz force give more resistance to the particles motion. Thus heat is generated and temperature enhances. Behavior of velocity for various estimations of n is displayed through Figs. $(2.9 - 2.11)$. These figures clearly show that particles motion increases for larger n. Physically the higher n reduces the viscosity of fluid which enhances velocity profile. However decreasing trend is observed for temperature and increasing behavior for concentration profile. Fig. 2.12 highlights the impact of (N^*) on velocity. This parameter increases the velocity field. Influence of Pr on temperature is drawn through Fig. 2.13. By increasing Pr number thermal diffusivity decreases. So thickness of thermal boundary layer decreases and also decays the temperature field. Fig. 2.14 is shown to present the behavior of temperature $\tilde{\theta}(\xi)$ for variations of R_d. Temperature enhances for higher R_d. This is due to the conversion of internal energy into thermal energy. More heat is produced in the system which increases temperature profile. Similarly, Fig. 2.15 shows the influence of temperature difference ratio parameter θ_w on $\tilde{\theta}(\xi)$. From this figure it is inspected that temperature rises for larger estimations of θ_w. Behavior of Sc on concentration is sketched in Fig. 2.16. Higher values of Sc reduces the concentration profile. Skin friction pertaining to magnetic variable Ha and mixed convection variables β_c and β_t are shown in Figs. $(2.17 - 2.19)$. Drag force increases for larger Ha, β_c and β_t. Fig. (2.20) presents the effect of sheet thickness parameter and Pr on heat transfer rate. It is investigated in this figure that rate of heat transfer increases for higher estimations of Prandtl number.
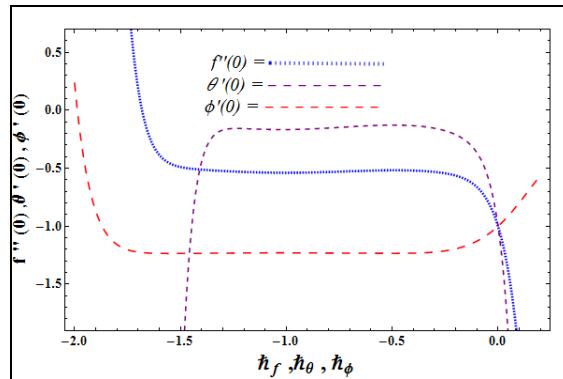
Fig. 2.2. $\hbar-$curves for $f''(0), \theta'(0)$ and $\phi'(0)$.

19
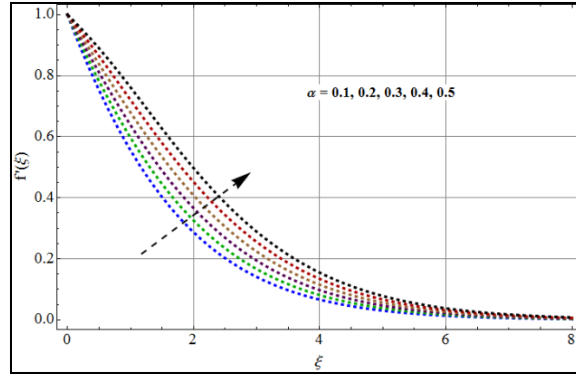
Fig. 2.3a: $f'(\xi)$ via α.
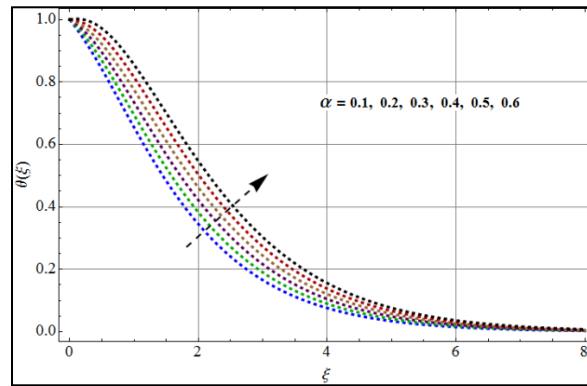
Fig. 2.3b: $\theta(\xi)$ via α.
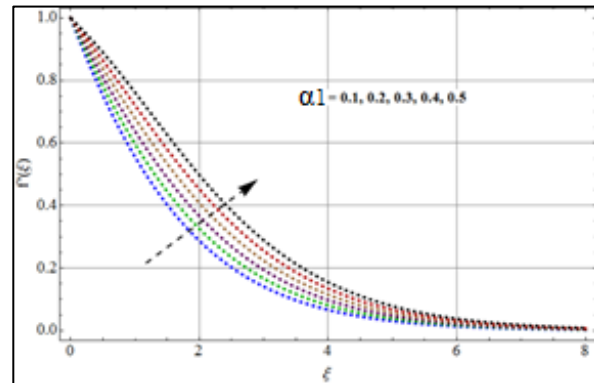
Fig. 2.4: $f'(\xi)$ via α_1.
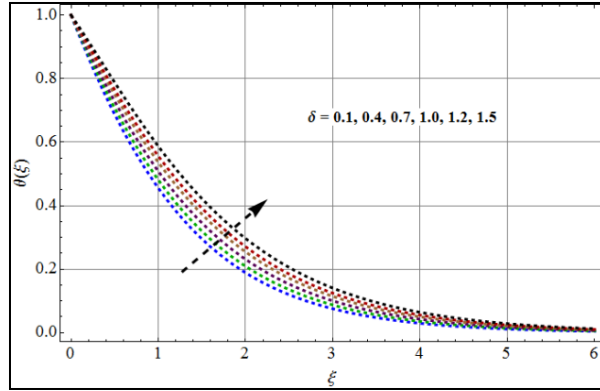
Fig. 2.5: $\theta(\xi)$ via δ.
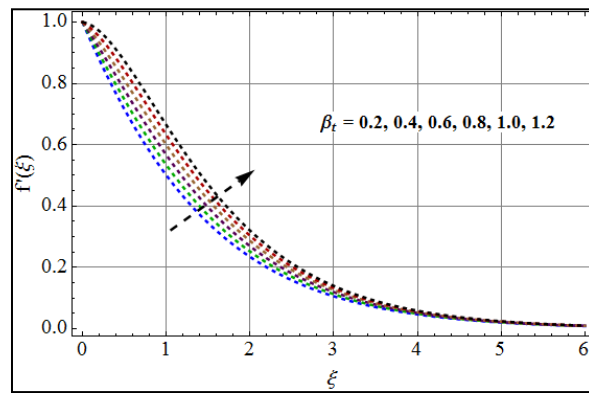
Fig. 2.6: $f'(\xi)$ via β_t.
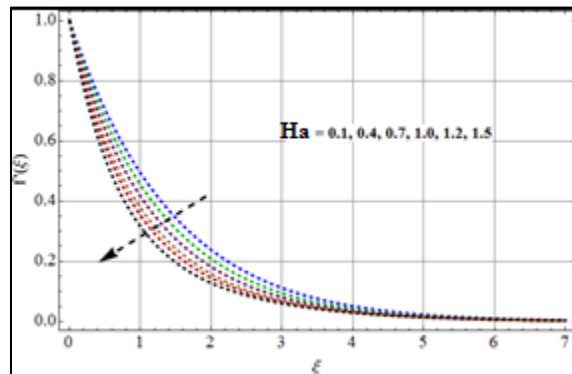
Fig. 2.7: $f'(\xi)$ via Ha.
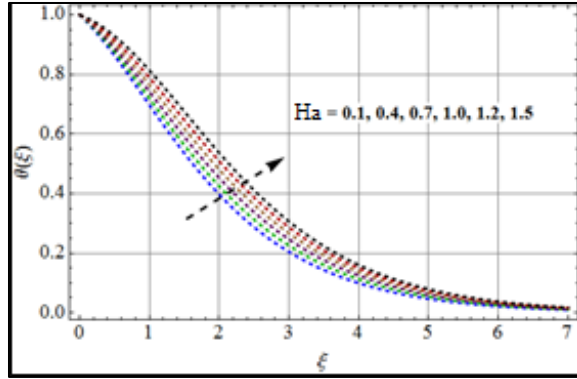
Fig. 2.8: $\theta(\xi)$ via Ha.
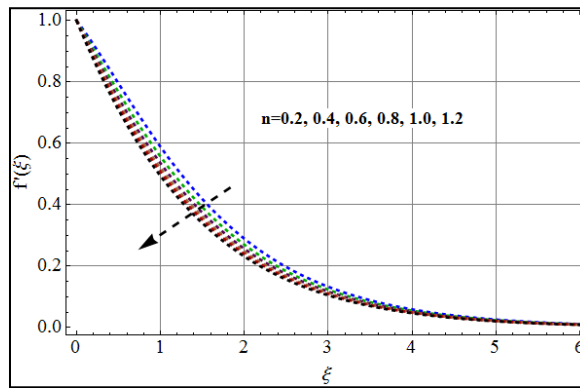
Fig. 2.9: $f'(\xi)$ via n.
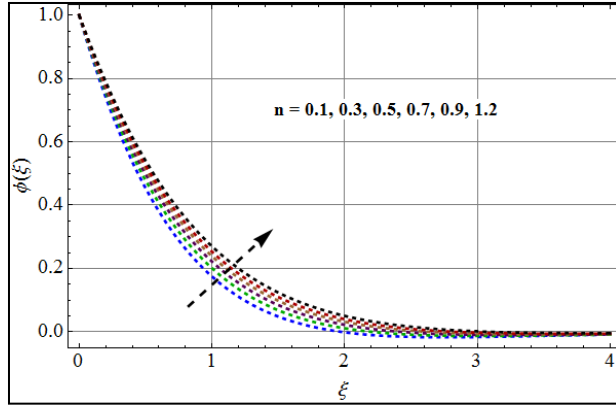

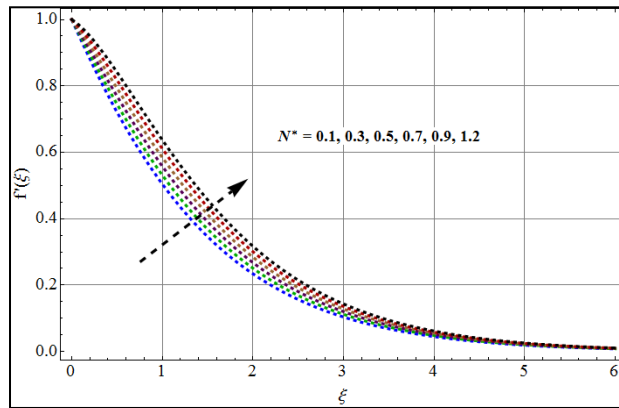Fig. 10: $\theta(\xi)$ via n.

22
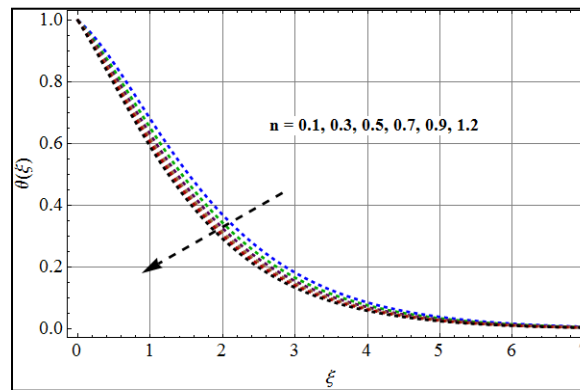
Fig. 2.11: $\phi(\xi)$ via n.

Fig. 2.12: $f'(\xi)$ via N^*.
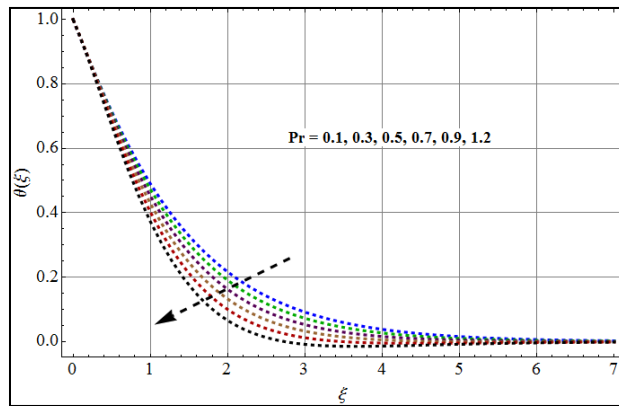
Fig. 2.13: $\theta(\xi)$ via Pr.
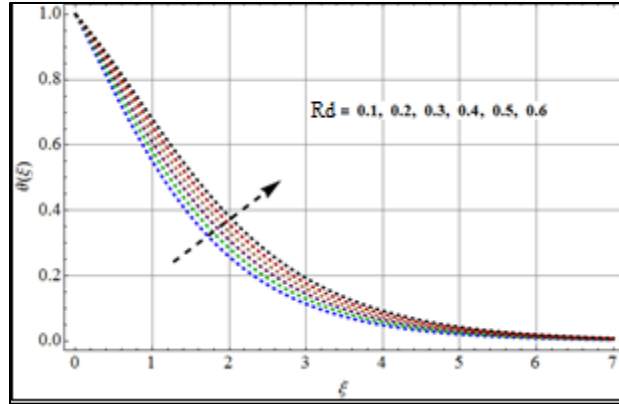
Fig. 2.14: $\theta(\xi)$ via R_d.
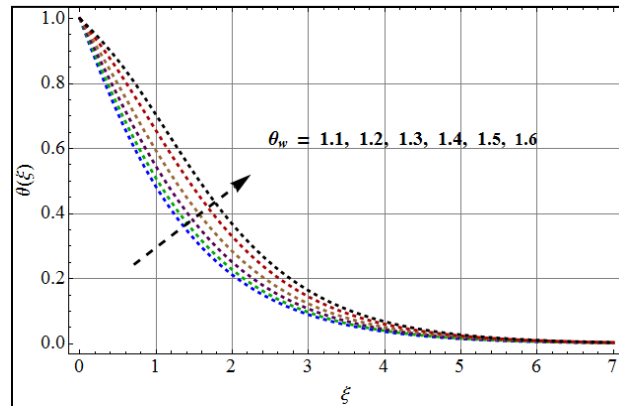
Fig. 2.15: $\theta(\xi)$ via θ_w.
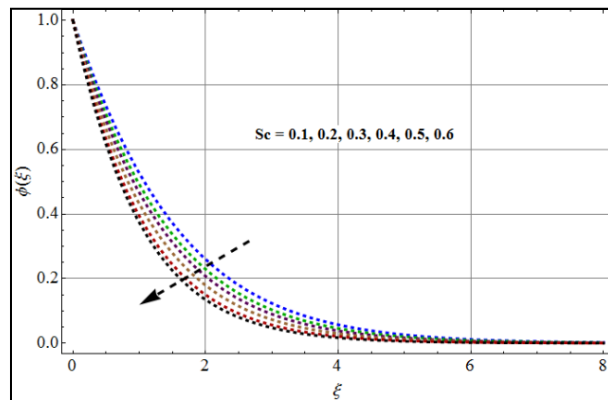
Fig. 2.16: $\phi(\xi)$ via Sc.
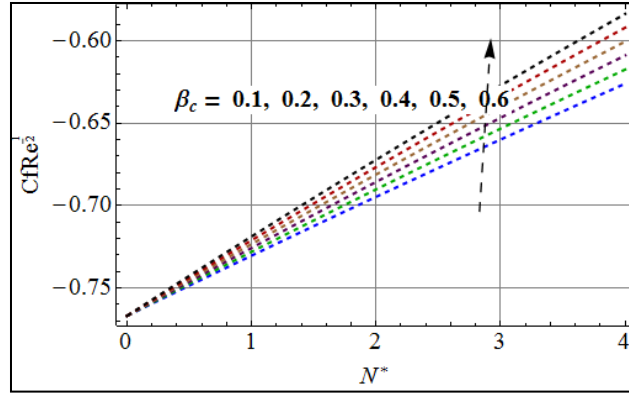
Fig. 2.17: Skin friction via N^* and β_c.
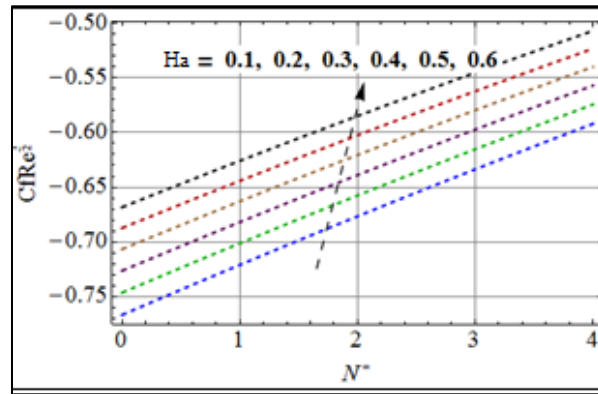
Fig. 2.18: Skin friction via N^* and Ha.
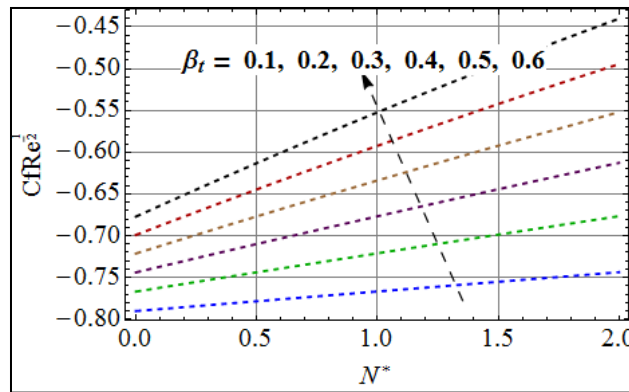
Fig. 2.19: Skin friction via N^* and β_t.
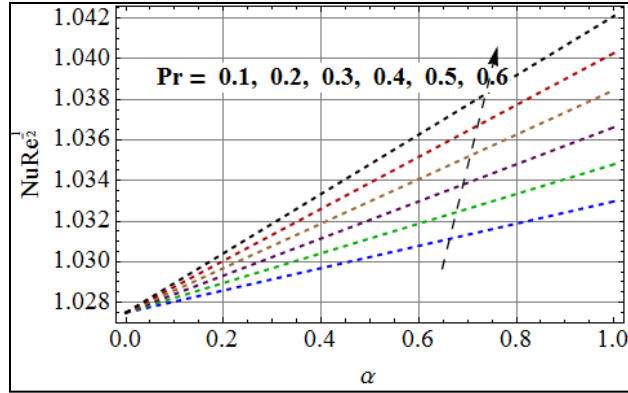
Fig. 2.20: Nusselt number via Pr and α.
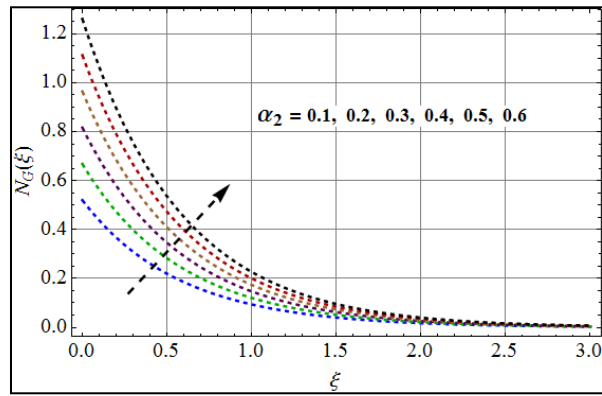
Fig. 2.21: Entropy generation N_G via α_2.
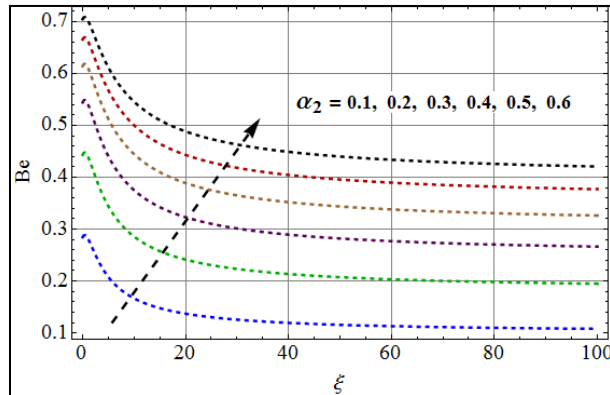
Fig. 2.22: Bejan number Be via α_2.
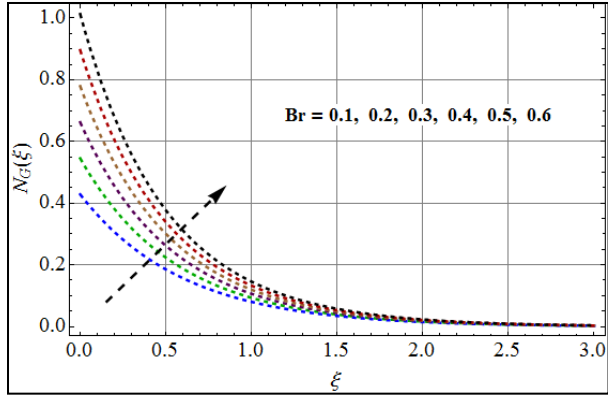
Fig. 2.23: Entropy generation N_G via Br.
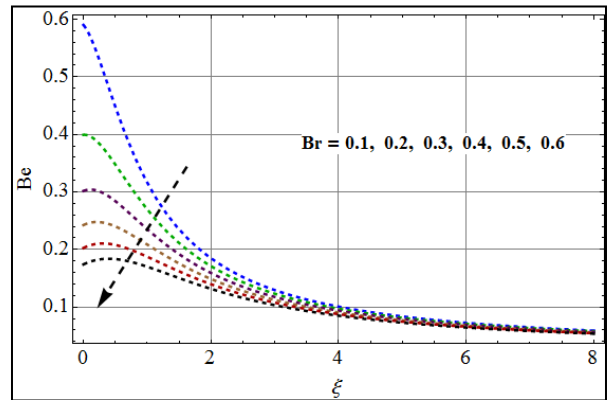
Fig. 2.24: Bejan number Be via Br.
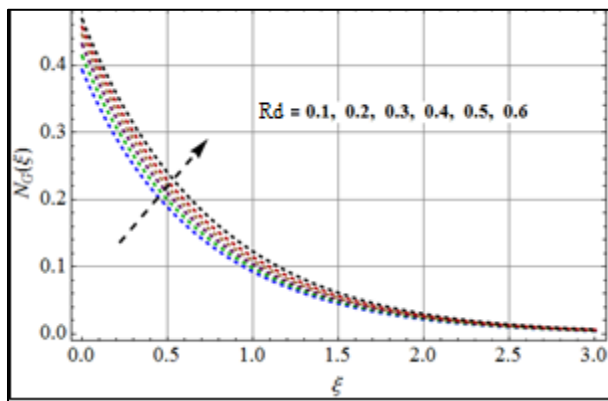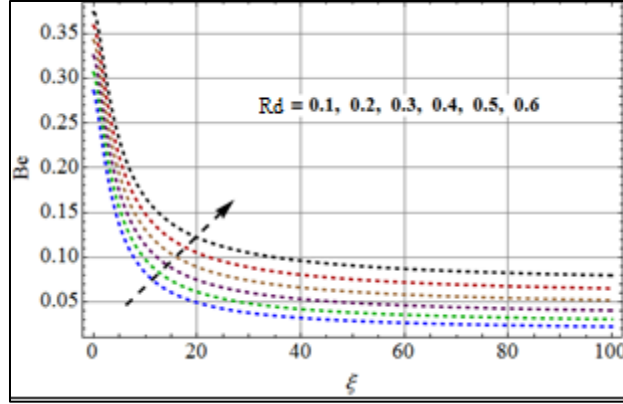

Fig. 2.25: Entropy generation N_G via R_d.

27

Fig. 2.26: Bejan number Be via R_d.

Entropy $(N_G(\xi))$ and Bejan number (Be)

Influences of the temperature difference ratio parameter α_2, thermal radiation parameter R_d and Brinkman number Br on entropy generation $N_G(\xi)$ and Bejan number Be are displayed graphically via Figs.$(2.21 - 2.26)$.

Figs. 2.21 and 2.22 exhibit the characteristics of local entropy generation rate as well as Bejan number for higher values of α_2. Magnitudes of entropy generation rate and Bejan number enhance for larger α_2. It is very clear that $N_G(\xi)$ vanishes far away from the surface. For higher values of α_2, the impact of heat transfer rate is more prominent in comparison to fluid friction and magnetic impacts. That is why Be number increase.

Figs. 2.23 and 2.24 show the effects of entropy generation $N_G(\xi)$ and Be number for higher Br. Brinkman number is specifically identified near the surface. The production of heat inside the layers of the fluid particles which enhances the entropy. Fig. 2.24 shows a decreasing behavior of Be for higher Br. Influences of R_d on $N_G(\xi)$ and Be are shown graphically through Figs. 2.25 and 2.26. $N_G(\xi)$ and Be number enhancement is observed for higher values of R_d. Larger values of R_d gives more heat to the system. Hence heat transfer rate enhances and additional entropy generation is noted.

Conclusions

Entropy production rate in nonlinear mixed convective flow phenomenon of viscous fluid towards a sheet surface is studied. Key points are summarized as follows:

- Velocity increases for higher power law index.
- Temperature $\tilde{\theta}(\xi)$ grows against R_d.
- Magnetic parameter enhances the coefficient of skin friction coefficient..

- Entropy generation $N_G(\xi)$ increases for R_d and Br.

- Bejan number Be decays for Br while reverse trend is noted for R_d.

Chapter 3

Numerical analysis of entropy optimization for MHD power law fluid with convective boundary conditions

Introduction

The present chapter is prepared for two-dimensional flow of power law liquid. Energy expression with convective boundary conditions is considered. Concentration expression subject to activation energy is employed. Relevant problems are numerically solved and analyzed.

Formulation

Here two-dimensional power law fluid flow caused by a plane stretched surface is taken. Magnetic field is applied orthogonally. Convective conditions and viscous dissipation effects are considered. Sheet is stretched with two equal and opposite forces along the x-axis. Flow geometry of the related problem is shown in Fig. 3.1.
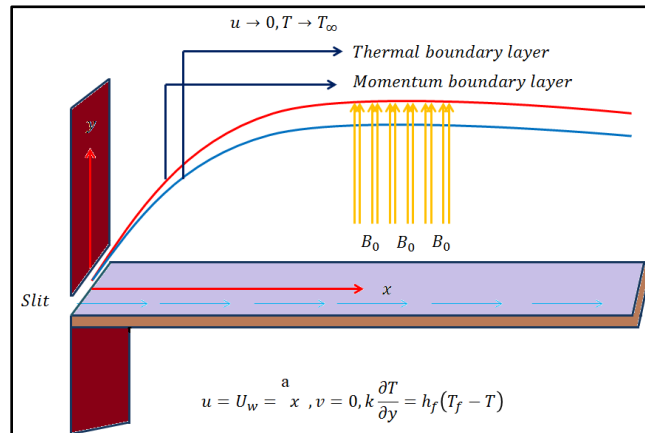
Fig 3.1 Geometry of flow problem

The given flow problems in mathematical form are given as

$$\frac{\partial \tilde{u}}{\partial x} + \frac{\partial \tilde{v}}{\partial y} = 0, \tag{3.1}$$

$$\tilde{u}\frac{\partial \hat{u}}{\partial x} + \tilde{v}\frac{\partial \tilde{u}}{\partial y} = \frac{K_0}{\rho}\frac{\partial}{\partial y}\left(\frac{\partial \tilde{u}}{\partial y}\right)^n - \frac{\sigma}{\rho}B_0^2\tilde{u}, \tag{3.2}$$

$$\left(\tilde{u}\frac{\partial \tilde{T}}{\partial x} + \tilde{v}\frac{\partial \tilde{T}}{\partial y}\right) = \frac{k}{\rho c_p}\frac{\partial^2 \tilde{T}}{\partial y^2} + \frac{k}{\rho c_p}\left(\frac{\partial \tilde{u}}{\partial y}\right)^{n+1} + \frac{\sigma}{\rho c_p}B_0^2\tilde{u}^2, \tag{3.3}$$

$$\tilde{u}\frac{\partial \tilde{C}}{\partial r} + \tilde{v}\frac{\partial \tilde{C}}{\partial y} = D_B \frac{\partial^2 \tilde{C}}{\partial y^2} - k_r^2\left(\tilde{C} - \tilde{C}_\infty\right)\left(\frac{\tilde{T}}{\tilde{T}_\infty}\right)^n Exp(-Ea/kT), \tag{3.4}$$

along with the corresponding boundary conditions

$$\left.\begin{array}{l} \tilde{u} = \tilde{u}_w = ax, v = 0, -k_f \hat{v}\dfrac{\partial \hat{T}}{\partial y} = h_f(T_\infty - T), C = C_w \text{ at } y = 0 \\[2mm] \tilde{u} = 0, v = 0, \hat{T} = T_\infty, C = C_\infty \text{ at } y \to \infty \end{array}\right\} \tag{3.5}$$

where $\hat{T}$ is the fluid temperature, k_r chemical reaction parameter, h_f dimensional coefficient, K_0 power law coefficient, dynamic viscosity μ, thermal conductivity k, density ρ_f, kinematic viscosity ν , electrical conductivity σ and heat capacitance c_p.

Using the following transformations

$$\left.\begin{array}{l} \eta = \sqrt{\dfrac{a}{\nu}}\, y, \tilde{u} = ax\, \tilde{f}'(x), \hat{v} = -\sqrt{ax}\, \tilde{f}'(x), \\[3mm] \tilde{\theta}'(\eta) = \dfrac{\hat{T} - \hat{T}_\infty}{\hat{T}_w - \hat{T}\infty}, \phi'(\eta) = \dfrac{C - C_\infty}{C_w - C_\infty}, \end{array}\right\} \tag{3.6}$$

one has

$$\left.\begin{array}{l} ff'' - f'^2 + nM(f'')^{n-1}f''' - Haf' = 0, \\[2mm] \dfrac{1}{\Pr}\theta'' + f\theta' + EcM(f'')^{n+1} + EcHaf'^2 = 0 \\[2mm] \dfrac{1}{Sc}\phi'' + f\phi' - \gamma\phi(1 + \theta_w\theta)^n Exp[\dfrac{-E}{1 + \theta_w\theta}] = 0, \\[2mm] f'(0) = 1, f'(\infty) = 0, \ \theta'(0) = \beta(1 - \theta(0))\, \theta(\infty) = 0\, \tilde{\phi}(0) = 1, \tilde{\phi}(\infty) = 0, \end{array}\right\} \tag{3.7}$$

with

$$\left.\begin{array}{l} Sc = \dfrac{\nu}{D_B}, \gamma = \dfrac{k_r^2}{a}, \theta_w = \dfrac{\hat{T}_w - \hat{T}_\infty}{\hat{T}_\infty}, M = \dfrac{K_0}{\rho\nu}(ax\sqrt{\dfrac{a}{\nu}})^{n-1}, \Pr = \dfrac{\mu c_p}{k}, \\[3mm] Ec = \dfrac{\tilde{u}_w^2}{c_p(\hat{T}_w - \hat{T}_\infty)}, E = \dfrac{Ea}{K(\hat{T}_w - \hat{T}_\infty)}, \beta = \dfrac{h_\infty}{k_\infty}\sqrt{\dfrac{\nu}{a}}, Ha = \dfrac{\sigma B_0^2}{a\rho} \end{array}\right\} \tag{3.8}$$

where Sc denotes Schmidt number, γ chemical reaction constant, θ_w temperature difference ratio parameter, M material parameter, $\Pr$ the Prandtl number , Ec Eckert number, E activation energy parameter, β the convective parameter and Ha the Hartman number.

Surface drag force

Mathematical equation for skin friction is

$$C_f = \frac{\tau_{xy}^2}{\rho_f^2 \tilde{u}_w^2},$$

(3.9)

where τ_{xy} denote shear stresses in transverse satisfying,

$$\tau_{xy} = k_0 \left(\frac{\partial \tilde{u}}{\partial y}\right)^{n-1}\Big|_{y=0}$$

(3.10)

Equations (3.9) and (3.10) imply that

$$C_{fx} = \frac{\tau_w|_{y=0}}{\rho_f \tilde{u}_w^2} = -2\, Re^{-\frac{1}{n+1}}[\,(\tilde{f}''(0))]^n.$$

(3.11)

Heat transfer rate

In mathematical form, the rate of heat transfer is

$$Nu_x = \frac{a q_w}{k_f (\hat{T}_w - \hat{T}_\infty)}\Big|_{y=0},$$

(3.12)

with wall heat flux q_w as

$$q_w|_{y=0} = -k_f \frac{\partial \hat{T}}{\partial y}\Big|_{y=0} = -k_f (\hat{T}_f - \hat{T}_\infty)\tilde{\theta}'(0).$$

(3.13)

Putting Eq. (3.13) in Eq. (3.12) the following dimensionless form is obtained

$$Nu_x = -\,Re^{-\frac{1}{n+1}}\tilde{\theta}'(0).$$

(3.14)

Similarly, the local Sherwood number is given by

$$Sh_x = \frac{a q_m}{D_B (C_w - C_\infty)}\Big|_{y=0},$$

(3.15)

where q_m is the mass flux and

$$Sh_x = -Re^{-\frac{1}{n+1}}\phi'(0). \tag{3.16}$$

Expression of entropy generation

Dimensional expression for entropy is given by

$$S_G = \frac{k_f}{\widehat{T}_\infty^2}\left(\frac{\partial \widehat{T}}{\partial y}\right)^2 + \frac{K_0}{\widehat{T}_\infty}\left(\frac{\partial \tilde{u}}{\partial y}\right)^{n+1} + \frac{\sigma}{\widehat{T}_\infty}B_0^2\tilde{u}^2. \tag{3.17}$$

We can write

$$S_G = \underbrace{\frac{k_f}{\widehat{T}_\infty^2}\left(\frac{\partial \widehat{T}}{\partial y}\right)^2}_{\text{Thermal irreversibility}} + \underbrace{\frac{\mu_f}{\widehat{T}_\infty}\left(\frac{\partial \tilde{u}}{\partial y}\right)^{n+1}}_{\text{Fluid friction irreversibility}} + \underbrace{\frac{\sigma}{\widehat{T}_\infty}B_0^2\tilde{u}^2}_{\text{Joule dissipation irreversibility}} \left.\vphantom{\begin{array}{c}1\\1\\1\\1\\1\end{array}}\right\}. \tag{3.18}$$

Equation (3.18) shows that entropy is generated by three main sources. First source is heat transfer generated by thermal radiation. The second source is friction of the fluid and third term appears due to Joule dissipation. Non-dimensional entropy generation N_g is defined as

$$N_g = N_{g0}\left[\left(\frac{\partial \theta}{\partial \eta}\right)^2 + PrEc\{M(f'')^{n+1} + Haf'^2\}\right], \tag{3.19}$$

Here Ha represents Hartmann number, M material parameter and $N_{g0}\left(=\frac{ak(\widehat{T}_w - \widehat{T}_\infty)}{\nu \widehat{T}_\infty}\right)$.
Definition of entropy generation satisfies

$$N_G = \frac{N_g}{N_{g0}} = \left[\left(\frac{\partial \theta}{\partial \eta}\right)^2 + PrEc\{M(f'')^{n+1} + Haf'^2\}\right], \tag{3.20}$$

Bejan number (Be) is given by

$$Be = \frac{\text{Entropy generated by heat transfer effect}}{\text{Total entropy of the system}},$$

or

$$Be = \frac{\left(\frac{\partial\theta}{\partial\eta}\right)^2}{\left[\left(\frac{\partial\theta}{\partial\eta}\right)^2 + Pr\, E\, c\{M(f'')^{n+1} + Haf'^2\}\right]}. \tag{3.21}$$

Solution procedure

The governing equations are computed through built in ND solve technique.

Discussion

The characteristics of pertinent dimensionless variables on flow of power law fluids produced by a stretched surface are displayed graphically. Figs. $(3.2 - 3.12)$ are sketched for impacts of velocity, temperature distribution $\tilde{\theta}(\eta)$, skin friction $C_{fx}Re^{\frac{1}{n+1}}$ and heat transfer $Nu_xRe^{\frac{1}{n+1}}$. Fig. (3.2) shows the influence of velocity for magnetic parameter Ha. As this parameter is associated with Lorentz force so higher Ha produce more resistance and consequently velocity reduces. Impact of velocity via material parameter M is represented in Fig. (3.3). Velocity enhances for higher M. It is due to decay in the viscosity of fluid. Since M is inversely proportional to viscosity. Therefore it causes an increase in velocity. Impact of velocity via power law index n is portrayed

in Fig. (3.4). It is clearly shown that movement in liquid particles enhances via n. Physically larger n decrease the fluid's viscosity and consequently velocity is enhanced.

Fig. (3.5) shows that concentration distribution increases for larger values of E. Physically for larger E the productive chemical reaction amount is increased. As a result concentration of fluid enhances. Impact of chemical reaction parameter γ on concentration of power law fluid with both shear thinning and thickening behavior is given in Fig. (3.6). There is decreasing trend for chemical reaction parameter. For higher γ the destructive amount of chemical reaction also enhances. Hence for larger γ the thickness of concentration boundary layer decays which decreases the concentration. Behavior of concentration via Schmidt number Sc is sketched in Fig. (3.7). Since Schmidt number Sc shows the relation between the thickness of the momentum layer with mass diffusivity. Hence larger values of Sc lead to decay of concentration. Fig. (3.8) is displayed to observe the effect of temperature $\tilde{\theta}(\eta)$ via Ec. An enhancement in temperature for higher Ec is shown. Internal friction converts mechanical energy into heat energy which is the reason for

34

enhancement of temperature. Magnetic parameter Ha on $\tilde{\theta}(\eta)$ is indicated in Fig. (3.9). Here temperature enhancement is noted for larger values of Ha. Lorentz forces gives resistance to the motion of particles. Hence more heat is generated inside the system and thus temperature enhanced. Fig. (3.10) displays the influence of temperature via Pr. As Pr is inversely related to thermal diffusivity so decrease in temperature is observed. Fig. (3.11) indicates the impact of material parameter M on temperature $\tilde{\theta}(\eta)$. It clearly shows increasing behavior due to growth in thickness thermal boundary layer.

Behaviors of skin friction with respect to magnetic and material parameters are shown in Table 3.1. Enhancement of drag force for larger Ha and M is observed. Similarly the influences of Eckert number Ec and magnetic variable M on Nusselt number are shown in Table. 3.4. Heat transfer rate decreases for Ec and M.
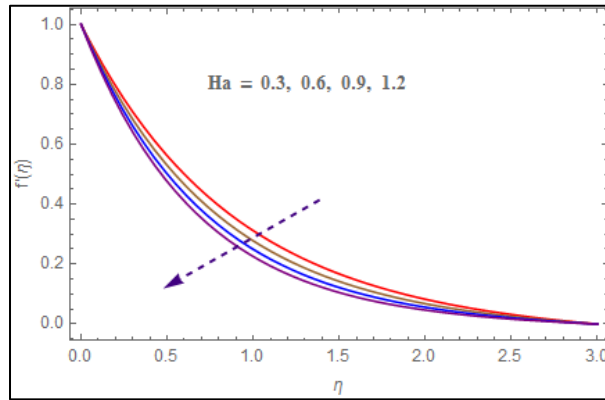
Fig 3.2 $f'(\eta)$ via Ha
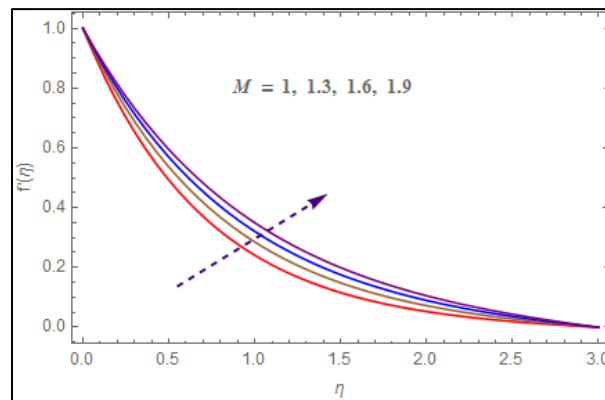
Fig 3.3 $f'(\eta)$ via M.
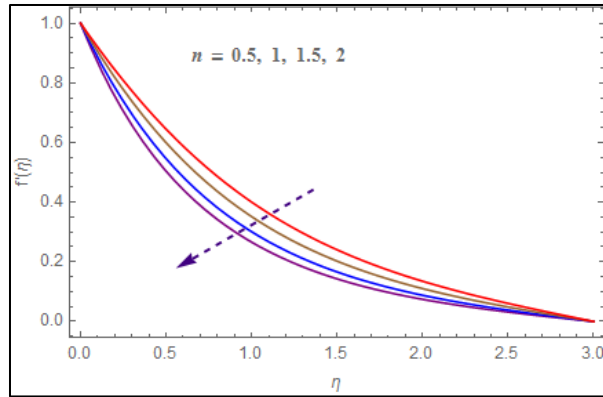
Fig 3.4 $f'(\eta)$ via n.
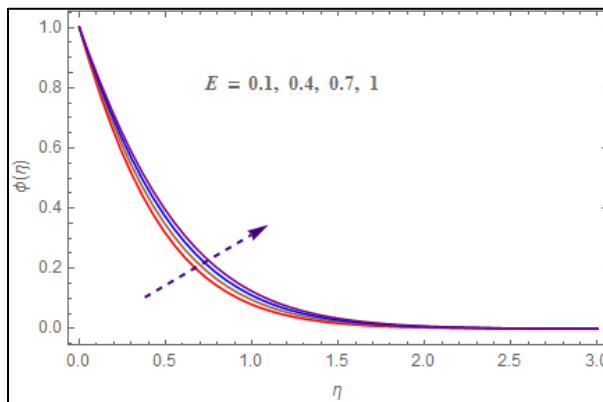
Fig 3.5 $\phi(\eta)$ via E.
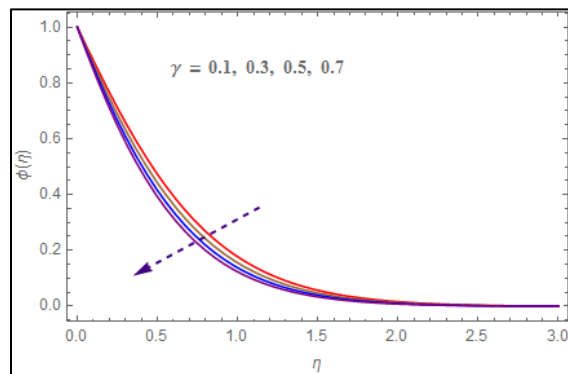
Fig 3.6 $\phi(\eta)$ via γ
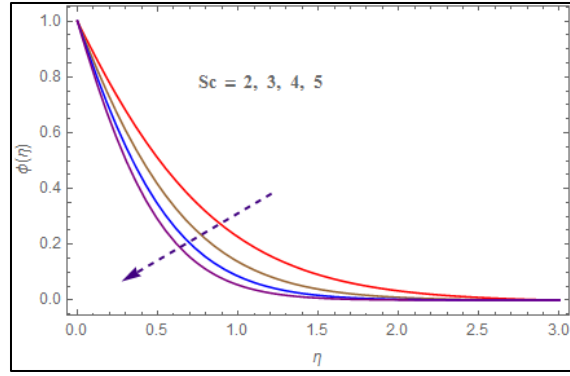
Fig 3.7 $\phi(\eta)$ via Sc.
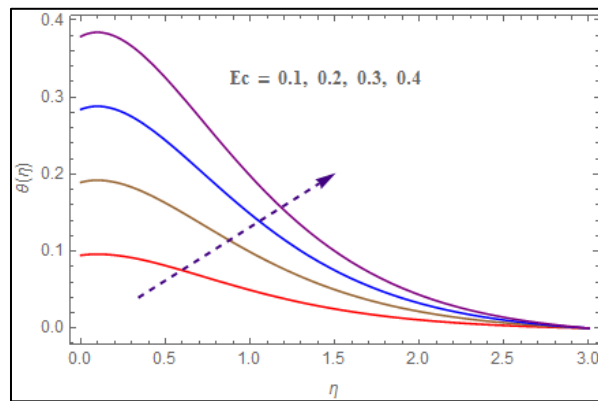
Fig 3.8. $\theta(\eta)$ via Ec.
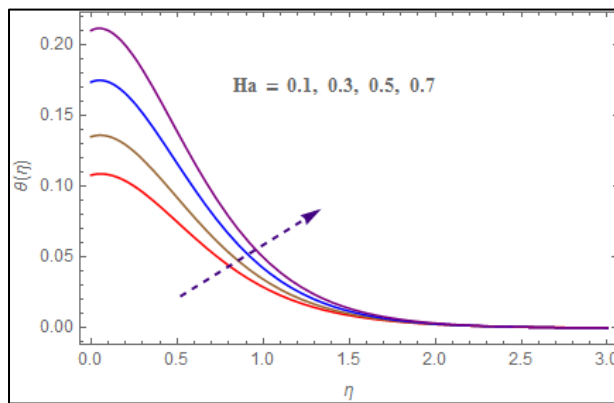
Fig 3.9 $\theta(\eta)$ via Ha.

Fig 3.10 θ(η) via Pr.

Fig 3.11 θ(η) via *M*.

Fig 3.12 θ(η) via *β*.
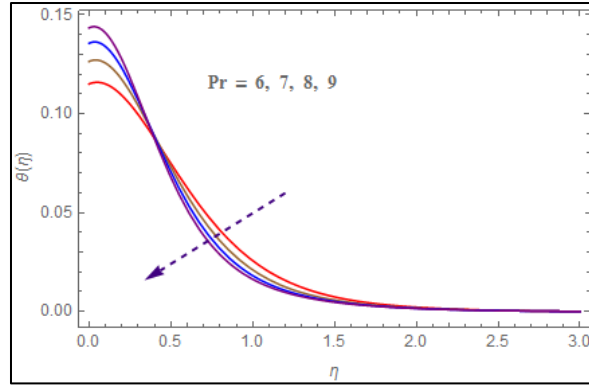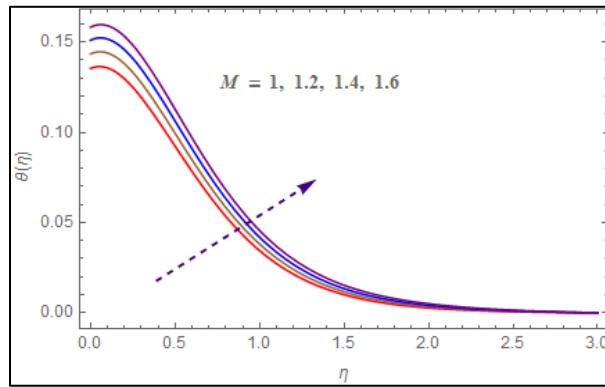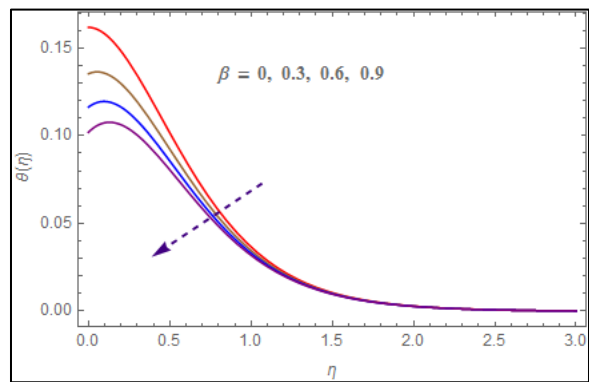
Table 3.1

M	Ha	Skin friction
1.0		2.2948
1.1		2.1915
1.2		2.1017
	0.3	2.2948
	0.4	2.3781
	0.5	2.4589

Table 3.2

Pr	Ec	M	Ha	β	Nusselt Number
6.0					0.0515
6.1					0.0518
6.2					0.0521
	0.1				0.0515
	0.2				0.1031
	0.3				0.1232
		1.0			0.0515
		1.1			0.0530
		1.2			0.0544

Table 3.3

Sc	γ	Ec	E	n	Sherwood Number
1.0					0.79298
1.1					0.83281
1.2					0.87167
	0.5				0.79298
	0.6				0.82696
	0.7				0.85977
		0.1			0.79298
		0.2			0.79415
		0.3			0.79532
			0.6		0.79298
			0.7		0.77652
			0.8		0.76136
				0.1	0.79298
				0.2	0.79315

Entropy generation and Bejan number

Behaviors of entropy generation $N_G(\eta)$ and Bejan number Be via pertinent parameters e.g Eckert number Ec, Hartman number Ha, material parameter M and Pr number are studied in Figs. [3.13 − 3.20].

Influences of $N_G(\eta)$ and Be for larger values of Ec are sketched in Figs. 3.13 and 3.14. These show that both quantities are directly related to Ec. Since Ec characterizes the heat dissipation in the system so more heat is dissipated which increases the entropy. For higher estimations of Ec the rate of heat transfer has more clear impact in comparison to magnetic and fluid friction effects. Due to this reason Bejan number tends to increase. Figs. 3.15 and 3.16 are drawn to show the effect of Ha on $N_G(\eta)$ and Be. Both $N_G(\eta)$ and Be number show increasing pattern for higher values of Ha. Physically production of more disturbance in the flow system is the reason for such

enhancement. That is why both $N_G(\eta)$ and Be are increased. Figs. 3.17 and 3.18 display $N_G(\eta)$ and Be for higher estimations of material parameter M. However entropy generation rate $N_G(\eta)$ and Bejan number Be show decreasing trend for increasing material parameter. For higher M concentration layer thickness decreases so less entropy is generated. Heat transfer for Be is less effective than magnetic and fluid friction effects. That is the Be decays. Figs. 3.19 and 3.20 demonstrate the essential impact of Pr on $N_G(\eta)$ and Be. We note that entropy generation increases for larger Pr but Bejan number decreases for higher Pr. Because larger values of Pr results to an increase in momentum diffusivity of the liquid so particles move rapidly inside the system. It enhances the disturbance in the system and thus more entropy is generated.
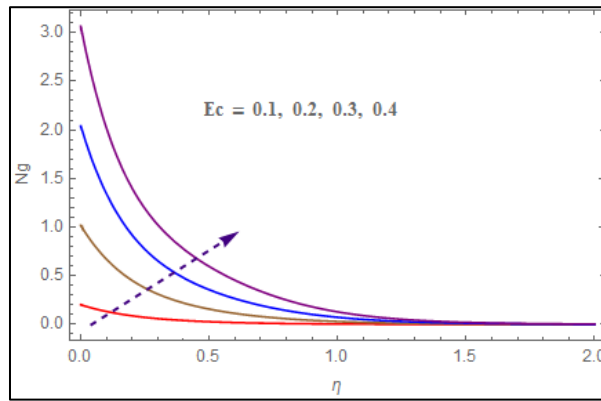
Fig. 3.13 $N_G(\eta)$ for Ec.
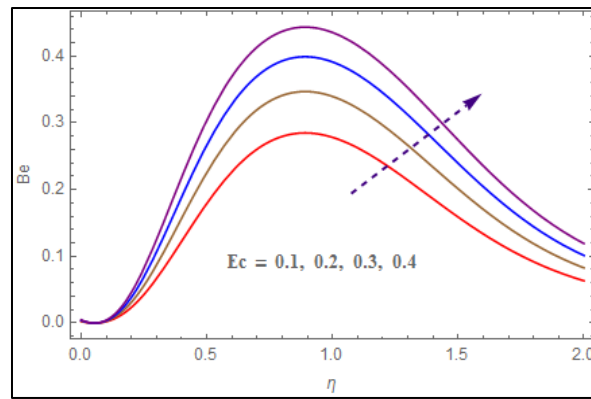
Fig. 3.14 Be for Ec.
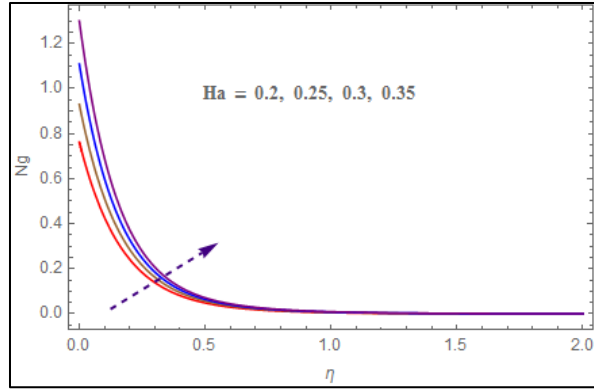
Fig. 3.15 $N_G(\eta)$ for Ha.
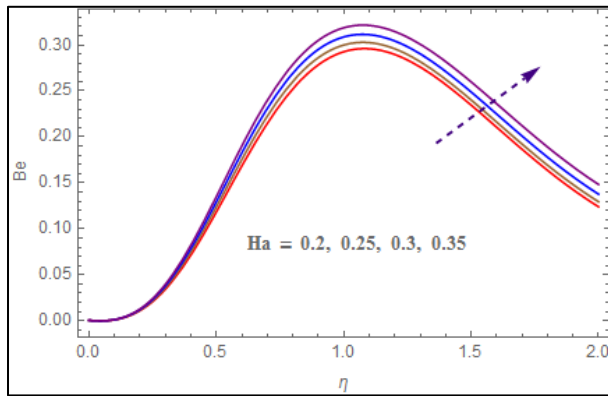
Fig. 3.16 Be for Ha.
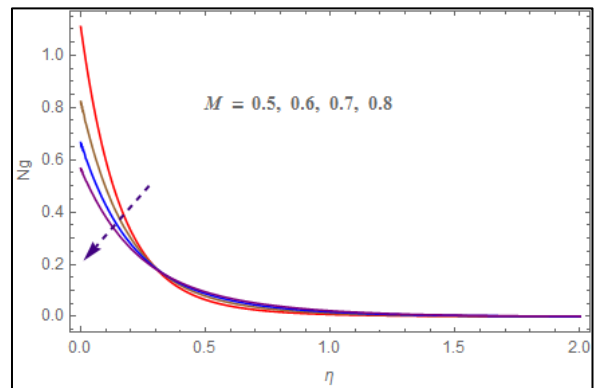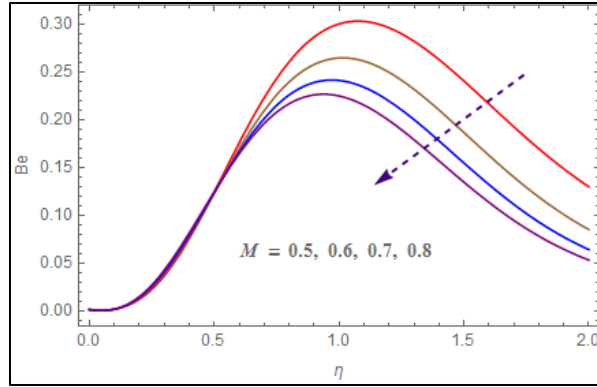

Fig. 3.17 $N_G(\eta)$ for M.
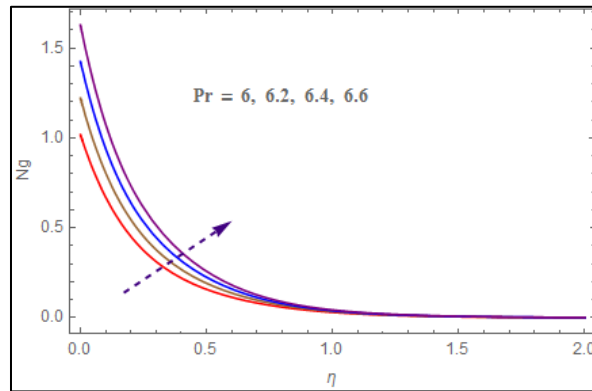
Fig.3. 18 Be for M.
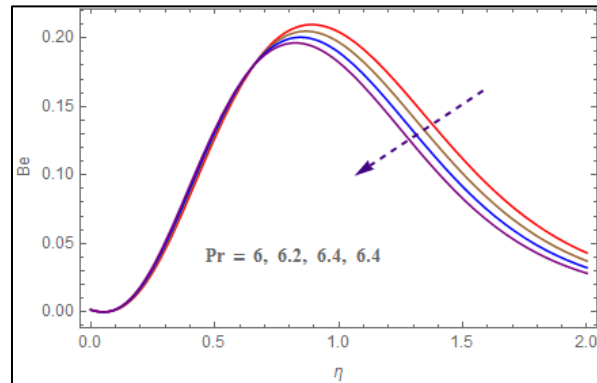

Fig. 3.19 $N_G(\eta)$ for Pr

Fig. 3.20 Be for Pr.

Conclusions

Stretched flow of power law fluid with convective conditions, Joule heating, Activation energy and viscous dissipation effects is examined. Key observations are concluded as follows:

- Velocity grows for larger estimations of power law index of fluid.

- Temperature $\tilde{\theta}(\eta)$ increases for Ec.

- Surface drag enhances for higher values of Ha.

- Temperature gradient $Nu_x Re^{\frac{-1}{n+1}}$ is inversely proportional to Ec and Ha.

- Entropy $N_G(\eta)$ is larger for higher Ec and Ha while reverse trend holds for M.

- Bejan number Be decreases with Pr and M while it increases with Ha and Ec.

Chapter 4

Non-linear radiative flow caused by a thin moving needle with entropy generation

Introduction

Entropy optimization and heat transfer phenomenon in non-linear flow of nanoparticles by a thin moving needle are analyzed. Energy expression is studied along with viscous dissipation and thermal radiation. Water is used as a base fluid while copper, titanium dioxide and aluminum oxide are the nanomaterials. Non-linear governing equations are first transformed into ordinary ones and solved by shooting method for obtaining numerical results. Entropy expression with temperature and velocity gradients is calculated. Pertinent variables are used to obtain the nondimensionalized form. Entropy generation is analyzed by the help of thermodynamics' second law. Results for temperature profile, velocity profile, concentration profile, surface drag and thermal transport are explored through graphical representation. Here outcomes disclose that surface drag and rate of heat transfer enhance for larger values of nanoparticle volume fraction. Drag force decreases for aluminum oxide while it increases for copper nanoparticles. Additionally the heat transfer rate reduces for higher radiation parameter. Temperature enhances for higher temperature ratio parameter.

Formulation

Flow of nanoparticles due to thin needle moving with constant velocity u_w is discussed. A schematic flow diagram is shown in Fig. 4.1. Here (x, r) denote the axial and radial directions and "a" the needle size (see Fig. 4.1). The continuously moving needle is considered thin when thickness of needle does not exceed that of momentum and thermal boundary layer. Viscous dissipation and non-linear thermal radiation effects are incorporated in the energy equation. Water is taken as base-fluid while nanoparticles comprise oxides of aluminum, titanium and copper and. Pressure gradient is neglected. Entropy generation is analyzed mathematically. Moreover it is also assumed that T_w and T_∞ denote the constant and ambient temperature of the needle $(T_w > T_\infty)$. The governing flow equations subject to above assumptions are:

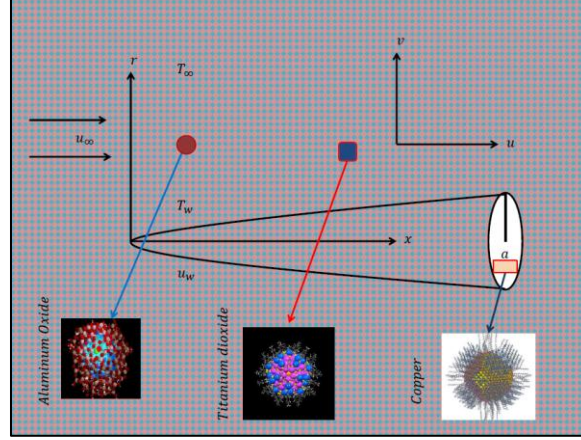Fig 4.1: Flow geometry

$$\frac{\partial}{\partial x}(ru) + \frac{\partial}{\partial x}(rv) = 0 \tag{4.1}$$

$$u\frac{\partial u}{\partial x} + v\frac{\partial u}{\partial r} = \frac{\mu_{nf}}{\rho_{nf}}\frac{1}{r}\frac{\partial}{\partial r}\left(r\frac{\partial u}{\partial r}\right) \tag{4.2}$$

$$u\frac{\partial T}{\partial x} + v\frac{\partial T}{\partial r} = \frac{k_{nf}}{(\rho c_p)_{nf}}\frac{1}{r}\frac{\partial}{\partial r}\left(r\frac{\partial T}{\partial r}\right) + \frac{1}{(\rho c_p)_{nf}}\left(\begin{array}{c}\frac{16\sigma^* T^3}{3k^*}\frac{\partial^2 T}{\partial r^2} + \\ \frac{16\sigma^* 3T^2}{3k^*}\left(\frac{\partial T}{\partial r}\right)^2\end{array}\right) + \frac{\mu_{nf}}{(\rho c_p)_{nf}}\left(\frac{\partial u}{\partial r}\right)^2, \tag{4.3}$$

with

$$\left.\begin{array}{c}u \to u_w, \ v = 0, \ T = T_w \ \text{at } r = R(x), \\ u \to u_\infty, \ T = T_\infty \ \text{as } r \to \infty,\end{array}\right\} \tag{4.4}$$

where (u, v) represent respectively axial and radial components of velocity, (x, r) the cylindrical coordinates, $R(x)$ the surface shape of axisymmetric body, $(c_p)_{nf}$ the specific heat, σ^* the Stefan-Boltzman constant, k^* the mean absorption coefficient, ρ_{nf} the density, T the temperature, k_{nf} the thermal conductivity, μ_{nf} the dynamic viscosity and $(\rho c_p)_{nf}$ the heat capacity. These definitions are

$$\left.\begin{array}{c}v_{nf} = \frac{\mu_f}{(1-\phi)^{2.5}[(1-\phi)\rho_f + \phi\rho_s]}, \ \rho_{nf} = (1-\phi)\rho_f + \phi\rho_s, \\ \alpha_{nf} = \frac{k_{nf}}{(\rho c_p)_{nf}}, \ (\rho c_p)_{nf} = (1-\phi)(\rho c_p)_f + \phi(\rho c_p)_s, \\ \frac{k_{nf}}{k_f} = \frac{(k_s + 2k_f) - 2\phi(k_f - k_s)}{(k_s + 2k_f) + \phi(k_f - k_s)},\end{array}\right\} \tag{4.5}$$

Here μ_f denotes the dynamic viscosity, ϕ the solid volume fraction of nanoliquid, ρ_f the density, ρ_s density of nanoparticle, k_f the thermal conductivity, $(\rho c_p)_s$ nanoparticles' heat capacity, (ρc_p) the heat capacity for base fluid and k_s the thermal conductivity of solid particles. Here nf stands for nanofluid and f for base fluid.

Table 4.1: Thermal properties of base fluid and nanoparticles.

Base fluid and nanomaterials	Water	Aluminum oxide	Titanium dioxide	Copper
Molecular formula	H_2O	Al_2O_3	Tio_2	Cu
$C_P (J/kgK)$	4179	765	686.2	385
$\rho (kg/m^3)$	997.1	3970	4250	8933
$k (W/mK)$	0.613	40.0	8.954	400.0
$\alpha * 10^7 (m^2/s)$	1.47	131.1	30.9	1163.1
$\beta * 10^{-5} (1/K)$	21	0.85	0.9	1.67

We consider the transformations

$$\Psi = v_f x f(\eta), \ \theta(\eta) = \frac{T - T_\infty}{T_w - T_\infty}, \ \eta = \frac{U r^2}{v_f x}, \ v = -\left(\frac{1}{r}\right)\frac{\partial \Psi}{\partial x}, \ u = \left(\frac{1}{r}\right)\frac{\partial \Psi}{\partial r},$$
$$u = 2U f'(\eta), v = -\frac{v_f}{r}(f(\eta) - \eta f'(\eta)). \tag{4.6}$$

Here Ψ indicates the stream function, $v \left(= -\left(\frac{1}{r}\right)\frac{\partial \Psi}{\partial x}\right)$ and $u \left(= \left(\frac{1}{r}\right)\frac{\partial \Psi}{\partial r}\right)$ the velocity components, v_f the kinematic viscosity and $f(\eta)$ the dimensionless stream function. Note that Eq. (4.5) depicts the size and shape of needle $r = R(x)$ by setting $\eta = a$ with its surface given by

$$R(x) = \left(\frac{v_f a x}{U}\right)^{\frac{1}{2}}. \tag{4.7}$$

Equation (4.1) is automatically verified and the other expressions give

$$\frac{2}{(1-\phi)^{2.5}} (\eta f'')' + \left(1 - \phi + \phi \left(\frac{\rho_s}{\rho_f}\right)\right) f f'' = 0, \tag{4.8}$$

$$\left.\begin{array}{c}
\dfrac{k_{nf}}{k_f}\dfrac{1}{Pr}\dfrac{1}{\left(1-\phi+\phi\dfrac{(\rho c_p)_s}{(\rho c_p)_f}\right)}[\theta'+\eta\theta'']+\dfrac{1}{2}f\theta'+\\[4mm]
+\dfrac{4}{3}R_d\dfrac{1}{Pr}\dfrac{1}{\left(1-\phi+\phi\dfrac{(\rho c_p)_s}{(\rho c_p)_f}\right)}\left(\theta\left(\theta_w-1\right)+1\right)^2\left[\left(\theta\left(\theta_w-1\right)+1\right)\left(\dfrac{\theta'}{2}+\eta\theta''\right)+3\theta'^2\left(\theta_w-1\right)\eta\right]\\[4mm]
+\dfrac{1}{\left(1-\phi\right)^{2.5}\left(1-\phi+\phi\dfrac{(\rho c_p)_s}{(\rho c_p)_f}\right)}Ec\eta f''^2=0,
\end{array}\right\} \tag{4.9}$$

with

$$\left.\begin{array}{c}
f(a)=\dfrac{a\varepsilon}{2},\ f'(a)=\dfrac{\varepsilon}{2},\ f'(\infty)=\dfrac{1-\varepsilon}{2},\\[2mm]
\theta(a)=1,\ \theta(\infty)=0.
\end{array}\right\} \tag{4.10}$$

Here $Pr\left(=\dfrac{(\rho c_p)_f \nu_f}{k_f}\right)$ denotes the Prandtl number, $R_d=\dfrac{4\sigma^* T_\infty^3}{k^* k_f}$ the radiative variable, $\theta_w=\dfrac{T_w}{T_\infty}$ the

heating variable, $Ec\left(=\dfrac{U^2}{(c_p)_f(T_w-T_\infty)}\right)$ the Eckert number and $\varepsilon\left(=\dfrac{u_w}{U}=\dfrac{\text{Needle velocity}}{\text{Composite velocity}}\right)$ the

velocity ratio variable.

Mathematically we have

$$\left.\begin{array}{c}
C_f=\dfrac{\tau_w}{\rho_f U^2},\\[3mm]
Nu_x=\dfrac{xq_w}{k_f(T_w-T_\infty)},
\end{array}\right\} \tag{4.11}$$

where τ_w and q_w are given by

$$\left.\begin{array}{c}
\tau_w=\mu_{nf}\left(\dfrac{\partial u}{\partial r}\right)_{r=a}=\mu_{nf}\dfrac{4aU^2}{\nu_f x}f''(a),\\[3mm]
q_w=-k_{nf}\left(\dfrac{\partial T}{\partial r}\right)_{r=a}=-k_{nf}\dfrac{2aU(T_w-T_\infty)}{\nu_f x}\theta'(a).
\end{array}\right\} \tag{4.12}$$

Using Eq. (4.11-4.12), one has

$$\left.\begin{array}{c}
Re_x^{0.5}C_f=\dfrac{4a^{\frac{1}{2}}}{\left(1-\phi\right)^{2.5}}f''(a),\\[3mm]
Re_x^{-0.5}Nu_x=-2a^{\frac{1}{2}}\dfrac{k_{nf}}{k_f}\theta'(a)\left(1+\dfrac{4R_d}{3}\theta_r^3\right),
\end{array}\right\} \tag{4.13}$$

where τ_w symbolizes the shear stress, q_w the wall heat flux and $Re_x\left(=\dfrac{Ux}{\nu_f}\right)$ the local Reynolds

number.

Implementation of entropy equation

The entropy generation per unit volume for incompressible two-dimensional flow with nonlinear thermal radiation is

$$\dot{S}_{gen}''' = \underbrace{\frac{k_f}{T^2}\left[\frac{k_{nf}}{k_f}\left(\frac{\partial T}{\partial r}\right)^2 + \frac{16\sigma^* T^3}{3k^* k_f}\left(\frac{\partial T}{\partial r}\right)^2\right]}_{\text{Entropy production due to thermal transport}} + \underbrace{\frac{\mu_{nf}}{T}\left(\frac{\partial u}{\partial r}\right)^2}_{\text{Entropy production due to fluid friction}}. \tag{4.14}$$

Basic form per unit volume of entropy generation rate is

$$\dot{S}_{gen}''' = \dot{S}_{gen,\Delta T}''' + \dot{S}_{gen,Frc}'''. \tag{4.15}$$

Using the transformations (4.6), equation (4.14) takes the form

$$N_G = \frac{\dot{S}_{gen}'''}{\frac{4k_f U}{v_f x}} = \left\{ \begin{array}{l} \eta\theta'^2\left(\theta_w - 1\right)^2\left(\dfrac{\dfrac{k_{nf}}{k_f}}{\left(\theta\left(\theta_w - 1\right) + 1\right)^2} + \dfrac{4}{3}R_d\left(\theta\left(\theta_w - 1\right) + 1\right)\right) \\[2em] + \dfrac{4\eta Ec\,Pr(\theta_w - 1)}{(1-\phi)^{2.5}\left(\theta\left(\theta_w - 1\right) + 1\right)}f''^2 \end{array} \right\} = N_{\Delta T} + N_{Frc}, \tag{4.16}$$

where

$$N_{\Delta T} = \eta\theta'^2\left(\theta_w - 1\right)^2\left(\underbrace{\frac{\frac{k_{nf}}{k_f}}{\left(\theta\left(\theta_w - 1\right) + 1\right)^2}}_{\text{Conductive irreversibility}} + \frac{4}{3}R_d\left(\theta\left(\theta_w - 1\right) + 1\right)\right), \left.\begin{array}{c} \\ \\ \\ \\ \\ \end{array}\right\} \tag{4.17}$$

$$N_{Frc} = \underbrace{\frac{4\eta Ec\,Pr(\theta_w - 1)}{(1-\phi)^{2.5}\left(\theta\left(\theta_w - 1\right) + 1\right)}}_{\text{Viscous irreversibility}}f''^2, \left.\begin{array}{c} \\ \\ \\ \end{array}\right\} \tag{4.18}$$

$$\left(\dot{S}_{gen}'''\right)_c = \underbrace{\frac{4k_f U}{\nu_f x}}_{\text{Characteristic entropy}}. \tag{4.19}$$

Bejan number is defined as follows:

$$Be = \frac{\frac{k_f}{T^2}\left[\frac{k_{nf}}{k_f}\left(\frac{\partial T}{\partial r}\right)^2 + \frac{16\sigma^* T^3}{3k^* k_f}\left(\frac{\partial T}{\partial r}\right)^2\right]}{\frac{k_f}{T^2}\left[\frac{k_{nf}}{k_f}\left(\frac{\partial T}{\partial r}\right)^2 + \frac{16\sigma^* T^3}{3k^* k_f}\left(\frac{\partial T}{\partial r}\right)^2\right] + \frac{\mu_{nf}}{T}\left(\frac{\partial u}{\partial r}\right)^2}, \tag{4.20}$$

By utilizing Eq. (4.6) we have

Be

$$= \frac{\eta\theta'^2\left(\theta_w - 1\right)^2\left(\dfrac{\dfrac{k_{nf}}{k_f}}{\left(\theta\left(\theta_w - 1\right) + 1\right)^2} + \dfrac{4R_d}{3}\left(\theta\left(\theta_w - 1\right) + 1\right)\right)}{\eta\theta'^2\left(\theta_w - 1\right)^2\left(\dfrac{\dfrac{k_{nf}}{k_f}}{\left(\theta\left(\theta_w - 1\right) + 1\right)^2} + \dfrac{4}{3}R_d\left(\theta\left(\theta_w - 1\right) + 1\right)\right) + \dfrac{4\eta Ec\,Pr(\theta_w - 1)}{(1 - \phi)^{2.5}\left(\theta\left(\theta_w - 1\right) + 1\right)}f''^2} \tag{4.21}$$

Discussion

Nonlinear radiative flow of nanomaterials (titanium dioxide, copper and aluminum oxide) over a thin moving needle is numerically examined with the help of Built-in-Shooting technique. Here results are well ordered for different parameters like the Prandtl number Pr, radiative parameter R_d, temperature ratio θ_w, Eckert number Ec and velocity ratio variable ε on temperature $\theta(\eta)$, entropy generation (N_G), skin friction coefficient, Nusselt number (Nu) and Bejan number (Be) (see Figs. 4.2–4.19). We take the value of Pr equal to 6.2 and the range of nanoparticle volume fraction $0 \leq \phi \leq 1$. Effect of radiative parameter (R_d) is illustrated in Fig. 4.4. Here the performance of temperature $\theta(\eta)$ and their associated layer is smaller for higher (R_d). Temperature of fluid particles at the needle surface is smaller when compared with ambient temperature for larger radiation parameter. Therefore, thermal field and associated layer thickness is decreased. Variation of temperature $\theta(\eta)$ for variable (θ_w) is shown in Fig. 4.3. Here temperature is enhanced for higher

θ_w. Physically internal temperature of liquid particles increases for rising θ_w. That is why temperature field is enhanced. The characteristics of velocity ratio variable (ε) on temperature is plotted in Fig. 4.4. Obviously temperature is enhanced with rising estimation of heating parameter. Temperature ($\theta(\eta)$) for (ϕ) is drawn in Fig. 4.5. Since larger (ϕ) result in improvement of convective heat transport. Therefore temperature field increases. Figs. 4.6 and 4.7 show the graphical performances for (N_G) and Be with ($a = 0.01$) and various estimations of radiative parameter. Both (Be) and (N_G) are decreased for higher (R_d). Physically inside energy source of flow system enhances for higher (R_d). Therefore (Be) and (N_G) decay. Effects of Eckert number (Ec) on entropy generation and Bejan number (Be) are revealed in Figs. 4.8 and 4.9 respectively. Entropy generation rate (N_G) is increased by enhancing Eckert number (Ec). However reverse trend is noted for Bejan number in case of Eckert number. Physically heat is a form of disorganized energy. Therefore, more heat transfer to the system is generated due to entropy. That is why kinetic energy of liquid particles converted low grade energy (heat energy) and consequently (N_G) enhances. Bejan number is decreasing function of (Ec). Physically in the absence of dissipation the Bejan number (Be=1) at the surface and within the layer, entropy generation is just due to heat transport. Figs. 4.10 and 4.11 are arranged for the impact of heating parameter (θ_w) on rate of entropy generation (N_G) and (Be). Clearly both (N_G) and (Be) enhance for different higher values of heating variable. Effect of velocity ratio variable (ε) on rate of entropy generation (N_G) and (Be) is displayed in Figs.4. 12 and 4.13. N_G decays with higher values of velocity ratio variable (ε) for both cases i.e., $0 \le \varepsilon \le 0.5$ and $0.5 \le \varepsilon \le 1.0$. The purpose of entropy generation analysis is to decay entropy by different flow parameters. Therefore the goal of entropy generation minimization is accomplished for larger values of velocity ratio variable when the needle travels slower than the free stream and the needle travels closer than the free stream. Figs. 4.14 and 4.15 disclosed that N_G and Be have reverse behavior for larger estimation of (ϕ). Influences of nanoparticle volume fraction (ϕ) and velocity ratio parameter (ε) on surface drag force $Re_x{}^{0.5}C_{f_x}$ are portrayed in Fig. 4.16. Clearly drag force is increased for all nanoparticles (titanium dioxide, copper and aluminum oxide). Surface drag force is larger for higher values of (ϕ) and velocity ratio parameter (ε). Fig. 4.17 revealed that magnitude of heat transfer rate $Re_x{}^{-0.5}Nu_x$ enhances with increasing values of (ϕ). Physically thermal conductivity of base liquid (water) enhances for varying values of (titanium dioxide, copper and aluminum oxide). Therefore rate of heat transfer is enhanced. Effects

of radiative and heating parameter on heat transfer rate are plotted in Figs. 4.18 and 4.19. Magnitude of heat transfer rate decays for radiative parameter (see Fig. 4.18). Initially heat transfer rate enhances in the range $0 \leq \varepsilon \leq 0.5$ and then it decays for $0.5 \leq \varepsilon \leq 1.0$. Magnitude of heat transfer rate increases for increasing range of heating parameter (see Fig. 4.19).
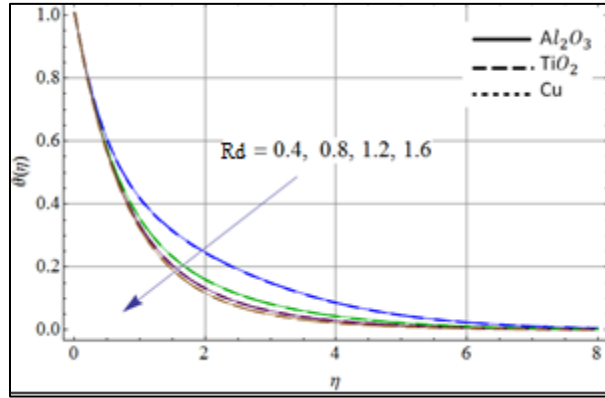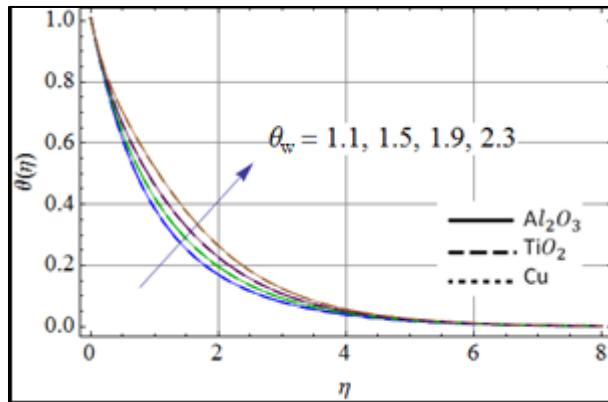
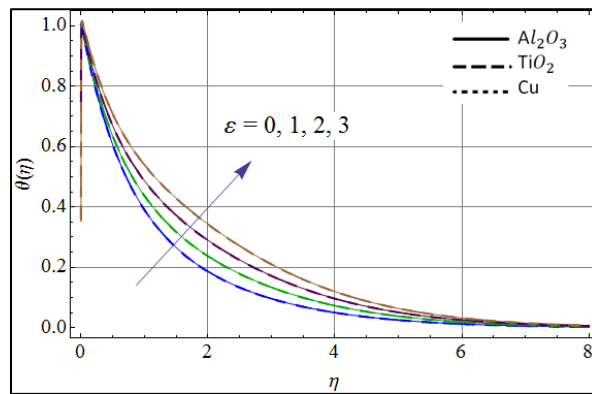

Fig. 4.2: $\theta(\eta)$ via R_d.

Fig. 4.3: $\theta(\eta)$ via θ_w.

Fig. 4.4: $\theta(\eta)$ via ε.
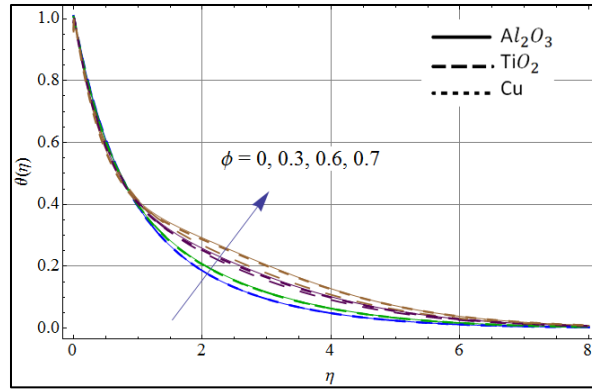
Fig. 4.5: $\theta(\eta)$ via ϕ.
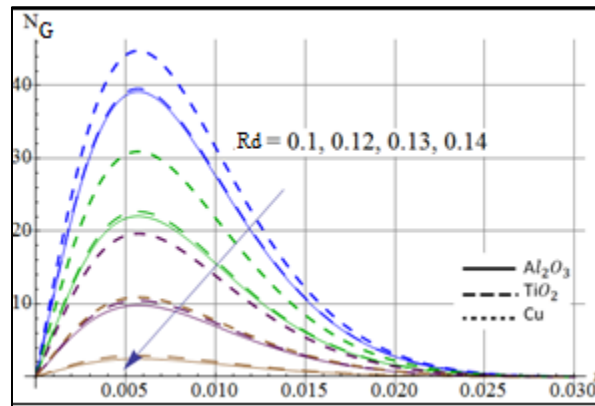
Fig. 4.6: N_G via R_d.

Fig. 4.7: Be via R_d.

53
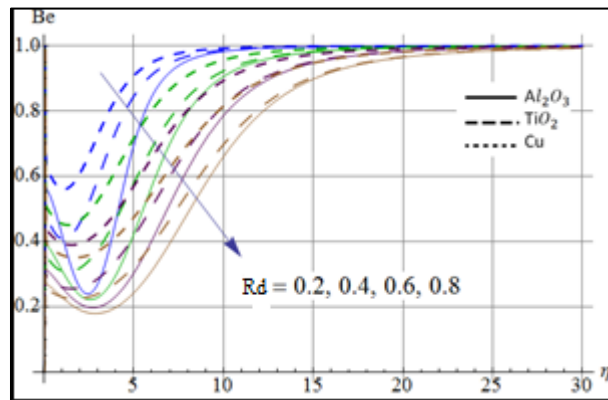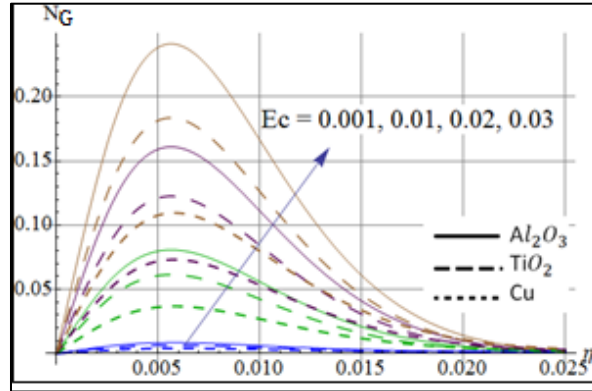
Fig. 4.8: N_G via Ec.
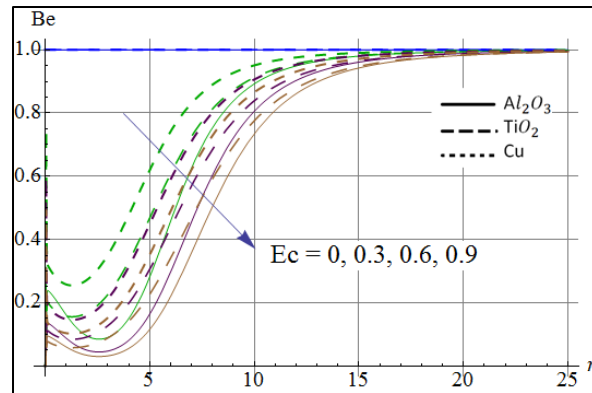
Fig. 4.9: Be via Ec.
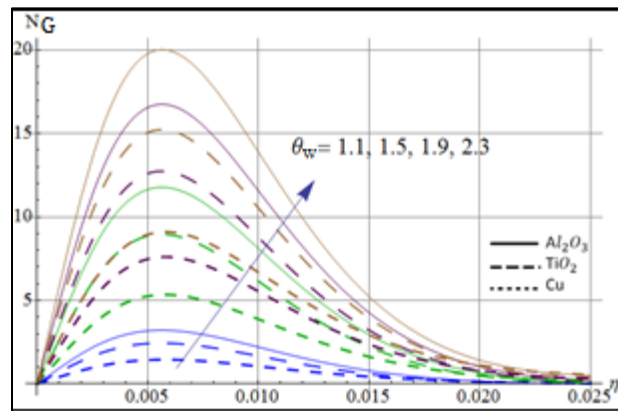
Fig. 4.10: N_G via θ_w.
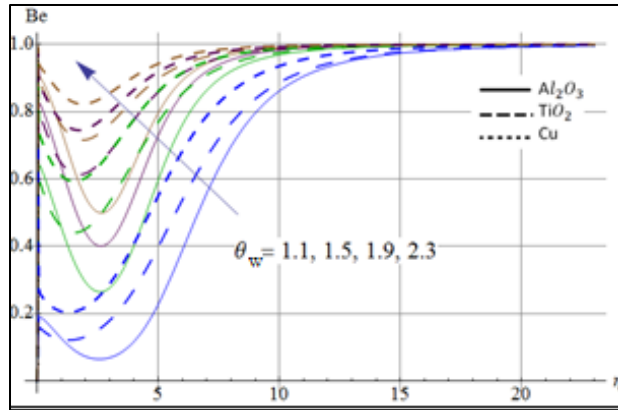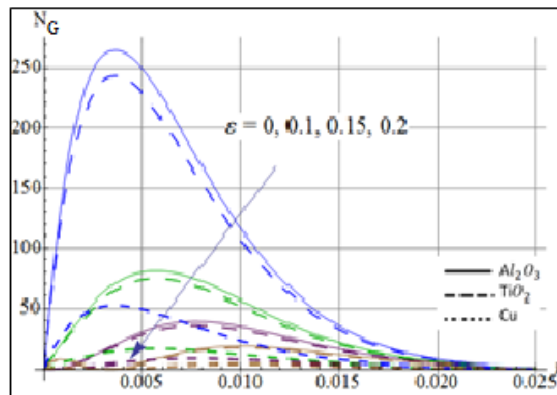
Fig. 4.11: *Be* via θ_w.

Fig. 4.12: N_G via ε.

Fig. 4.13: *Be* via ε.

55
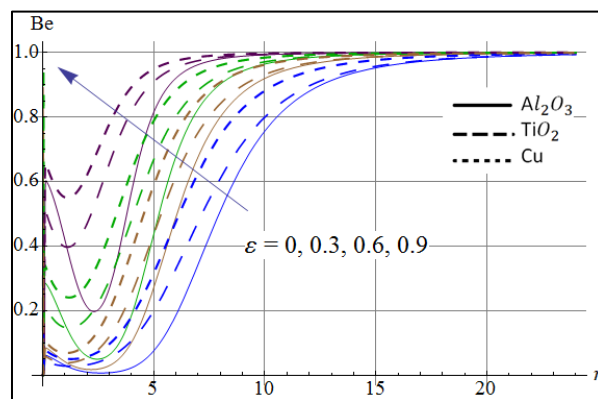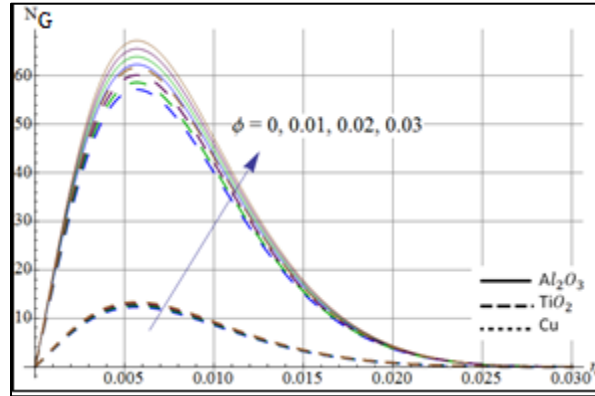
Fig. 4.14: N_G via ϕ.
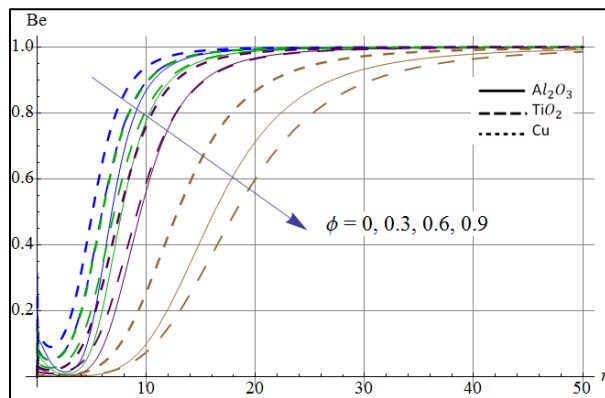
Fig. 4.15: Be via ϕ.
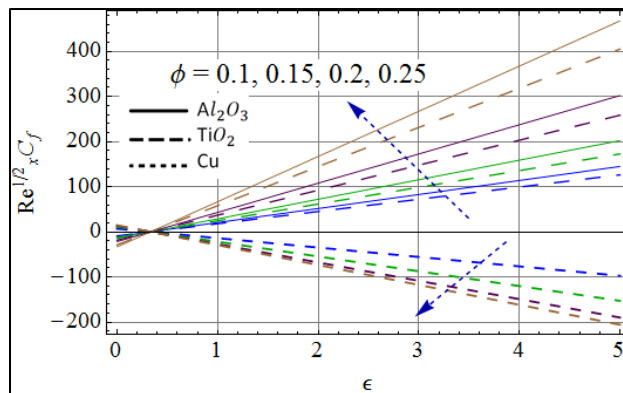
Fig. 4.16: Effects of ϕ and ε on $Re_x^{0.5} C_f$.
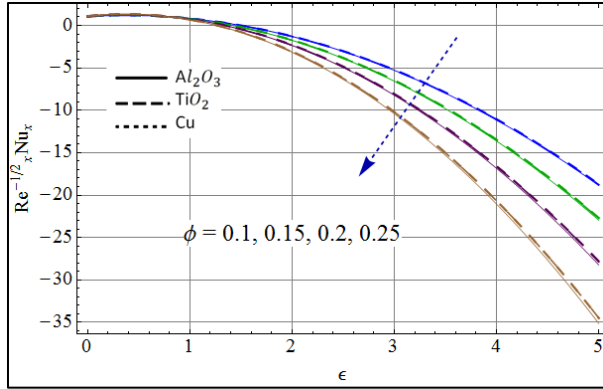
Fig. 4.17: Effects of ϕ and ε on $Re_x^{-0.5} N u_x$.
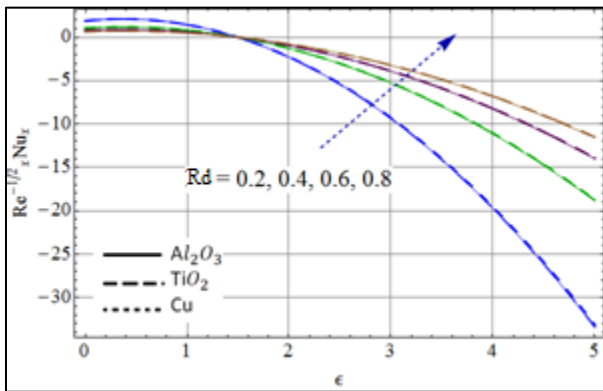
Fig. 4.18: Effects of ϕ and ε on $Re_x^{-0.5} N u_x$.
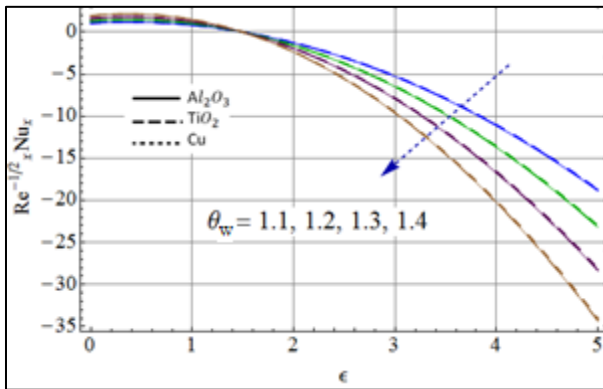
Fig. 4.19: Effects of ϕ and ε on $Re_x^{-0.5} N u_x$.

Conclusions

Entropy generation in thermally radiative flow of titanium dioxide, copper and aluminum oxide nanomaterials over a thin moving needle is examined. Main points are given as follows:

• Enhancement in radiative parameter (R_d) reduces in temperature.

• Thermal field enhances with increasing velocity ratio parameter (ε), heating parameter (θ_w) and (ϕ).

• N_G and Be are decreased for higher R_d.

• Skin friction $Re_x{}^{0.5}C_{fx}$ and ($Re_x{}^{-0.5}Nu_x$) increase via (ϕ).

• Heat transfer $Re_x{}^{-0.5}Nu_x$ for radiative parameter is decreased.

Chapter 5

Entropy minimization in Sisko fluid flow with nonlinear thermal radiation

Introduction

This chapter demonstrates the salient characteristics of entropy minimization for the flow of Sisko fluid. Source for fluid motion is the stretchable rotating disk. Nonlinear mixed convection, viscous dissipation and Brownian motion are discussed. Entropy is calculated and discussed through graphical representation. Properties of heat transfer are examined with heat source/sink and nonlinear thermal radiation. The governing equations are solved for convergent solutions. Results are graphically shown.

Formulation

Here Sisko fluid flow generated by a rotating stretchable disk is presented. The rotating disk at $z = 0$ has an angular speed Ω. Stretching velocity of the disk is $u = ra$ (see Fig. 5.1). Thermal characteristics are scrutinized alongwith heat source/sink, nonlinear radiation and dissipation effects. Additionally nonlinear mixed convection is also considered. Furthermore thermophoresis as well as Brownian motion parameters are present. Entropy generation and dimensionless Bejan number are discussed graphically. The conservations laws of mass, momentum, energy as well as concentration for Sisko fluid flow yield:
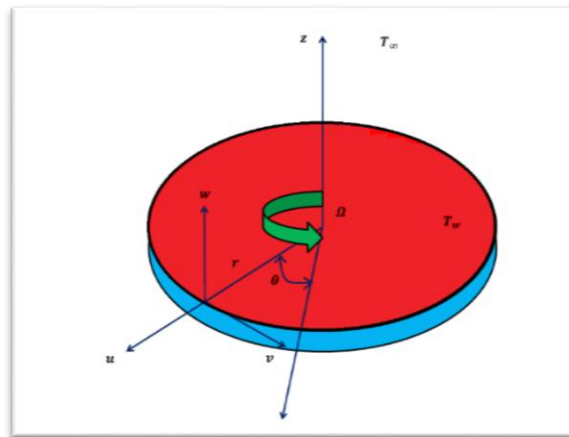
Fig. 5.1 Flow geometry

$$\frac{\partial \hat{u}}{\partial r} + \frac{\hat{u}}{r} + \frac{\partial \hat{w}}{\partial z} = 0,$$

(5.1)

$$\rho\left(\hat{u}\frac{\partial \hat{u}}{\partial r} + \hat{w}\frac{\partial \hat{u}}{\partial z} - \frac{\hat{v}^2}{r}\right) = \alpha^*\frac{\partial^2 \hat{u}}{\partial z^2} + \beta^*\frac{\partial}{\partial z}\left[\frac{\partial \hat{u}}{\partial z}\left(\left(\frac{\partial \hat{u}}{\partial z}\right)^2 + \left(\frac{\partial \hat{v}}{\partial z}\right)^2\right)^{\frac{n-1}{2}}\right] + \Bigg\}$$
$$g\left[\lambda_1(\hat{T} - \hat{T}_\infty) + \lambda_2(\hat{T} - \hat{T}_\infty)^2\right] + g\left[\lambda_3(\hat{C} - \hat{C}_\infty) + \lambda_4(\hat{C} - \hat{C}_\infty)^2\right], \Bigg\} \tag{5.2}$$

$$\rho\left(\hat{u}\frac{\partial \hat{v}}{\partial r} + \hat{w}\frac{\partial \hat{v}}{\partial z} + \frac{\hat{u}\hat{v}}{r}\right) = \alpha^*\frac{\partial^2 \hat{v}}{\partial z^2} + \beta^*\frac{\partial}{\partial z}\left[\frac{\partial \hat{v}}{\partial z}\left(\left(\frac{\partial \hat{u}}{\partial z}\right)^2 + \left(\frac{\partial \hat{v}}{\partial z}\right)^2\right)^{\frac{n-1}{2}}\right], \tag{5.3}$$

$$\left(\hat{u}\frac{\partial \hat{T}}{\partial r} + \hat{w}\frac{\partial \hat{T}}{\partial z}\right) = \frac{k}{\rho c_p}\frac{\partial^2 \hat{T}}{\partial z^2} + D_B\left(\frac{\partial \hat{T}}{\partial z}\frac{\partial \hat{C}}{\partial z}\right) + \frac{D_T}{T_\infty}\left(\frac{\partial \hat{T}}{\partial z}\right)^2 + \frac{\alpha^*}{\rho c_p}\left[\left(\frac{\partial \hat{u}}{\partial z}\right)^2 + \left(\frac{\partial \hat{v}}{\partial z}\right)^2\right] + \Bigg\}$$
$$\frac{\beta^*}{\rho c_p}\left[\left(\left(\frac{\partial \hat{u}}{\partial z}\right)^2 + \left(\frac{\partial \hat{v}}{\partial z}\right)^2\right)^{\frac{n-1}{2}}\right] + \frac{Q^*}{\rho c_p}(\hat{T} - \hat{T}_\infty) + \frac{1}{\rho c_p}\frac{16\sigma^*}{3k^*}\frac{\partial}{\partial z}\left(\hat{T}^3\frac{\partial \hat{T}}{\partial z}\right), \Bigg\} \tag{5.4}$$

$$\hat{u}\frac{\partial \hat{C}}{\partial r} + \hat{w}\frac{\partial \hat{C}}{\partial z} = \frac{D_T}{T_\infty}\frac{\partial^2 \hat{T}}{\partial z^2} + D_B\frac{\partial^2 \hat{C}}{\partial z^2}, \tag{5.5}$$

subject to the conditions

$$\left.\begin{array}{l} \hat{u} = ra, \hat{v} = r\Omega, \hat{w} = 0, \hat{T} = \hat{T}_w, \hat{C} = \hat{C}_w, \text{ at } z = 0, \\ \hat{u} = 0, \hat{v} = 0, \hat{T} \to \hat{T}_\infty, C \to C_\infty \text{ when } z \to \infty. \end{array}\right\} \tag{5.6}$$

Here $\hat{T}$ is the fluid temperature, σ^* Stefan-Boltzman constant, k^* the mean absorption coefficient, a dimensional constant, density ρ, absolute viscosity μ, kinematic viscosity v, thermal conductivity k, electrical conductivity σ and heat capacitance c_p.

We consider Von-Karman transformations:

$$\left.\begin{array}{l} \hat{u} = r\Omega\tilde{f}(\xi), \hat{v} = r\Omega\tilde{g}(\xi), w = r^*\left(\frac{n-1}{n+1}\right)\left(\frac{\Omega^{1-2n}}{\sigma/\rho}\right)^{\frac{1}{n-1}}h(\xi) \\ \\ \theta = \frac{\hat{T} - \hat{T}_\infty}{\hat{T}_f - \hat{T}_\infty}, \phi = \frac{\hat{C} - \hat{C}_\infty}{\hat{C}_f - \hat{C}_\infty}, \xi = z\left(\frac{\Omega^{2-n}}{\sigma/\rho}\right)^{\frac{1}{n+1}}r^{\left(\frac{1-n}{n+1}\right)} \end{array}\right\} \tag{5.7}$$

where n denotes the power law index, $\tilde{f}, \tilde{g}, \tilde{h}$, are velocity components and r^* the radius. We obtain

$$\tilde{h}' + 2\tilde{f} + \frac{1-n}{1+n}\xi\tilde{f}' = 0, \tag{5.8}$$

$$A\tilde{f}'' - \tilde{f}^2 + \tilde{g}^2 - \left[\frac{1-n}{1+n}\xi\tilde{f} + \tilde{h}\right]\tilde{f}' + \left[\tilde{f}'\left(\tilde{f}'^2 + g'^2\right)^{\frac{n-1}{2}}\right]'$$
$$+ Re\left[\alpha_1\tilde{\theta}(1 + \beta_t\tilde{\theta}) + \alpha_1 N^*\phi(1 + \beta_c\phi)\right] = 0, \tag{5.9}$$

$$A\widetilde{g''} - 2\tilde{f}\tilde{g} - \left[\frac{1-n}{1+n}\xi\tilde{f} + \tilde{h}\right]\tilde{g}' - \left[\tilde{g}'\left(\tilde{f}'^2 + \tilde{g}'^2\right)^{\frac{n-1}{2}}\right]' = 0, \tag{5.10}$$

$$\frac{1}{Pr}\frac{4}{3}R_d\left(\tilde{\theta}(\tilde{\theta}_w - 1) + 1\right)^2\left(3\tilde{\theta}'^2(\tilde{\theta}_w - 1) + \tilde{\theta}(\tilde{\theta}_w - 1) + 1\right)\tilde{\theta}''$$
$$-\tilde{h}\tilde{\theta}' - \tilde{f}\tilde{\theta}'\xi\frac{1-n}{1+n} + A^*Ec\left(\tilde{f}'^2 + \tilde{g}'^2\right)^{\frac{n+1}{2}} + N_t\tilde{\theta}'^2 + Q^*\theta + N_b\tilde{\theta}'\phi' = 0, \tag{5.11}$$

$$\frac{1}{Sc}\frac{N_t}{N_b}\vartheta'' + \frac{1}{Sc}\phi'' - \tilde{h}\phi' - \frac{1-n}{1+n}\xi\tilde{f}\phi' = 0, \tag{5.12}$$

$$\tilde{h}(0) = 0, \tilde{f}(0) = A_1, \tilde{f}(\infty) = 0, \tilde{g}(0) = 1,$$
$$\tilde{\theta}(0) = 1, \tilde{g}(\infty) = 0, \ \phi(0) = 1$$
$$\tilde{\theta}(\infty) = 0, \phi(\infty) = 1, \tag{5.13}$$

$$Re = \frac{\Omega R_0^2}{v}, Ha = \frac{\sigma_f B_0^2}{\rho_f\Omega}, \ Pr = \frac{\rho c_p\Omega}{k}\left(\frac{\Omega^{2-n}}{\sigma/\rho}\right)^{\frac{-2}{1+n}} \ A_1 = \frac{a}{\Omega}, Sc = \frac{\Omega}{D_B}(\frac{\Omega^{2-n}}{\beta/\rho})^{2/1+n}r^{-2(\frac{1-n}{1+n})}, \beta_c = \frac{\lambda_4}{\lambda_3}(C_w - C_\infty)$$

$$Ec = \frac{r^2\Omega^2}{c_p(\hat{T}_w - \hat{T}_\infty)}, \lambda = \frac{g\beta}{r^3\Omega^3}\lambda_1 \frac{(\hat{T}_w - \hat{T}_\infty)}{r^3\Omega^3}, \ Q^* = \frac{Q_0}{\rho c_p\Omega}, \alpha = \frac{a}{R_0^2}\left(\frac{\Omega R_0^2\rho}{\mu}\right)^{\frac{-1}{n+1}}, \beta_t = \frac{\lambda_2}{\lambda_1}(T_w - T_\infty), \theta_w = \frac{T_w}{T_\infty}$$

$$N_t = \frac{\tau D_T(\hat{T}_w - \hat{T}_\infty)}{\Omega\,\hat{T}_\infty}\left(\frac{\Omega^{2-n}}{\beta/\rho}\right)^{\frac{2}{1+n}}r^{2\left(\frac{1-n}{n+1}\right)}, N_b = \frac{\tau D_B(C_f - C_\infty)}{v}\left(\frac{\Omega^{2-n}}{\beta/\rho}\right)^{\frac{2}{1+n}}r^{2\left(\frac{1-n}{n+1}\right)}, A = \frac{\alpha}{\rho\Omega}\left|\frac{\Omega^{2-n}}{\beta/\rho}\right|^{\frac{-2}{n+1}}r^{2\left(\frac{1-n}{1+n}\right)}, N^* = \frac{\lambda_3}{\lambda_1}\frac{(C_w - C_\infty)}{(T_w - T_\infty)} \tag{5.14}$$

where Re denotes the Reynold number, Ha magnetic interaction parameter, Pr the Prandtl number, A the ratio of stretching rate and angular velocity, Sc Schmidt number, β_t non-linear mixed convection parameter due to temperature, Ec the Eckert number, λ the mixed convection parameter, Q^* heat source/sink parameter, ε the dimensionless constant, α disk thickness

coefficient, β_c non-linear mixed convection parameter for concentration, N_t thermophoresis parameter, N_b Brownian motion, θ_w temperature ratio parameter, A material parameter and N^* ratio of thermal to buoyancy forces parameter.

Surface drag force

We have

$$C_f = \frac{\tau_w}{1/2\rho_f U_w^2},$$
(5.15)

in which τ_w satisfies

$$\tau_w = (\alpha^* + \beta^* \frac{\partial u}{\partial z})^{n-1} \frac{\partial u}{\partial z}_{z=0}$$
(5.16)

From Eqs. (5.15) and (5.16) we get

$$\frac{1}{2} C_{fx} Re^{\frac{1}{n+1}} = A \tilde{f}'(0) - f'(0)^n$$
(5.17)

Heat transfer rate

Mathematically heat transfer is given as

$$Nu_x = \frac{q_w a}{k(\hat{T}_w - \hat{T}_\infty)}\bigg|_{z=0},$$
(5.18)

where the wall heat flux q_w is

$$q_w|_{z=0} = -k \left(1 + \frac{16\sigma^* T^3}{3kk^*}\right)^{\frac{1}{n+1}} \frac{\partial \hat{T}}{\partial z}.$$
(5.19)

Putting Eq. (5.19) in Eq. (5.18), one has

(5.20)

$$Re^{\frac{-1}{2}} N u_x = -(1 + 4/3R_d(1 + (\theta_w - 1)\tilde{\theta}(0))^{3\varsigma}\tilde{\theta}'(0).$$

Local Sherwood number is

$$Sh_x = \frac{a q_m}{D_B (C_w - C_\infty)}\bigg|_{z=0},$$
(5.21)

where q_m denotes the mass flux and

(5.22)

$$Sh_x Re^{\frac{-1}{n+1}} = -\phi'(0).$$

Entropy generation

Mathematically volumetric entropy rate in dimensional form after using boundary layer assumptions is

$$S_G = \frac{k}{\hat{T}_\infty^2}\left(1+\frac{16\sigma^*}{3kk^*}\right)\left(\frac{\partial \hat{T}}{\partial z}\right)^2 + \frac{RD}{\hat{T}_\infty}\left(\frac{\partial \hat{C}}{\partial z}\frac{\partial \hat{T}}{\partial z}\right) + \frac{RD}{\hat{C}_\infty}\left(\frac{\partial \hat{C}}{\partial z}\right)^2 +$$

$$+\frac{\mu}{\hat{T}_\infty}\alpha^*\left[\left(\frac{\partial \hat{u}}{\partial z}\right)^2 + \left(\frac{\partial \hat{v}}{\partial z}\right)^2\right] + \beta^*\left[\left(\left(\frac{\partial \hat{u}}{\partial z}\right)^2 + \left(\frac{\partial \hat{v}}{\partial z}\right)^2\right)^{\frac{n-1}{2}}\right].$$

(5.23)

In dimensionless form entropy generation number N_G is given by

$$N_G = (\frac{n+1}{2} + R_d)\tilde{\theta}'^2\alpha_1^*$$

$$+Br\left[\frac{n+1}{2}\lambda_1^*\tilde{\theta}'\phi' + \frac{n+1}{2}\lambda_2\phi'^2\right]$$

$$+\frac{n+1}{2}Br(\tilde{f}''^2) + HaBr(\tilde{f}'^2)$$

(5.24)

$$\alpha_1^* = \frac{\hat{T}_w - \hat{T}_\infty}{\hat{T}_f} = \frac{\Delta T}{\hat{T}_f}, N_G = \frac{\hat{T}_\infty S_G}{k\Delta T\Omega}\left(\frac{\Omega^{2-n}}{\beta/\rho}\right)^{\frac{-2}{n+1}}(r^*)^{-2\frac{1-n}{n+1}}$$

$$\lambda_1^* = \frac{RD}{k}(C_w - C_\infty), \ \lambda_2 = \frac{D\hat{T}_w}{C_\infty k\Delta T}(C_w - C_\infty)^2, Br = \frac{ar^2\Omega^2}{k\Delta T}.$$

(5.25)

Here α_1^* is the dimensionless temperature difference variable, N_G entropy generation rate, λ_1^* diffusion parameter and Br Brinkman number.

Bejan number (Be) is

$$Be = \frac{\text{Thermal entropy generation}}{\text{Total entropy generation}},$$

(5.26)

$$Be = \frac{(\frac{n+1}{2} + R_d)\tilde{\theta}'^2\alpha_1^*}{(\frac{n+1}{2} + R_d)\tilde{\theta}'^2\alpha_1^*} + Br\left[\frac{n+1}{2}\lambda_1^*\tilde{\theta}'\phi' + \frac{n+1}{2}\lambda_2\varphi'^2\right] + \frac{n+1}{2}Br(\tilde{f}''^2) + HaBr(\tilde{f}'^2)}.$$

(5.27)

Homotopy analysis

The initial approximations and corresponding operators are

$$\tilde{f}_0(\xi) = A_2\, exp(-\xi),$$
$$\tilde{\theta}_0(\xi) = exp(-\xi),$$
$$\phi_0(\xi) = exp(-\xi),$$

(5.28)

$$L_{\tilde{f}} = \tilde{f}'' - \tilde{f}, L_{\tilde{\theta}} = \tilde{\theta}'' - \tilde{\theta},$$
$$L_\phi = \phi'' - \phi,$$

(5.29)

with

$$
\left.\begin{aligned}
L_{\tilde{f}}\left[c_2 e^{\xi} + c_3 e^{-\xi}\right] &= 0, \\
L_{\tilde{\theta}}\left[c_6 e^{\xi} + c_7 e^{-\xi}\right] &= 0, \\
L_{\phi}\left[c_8 e^{\xi} + c_9 e^{-\xi}\right] &= 0,
\end{aligned}\right\}
\tag{5.30}
$$

In which c_i $(i = 1 - 9)$ represent the arbitrary constants.

Convergence

Homotopy analysis technique is utilized for solving system of nonlinear equations. Convergent solutions are found using this technique. The selection of initial guesses and linear operators is a key tool in this method. A better choice will provide us more accurate result. The graphs for h-curves are shown in Fig. (5.2). At $15th$ order of approximations, the ranges of convergence are $-1.5 \leq \hbar_{\tilde{f}} \leq -0.3$, $-1.6 \leq \hbar_{\tilde{g}} \leq -0.3$, $-4.0 \leq \hbar_{\tilde{\theta}} \leq -0.5$ and $-1.6 \leq \hbar_{\phi} \leq -0.5$. We note that 10th, 15th, 20th and 25th order of approximations are best for solutions convergence.

Discussion

Velocity

Here velocity distribution, temperature as well as concentration are discussed through graphical representation Figs. $(5.3 - 5.5)$ show the effect of A on velocity profile. The axial, radial as well as tangential velocity components show increasing trend for material parameter A. The reason for this increase is the decrease in fluid viscosity. Hence velocity increases. Figs. (5.6) and (5.7) are portrayed to show effect of power index on velocity. For shear thinning fluids $(n < 1)$ more increase in velocity is observed as compared to shear thickening case $(n > 1)$. Figs. (5.8) and (5.9) are sketched for impact of stretching parameter A₁ on velocity. Velocity increases for higher stretching parameter. The behavior of velocity through mixed convection parameter (α_1) is given through Figs. $(10 - 12)$. Velocity shown an increasing behavior for higher (α_1). Which is due to an enhancement in thermal buoyancy forces. Fig. (5.13) is shown for impact of ratio of thermal to buoyancy forces parameter (N^*) on velocity. It assists the velocity of fluid to increase.

Temperature

Figs. $(5.14 - 5.19)$ show the impacts of various parameters like Prandtl number (Pr), heat source parameter (Q^*), Brownian motion parameter, Eckert number (Ec) as well as thermophoresis

parameter (Nt) on temperature. For higher Pr the thermal diffusivity decreases. It results to a decrement in temperature profile as given in Fig. (5.14). Fig. (5.15) portrayed the effect of Ec on temperature. For larger values of Eckert number, large amount of kinetic energy is noticed. Thus temperature profile increases. Impact of heat source parameter (Q^*) on temperature distribution is given in Fig. (5.16). More heat is produced inside the system that is why temperature increases. Fig. (5.17) displays the influence of N_t on temperature. Temperature is enhanced for higher thermophoresis effects. The impact of Brownian motion parameter on temperature profile is graphically shown in Fig. (5.18) for both shear thickening as well as shear thinning i.e. $n > 1$ and $n < 1$. We have seen that temperature enhances for larger values of N_b. Impact of R_d on temperature profile is observed in Fig. (5.19). Larger R_d convert the internal kinetic energy to thermal energy, which is the reason for temperature to increase.

Concentration

Figs. $(5.20 - 5.22)$ explains the behaviors of pertinent parameters like thermophoresis N_t, Brownian motion N_b and Schmidt number on concentration profile. Impact of thermophoresis parameter on concentration is presented via Fig. (5.20). We know that $\phi\ (\xi)$ directly depends on temperature gradient and N_t shows increasing behavior due to temperature gradient. That is why concentration profile increases (see Fig. [5.20]). Impact of Brownian motion on concentration is described in Fig. (5.21). The zig-zag collision of particles produces more resistance to motion of the particles. Heat is generated and consequently the concentration is decreased. Fig. (5.22) portrayed the behavior of Sc number on concentration field. Larger values of Sc decreases mass diffusivity. Thus concentration tends to decrease in both the cases $n < 1$ and $n > 1$.
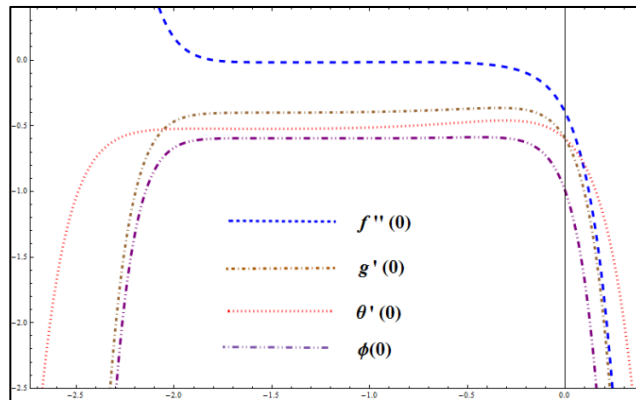
Fig. 5.2: $\hbar -$ curves.
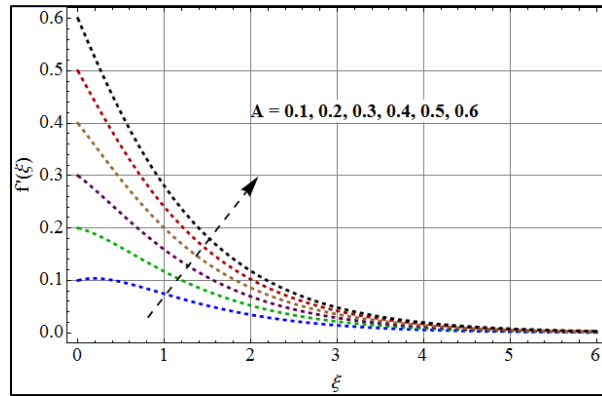
Fig. 5.5. $f(\xi)$ via A.
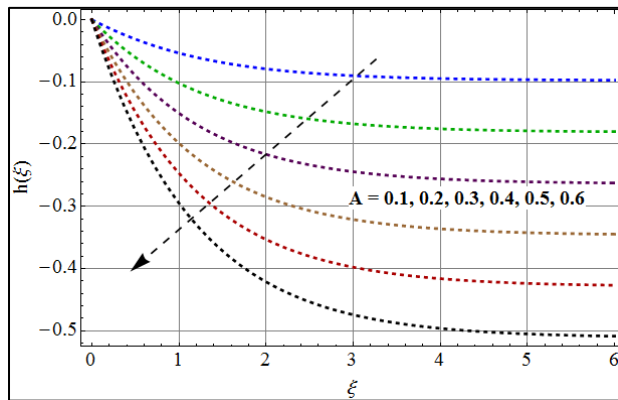
Fig. 5.4 $h(\xi)$ via A.
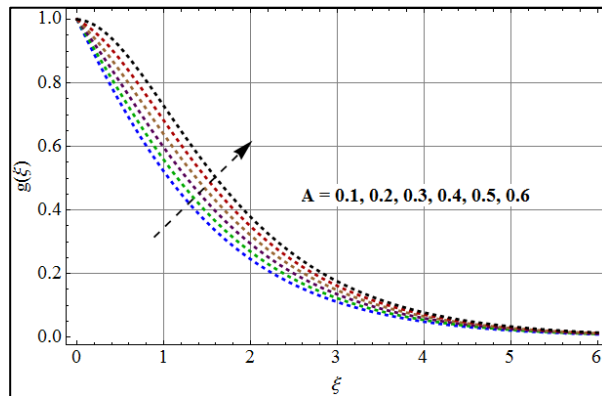
Fig. 5.5 $g(\xi)$ via A.
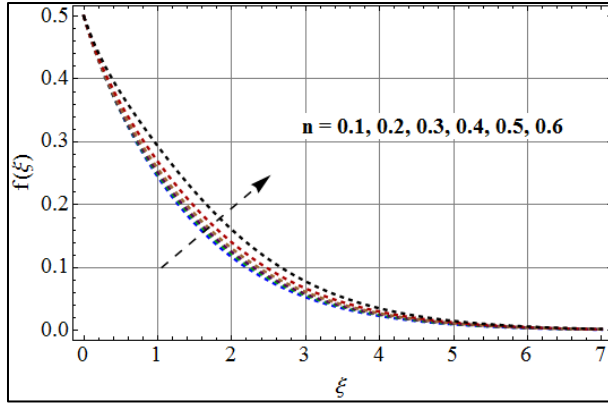
Fig. 5.6 $f(\xi)$ via n.
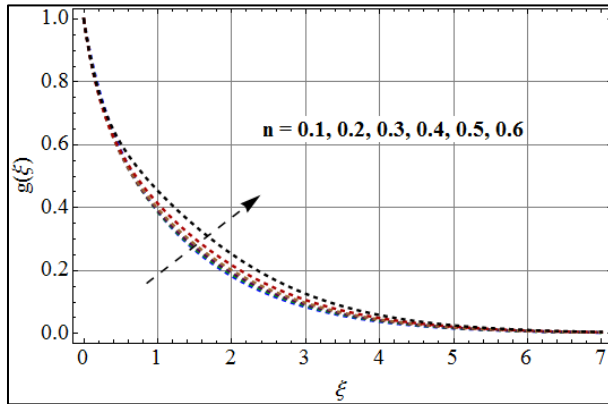
Fig. 5.7 $g(\xi)$ via n.
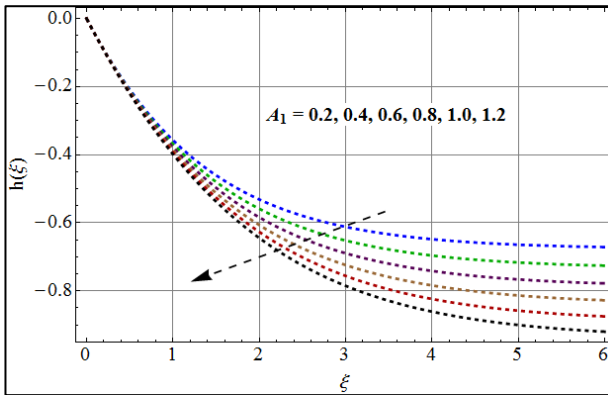
Fig. 5.8 $h(\xi)$ via A_1.
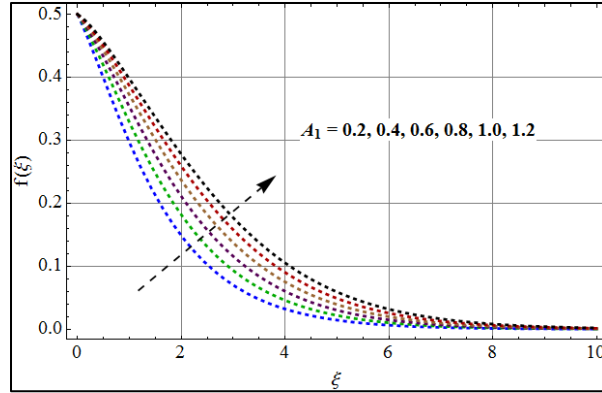
Fig. 5.9 $f(\xi)$ via A_1.
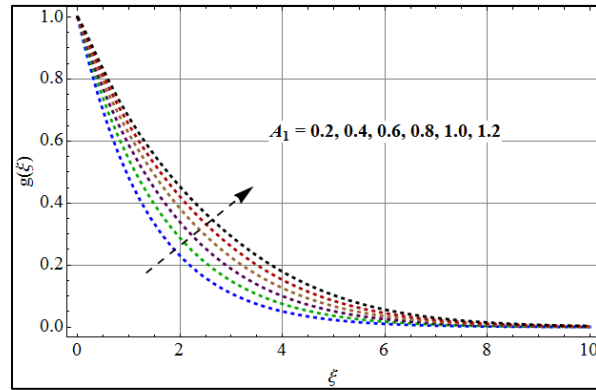
Fig. 5.10 $g(\xi)$ via A_1.
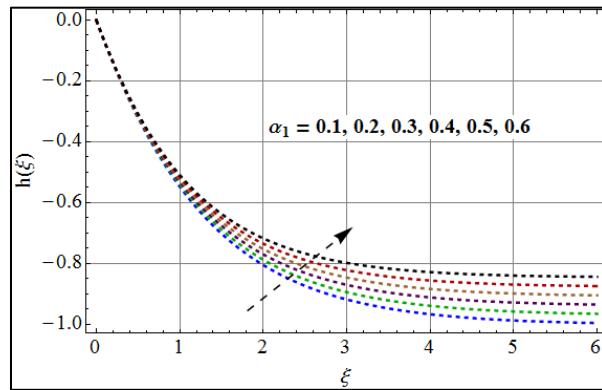
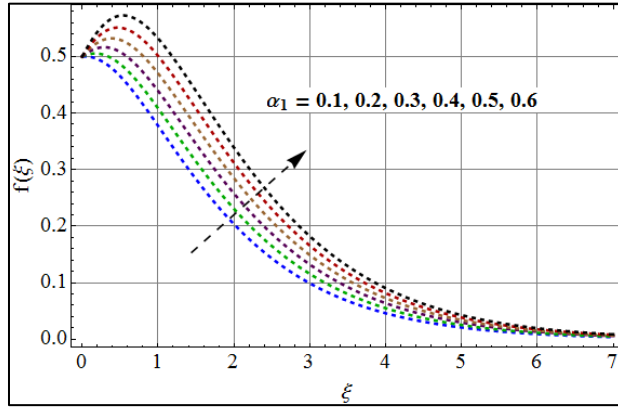Fig. 5.11 $h(\xi)$ via α_1.

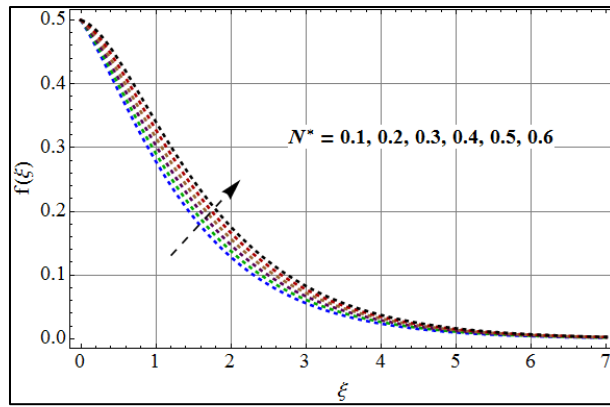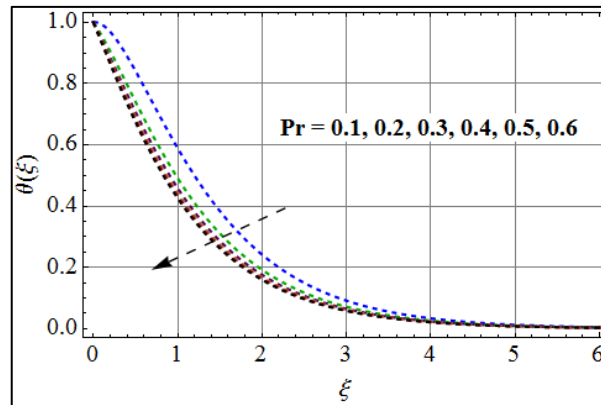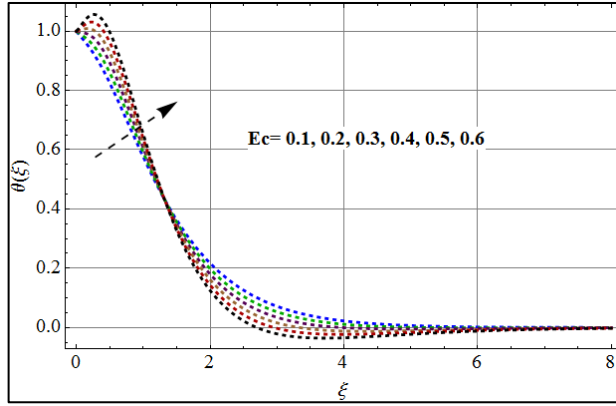Fig. 5.12 $f(\xi)$ via α_1.

Fig. 5.13 $f(\xi)$ via N^*.

Fig. 5.14 $\theta(\xi)$ via Pr.

Fig. 5.15 $\theta(\xi)$ via Ec.
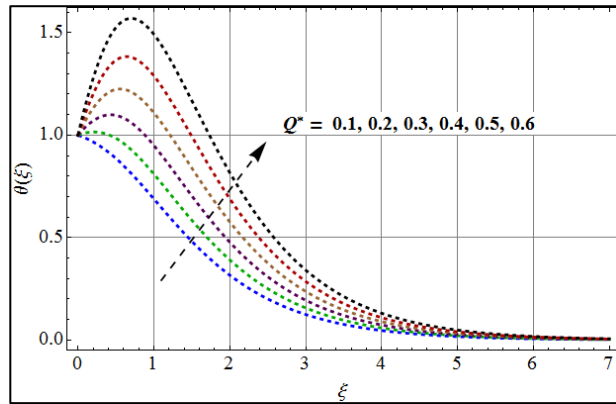
Fig. 5.16 $\theta(\xi)$ via Q^*.
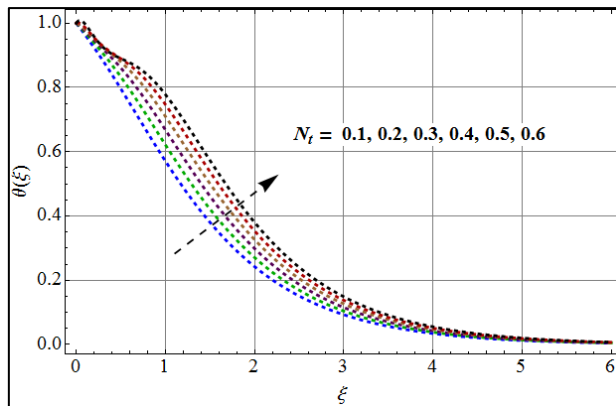
Fig. 5.17 $\theta(\xi)$ via N_t.
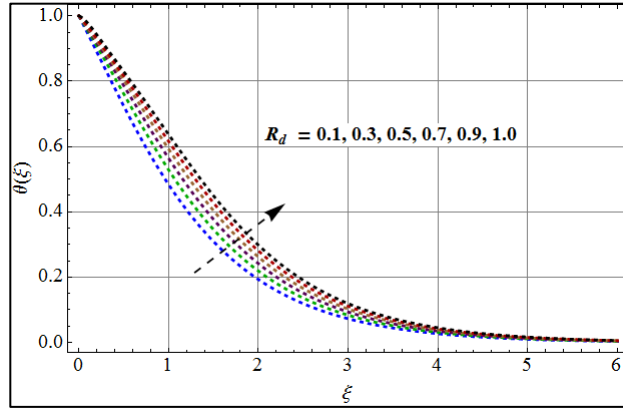
Fig. 5.18 $\theta(\xi)$ via R_d.
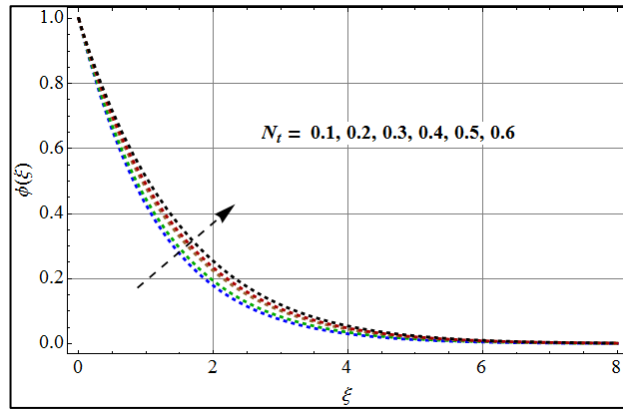
Fig. 5.19 $\phi(\xi)$ via N_t.
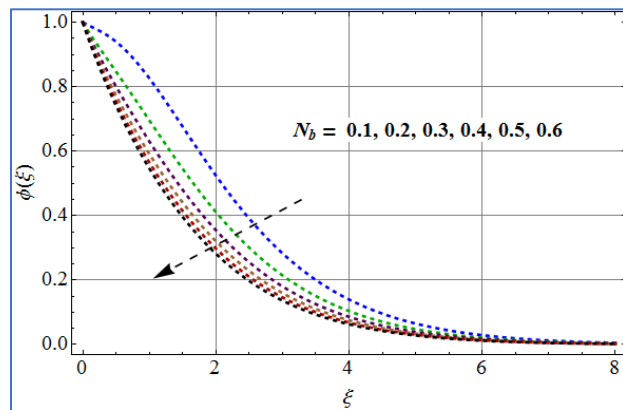
Fig. 5.20 $\phi(\xi)$ via N_b.
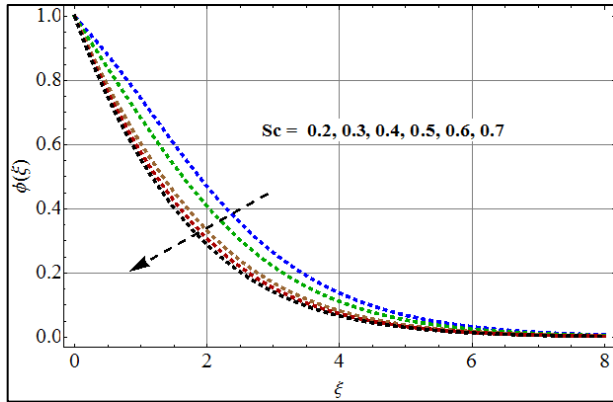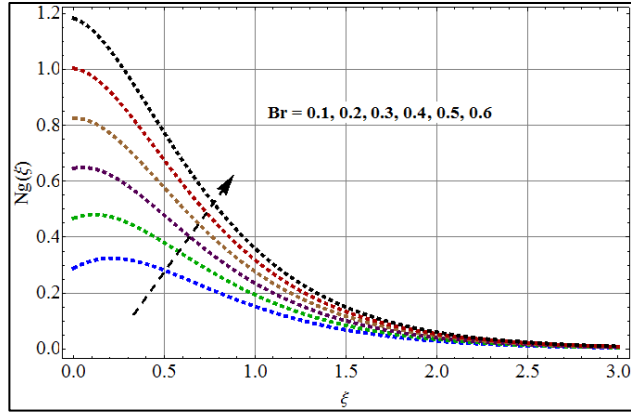
Fig. 5.21 $\phi\,(\xi)$ via Sc.
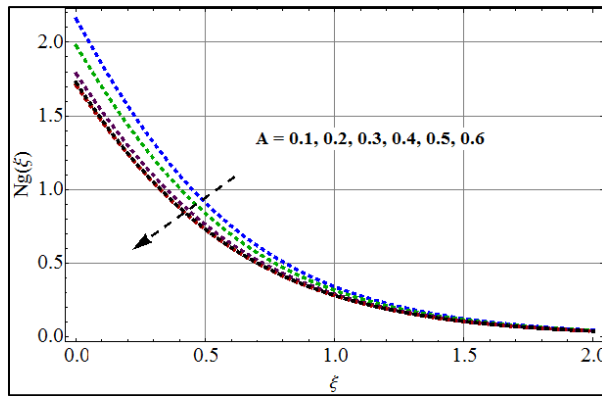
Fig. 5.22 $N_g(\xi)$ via A.
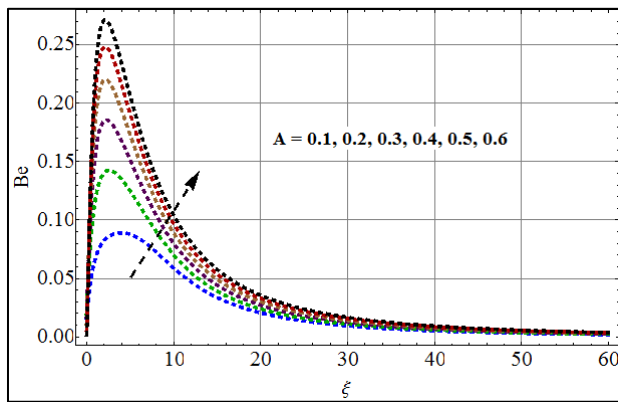
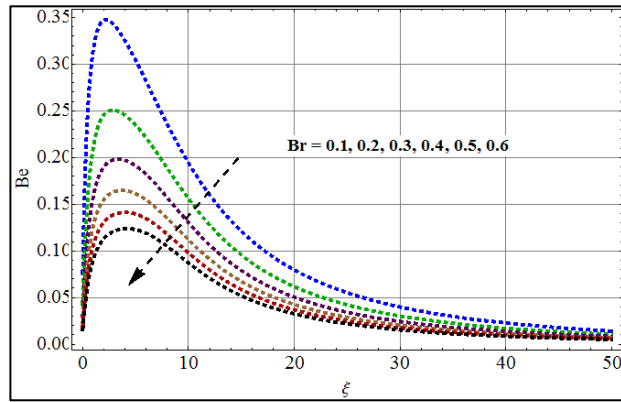Fig. 5.23 Be via A.

Fig. 5.24 $N_g(\xi)$ via Br.

Fig. 5.25 Be via Br.
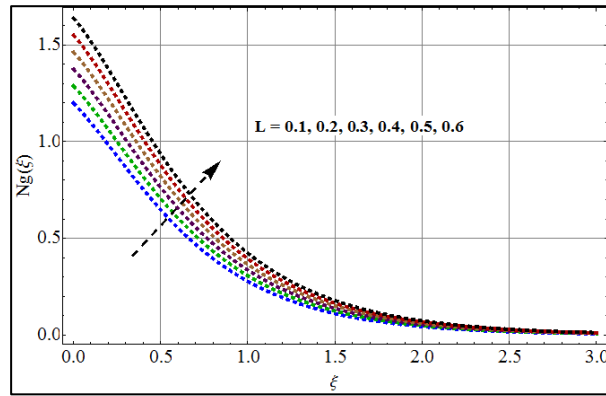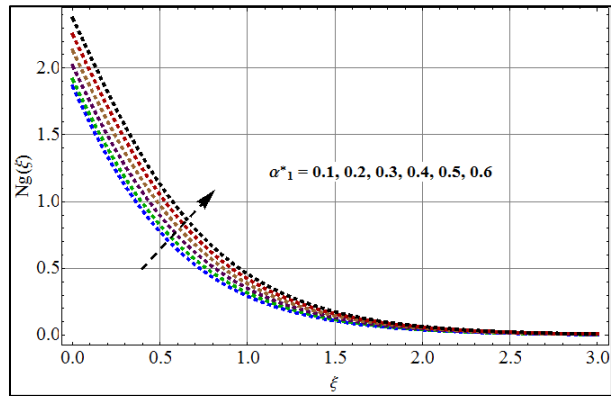

Fig. 5.26 $N_g(\xi)$ via L.
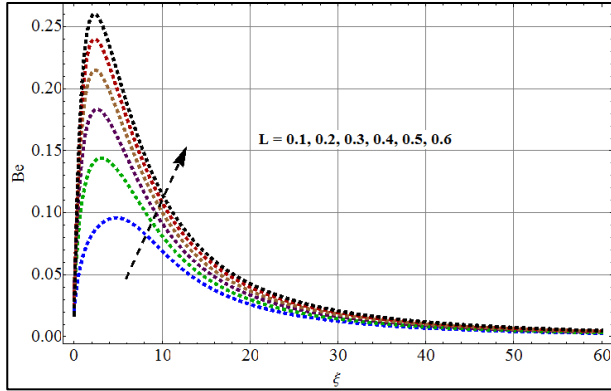
Fig. 5.27 *Be* via *L*.

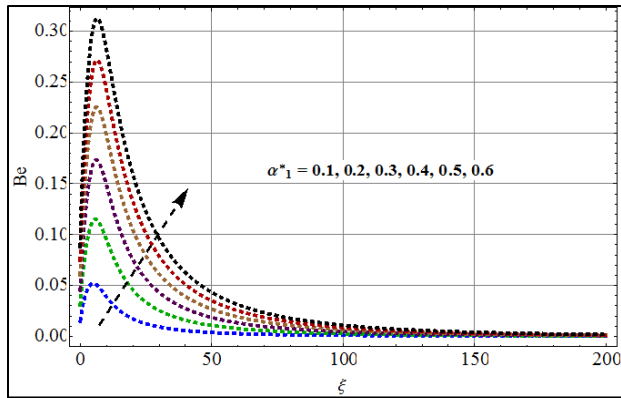Fig. 5.28 $N_g(\xi)$ via α_1^*.
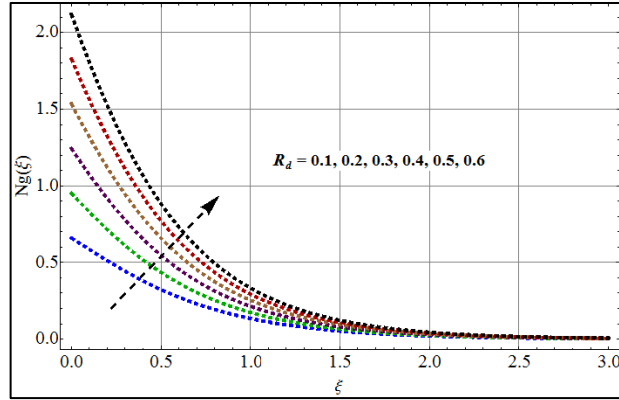

Fig. 5.29 *Be* via α_1^*.
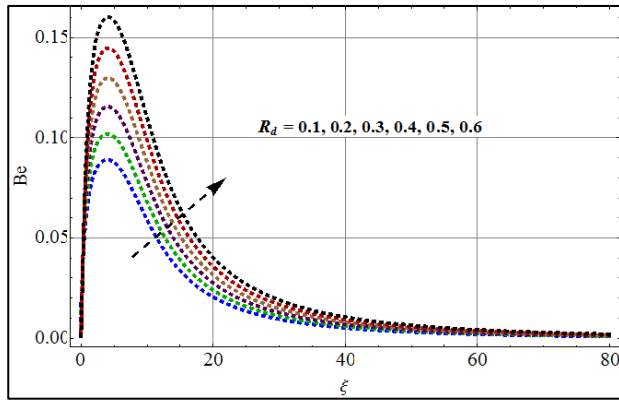
Fig. 5.30 $N_g(\xi)$ via R_d.

Fig. 5.31 Be via R_d.

8: Entropy generation and Bejan number (Be)

Our main aim here is to study entropy and Bejan number. Expression for irreversibilities is deliberated through entropy generation rate. The effects of various variables on entropy have been discussed here. Figs. $(5.22 - 5.31)$ are plotted to present the impacts of Brinkman number (Br), temperature ratio parameter α_1, diffusion parameter λ_1^*, radiation parameter R_d and Schmidt on entropy generation and Be number Fig. (5.22) portrays the behavior of fluid parameter on entropy generation rate $N_g(\xi)$. Higher fluid parameter A increases the shear rate which decreases motion of the fluid. Consequently less entropy is produced inside the system. But larger values of A, increases Bejan number near the disk by providing more thermal energy to the system due to higher viscous effects while decreasing trend is observed away from the disk in case of shear thickening fluids (see Fig. (5.23)). Figs. (5.24) and (5.25) portray the effects of Brinkman number on entropy generation rate $N_g(\xi)$ and Bejan number Be. For larger values of Br, entropy of the system

increases while decreasing behavior is noted for Bejan number. Since Br is the ratio of heat transfer due to conduction with the heat produced by viscous heating. Higher values of Br produces heat inside the system. Thus an increase in the disturbance of the whole system occurs for both $n < 1$ and $n > 1$. Reverse trend is seen for Be. Figs. (5.26) and (5.27) are sketched for impacts of diffusion parameter L on $N_g(\xi)$ and Bejan number. More disorderliness inside the system is observed due to diffusivity of the fluid. Thus more entropy is generated for diffusion parameter. Impact of thermal as well as fluid transfer irreversibilities are more dominant than viscous irreversibilities. That is why Bejan number shows increasing behavior. Effect of temperature ratio parameter α_1^* on $N_g(\xi)$ and Bejan number is designed via Figs. (5.28) and Fig. (5.29). Temperature difference always produces more disturbance inside the system, which results an enhancement in entropy. For higher α_1^*, the heat transfer irreversibilities are dominant than the fluid friction and viscous irrversibilities. That is the reason for Bejan number to increase. Increasing values of R_d provides more heat to system which increases heat transfer rate. So more entropy generation is shown. See Figs. (5.30) and (5.31).

Conclusions

Sisko fluid flow caused by a stretchable rotating disk along with entropy has been analyzed. Main results include the following points:

- Velocity is increased for larger values A and A_1.
- Higher estimations of N_t, Ec and Q^* enhance the temperature ditribution.
- Reverse trend on concentration is noted for N_t and N_b.
- Entropy increases for higher values of Br, α, R_d and diffusion parameter L while decreasing effect is seen for Sc.
- Entropy decreases in case of shear thinning fluids than for shear thickening fluids.
- Bejan number Be decreases for higher values of Br while increases for R_d.

Chapter 6

Rotating disk of nanofluid with entropy generation

Introduction

This chapter addresses magnetohydrodynamic viscous nano-fluid flow caused by a variable thicked rotatable disk. Entropy is determined in terms of velocity and temperature. Nanofluid properties are studied along with thermophoresis and Brownian motion. Conservation of energy comprises of dissipation, convective heat transport and Joule heating. Entropy generation is studied. Nonlinear stretching velocity of the disk causes the flow. Transformations lead to ordinary differential system. Total entropy generation rate is analyzed. Nonlinear computations have been carried out. Convergent series solutions are established. Radial, axial and tangential velocities are plotted and interpreted. Entropy equation for dissipation, Brownian diffusion and thermophoresis effects is examined. Velocity profile and temperature in dimensionless form are graphically shown and described in detail. Key outcomes are summed up in the conclusions.

Formulation

Consider steady mixed convective nanofluid flow caused by a rotating disk with variable surface thickness. Magnetic field of constant strength B_0 is exerted in $z -$ direction. Convective boundary conditions and Joule heating are studied. Additionally the impacts of mixed convection and viscous dissipation are examined. Disk at $z = a \left(\frac{r}{R_0} + 1 \right)^{-\varsigma}$ is stretched with stretching rate a (in radial direction) and angular speed Ω. The velocity components $(\hat{u}, \hat{v}, \hat{w})$ in the direction of (r, θ, z) are shown. Here $\hat{T}_f$ is the disk temperature while $\hat{T}_\infty$ being the ambient temperature. Geometry regarding the flow situation and coordinates are given in Fig. 6.1.
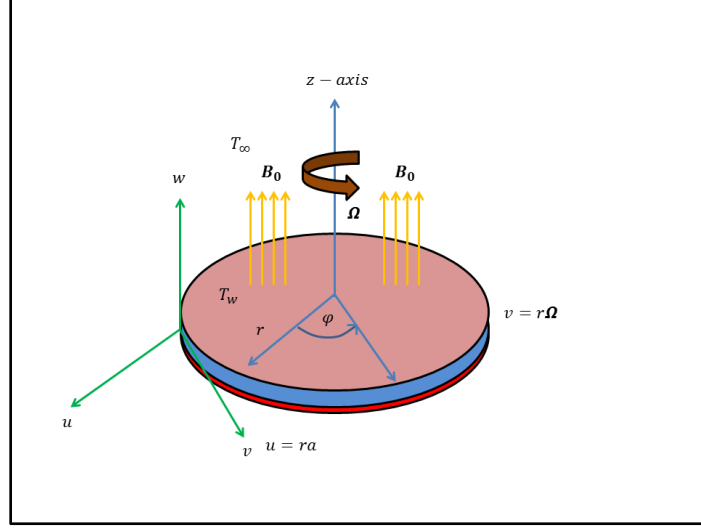
Fig 6.1 Geometry of flow problem

The equations and conditions relevant under consideration are

$$\frac{\partial \hat{u}}{\partial r} + \frac{\hat{u}}{r} + \frac{\partial \hat{w}}{\partial z} = 0,$$ (6.1)

$$\hat{u}\frac{\partial \hat{u}}{\partial r} + \hat{w}\frac{\partial \hat{u}}{\partial z} - \frac{\hat{v}^2}{r} = \nu\frac{\partial^2 \hat{u}}{\partial z^2} - \frac{\sigma_f}{\rho_f}B_0^2\hat{u} + g\beta(\hat{T} - \hat{T}_\infty),$$ (6.2)

$$\hat{u}\frac{\partial \hat{v}}{\partial r} + \hat{w}\frac{\partial \hat{v}}{\partial z} + \frac{\hat{u}\hat{v}}{r} = \nu\frac{\partial^2 \hat{v}}{\partial z^2} - \frac{\sigma_f}{\rho_f}B_0^2\hat{v},$$ (6.3)

$$(\rho c_p)_f \left(\hat{u}\frac{\partial \hat{T}}{\partial r} + \hat{w}\frac{\partial \hat{T}}{\partial z}\right)$$
$$= k_f\frac{\partial^2 \hat{T}}{\partial z^2} + (\rho c_p)_p\left[\frac{D_T}{T_\infty}\left(\frac{\partial \hat{T}}{\partial z}\right)^2 + D_B\left(\frac{\partial \hat{T}}{\partial z}\frac{\partial C}{\partial z}\right) + \sigma_f B_0^2(\hat{u}^2 + \hat{v}^2) + \mu_f\left(\frac{\partial \hat{u}}{\partial z}\right)^2\right],$$ (6.4)

$$\hat{u}\frac{\partial C}{\partial r} + \hat{w}\frac{\partial C}{\partial z} = \frac{D_T}{T_\infty}\frac{\partial^2 \hat{T}}{\partial z^2} + D_B\frac{\partial^2 C}{\partial z^2},$$ (6.5)

$$\left.\begin{array}{l}\hat{u} = ra, \hat{v} = r\Omega, \hat{w} = 0, -k\frac{\partial \hat{T}}{\partial z} = h_1(\hat{T}_f - \hat{T}), -D_m\frac{\partial C}{\partial z} = h_2(C_f - C) \text{ at } z = a\left(\frac{r}{R_0} + 1\right)^{-\varsigma}, \\ \hat{u} = 0, \hat{v} = 0, \hat{T} = \hat{T}_\infty, C = C_\infty \text{ when } z \to \infty,\end{array}\right\}$$ (6.6)

where $\hat{T}$ denotes fluid temperature, $\sigma°$ Stefan-Boltzman constant, $k°$ mean absorption coefficient, a dimensional constant, η scaled boundary layer coordinate, dynamic viscosity μ_f, density ρ_f, thermal conductivity k_f, kinematic viscosity ν_f, electrical conductivity σ_f and heat capacitance

c_{p_f}.

We consider

$$\hat{u} = r^* R_0 \Omega \tilde{F}(\eta), \hat{v} = r^* R_0 \Omega \tilde{G}(\eta), \hat{w} = R_0 \Omega (1 + r^*)^{-\varsigma} \left(\frac{\Omega R_0^2 \rho_f}{\mu_f}\right)^{\frac{-1}{n+1}} \tilde{H}(\eta), \Bigg\}$$

$$\tilde{\vartheta} = \frac{\hat{T} - \hat{T}_\infty}{\hat{T}_f - \hat{T}_\infty}, \Phi = \frac{C - C_\infty}{C_f - C_\infty}, \eta = \frac{z}{R_0}(1 + r^*)^{\varsigma} \left(\frac{\Omega R_0^2 \rho_f}{\mu_f}\right)^{\frac{1}{n+1}}, \Bigg\} \quad (6.7)$$

where R_0 represents the radius, ς thickness index, n the power law index, F the radial component of velocity, G the tangential component, H the axial component and r^* the nondimensional radius constant.

Using appropriate transformations, the Eqs. $(6.1 - 6.7)$ become

$$2\tilde{F} + \tilde{H}' + \eta \varepsilon \varsigma \tilde{F}' = 0, \quad (6.8)$$

$$(Re)^{\frac{1-n}{1+n}} (1 + r^*)^{2\varsigma} \tilde{F}'' - \tilde{F}^2 + \tilde{G}^2 - \tilde{H}\tilde{F}' - \tilde{F}\tilde{F}'\varsigma\eta\varepsilon$$
$$-Ha\tilde{F} + \lambda\tilde{\vartheta} = 0,\Big) \quad (6.9)$$

$$(Re)^{\frac{1-n}{1+n}} (1 + r^*)^{2\varsigma} \tilde{G}'' - 2\tilde{F}\tilde{G} - \tilde{H}\tilde{G}' - \tilde{F}\tilde{G}'\varsigma\eta\varepsilon - Ha\tilde{G} = 0, \quad (6.10)$$

$$\frac{1}{Pr\,Re^{\frac{1-n}{1+n}*2\varsigma}}$$
$$N_T (Re)^{\frac{1-n}{1+n}} (1 + r^*)^{2\varsigma} \tilde{\vartheta}'^2 + N_B (Re)^{\frac{1-n}{1+n}} \tilde{\vartheta}'\Phi' \Bigg\}$$
$$+HaEc(\tilde{F}^2 + \tilde{G}^2) + Ec(Re)^{\frac{1-n}{1+n}} (1 + r^*)^{\varsigma} \tilde{F}'^2 = 0\Big), \Bigg\} \quad (6.11)$$

$$\frac{N_T}{N_B}(Re)^{\frac{1-n}{1+n}} (1 + r^*)^{2\varsigma} \tilde{\vartheta}'' + (Re)^{\frac{1-n}{1+n}} (1 + r^*)^{2\varsigma} \Phi'' - Sc\varsigma\eta\varepsilon\tilde{F}\tilde{\vartheta}' - Sc\tilde{H}\Phi' = 0, \quad (6.12)$$

$$\tilde{H}(\alpha) = 0, \tilde{F}(\alpha) = A, \tilde{G}(\alpha) = 1,$$
$$\tilde{\vartheta}'(\alpha) = -r_1(1 - \tilde{\vartheta}(\alpha)), \Phi'(\alpha) = -r_1(1 - \Phi(\alpha)) \Bigg\} \quad (6.13)$$
$$\tilde{F}(\infty) = 0, \Phi(\infty) = 0, \tilde{G}(\infty) = 0, \tilde{\vartheta}(\infty) = 0.$$

Considering,

$$\left.\begin{array}{l}\tilde{H}(\eta) = \tilde{h}(\eta - \alpha) = \tilde{h}(\xi),\\ \tilde{F}(\eta) = \tilde{f}(\eta - \alpha) = \tilde{f}(\xi),\\ \tilde{G}(\eta) = \tilde{g}(\eta - \alpha) = \tilde{g}(\xi),\\ \tilde{\vartheta}(\eta) = \tilde{\theta}(\eta - \alpha) = \tilde{\theta}(\xi),\\ \Phi(\eta) = \Phi(\eta - \alpha) = {}_{\phi}(\xi),\end{array}\right\} \tag{6.14}$$

we obtain

$$2\tilde{f} + \tilde{h}' + (\xi + \alpha)\varepsilon\varsigma\tilde{f}' = 0, \tag{6.15}$$

$$\tilde{f}''(Re)^{\frac{1-n}{1+n}}(1 + r^*)^{2\varsigma} - \tilde{f}^2 + \tilde{g}^2 - \tilde{h}\tilde{f}' - \tilde{f}\tilde{f}'\varsigma(\xi + \alpha)\varepsilon \tag{6.16}$$
$$-Ha\tilde{f} + \lambda\tilde{\theta} = 0,\big)$$

$$\tilde{g}''(Re)^{\frac{1-n}{1+n}}(1 + r^*)^{2\varsigma} - 2\tilde{f}\tilde{g} - \tilde{h}\tilde{g}' - \tilde{f}\tilde{g}'\varsigma(\xi + \alpha)\varepsilon - Ha\tilde{g} = 0, \tag{6.17}$$

$$\left.\begin{array}{l}\dfrac{1}{Pr\,Re)^{\frac{1-n}{1+n}*2\varsigma}}\\ N_T(Re)^{\frac{1-n}{1+n}}(1 + r^*)^{2\varsigma}\tilde{\theta}'^2 + N_B(Re)^{\frac{1-n}{1+n}}\tilde{\theta}'{}_{\phi}'\\ +HaEc(\tilde{f}^2 + \tilde{g}^2) + Ec(Re)^{\frac{1-n}{1+n}}(1 + r^*)^{\varsigma}\tilde{f}'^2 = 0,\end{array}\right\} \tag{6.18}$$

$$\frac{N_T}{N_B}(Re)^{\frac{1-n}{1+n}}(1 + r^*)^{2\varsigma}\tilde{\vartheta}'' + (Re)^{\frac{1-n}{1+n}}(1 + r^*)^{2\varsigma}{}_{\phi}'' - Sc\varsigma\eta\varepsilon - Sc\tilde{h}{}_{\phi}' = 0, \tag{6.19}$$

$$\left.\begin{array}{l}\tilde{h}(0) = 0, \tilde{f}(0) = A, \tilde{f}(\infty) = 0, \tilde{g}(0) = 1,\\ \tilde{\theta}'(0) = -r_1(1 - \tilde{\theta}(0)), {}_{\phi}'(0) = -r_2(1 - {}_{\phi}(0))\\ \tilde{g}(\infty) = 0, \tilde{\theta}(0) = 1, \tilde{\theta}(\infty) = 0,\end{array}\right\} \tag{6.20}$$

$$\left.\begin{array}{l}Re = \dfrac{\Omega R_0^2}{\nu_f}, Ha = \dfrac{\sigma_f B_0^2}{\rho_f \Omega}, Pr = \dfrac{(\rho c_p)_f \nu_f}{k_f}, A = \dfrac{a}{\Omega},\\ \varepsilon = \dfrac{r^*}{1 + r^*}, \tau = \dfrac{(\rho c_p)_p}{(\rho c_p)_f}, N_T = \dfrac{\tau D_T(\hat{T}_f - \hat{T}_\infty)}{\nu_f \hat{T}_\infty}, N_B = \dfrac{\tau D_B(C_f - C_\infty)}{\nu_f},\\ Ec = \dfrac{r^2 \Omega^2}{c_p(\hat{T}_f - \hat{T}_\infty)}, \lambda = \dfrac{g\beta_f(\hat{T}_f - \hat{T}_\infty)}{r\Omega^2}, \alpha = \dfrac{a}{R_0^2}\left(\dfrac{\Omega R_0^2 \rho_f}{\mu_f}\right)^{\frac{-1}{n+1}},\end{array}\right\} \tag{6.21}$$

where Re is the Reynold number, Ha magnetic parameter, Pr the Prandtl number, A the ratio of

velocity to stretching parameter, ε the nondimensional constant, τ the ratio of specific heats, N_T, thermophoresis, N_B Brownian motion, Ec the Eckert number, λ the mixed convection and α the thickness coefficient.

Quantities of interest

Surface drag force

Mathematically surface drag force is

$$C_f = \frac{\sqrt{\tau_{zr}^2 + \tau_{z\theta}^2}}{\rho_f(\Omega r)^2},$$

(6.22)

where τ_{zr} and $\tau_{z\theta}$ are shear stresses in radial and tangential directions respectively. We have

$$\tau_{zr} = \mu_{nf}\frac{\partial \hat{u}}{\partial z}\bigg|_{z=0} = \mu_f r^* \Omega_1 (1+r^*)^\varsigma \left(\frac{\Omega R_0^2 \rho_f}{\mu_f}\right)^{\frac{1}{n+1}} \tilde{f}'(0),$$

(6.23)

$$\tau_{z\theta} = \mu_{nf}\frac{\partial \hat{v}}{\partial z}\bigg|_{z=0} = \mu_f r^* \Omega_1 (1+r^*)^\varsigma \left(\frac{\Omega R_0^2 \rho_f}{\mu_f}\right)^{\frac{1}{n+1}} \tilde{g}'(0).$$

(6.24)

Total shear stress τ_w is defined as

$$\tau_w = \sqrt{\tau_{zr}^2 + \tau_{z\theta}^2}.$$

(6.25)

Equations $(22) - (25)$ imply that

$$C_{fx} Re^{\frac{n-1}{n+1}} = \frac{\tau_w|_{z=0}}{\rho_f(r\Omega)^2} = \frac{1}{r^*}(1+r^*)^\varsigma[(\tilde{f}'(0))^2 + (\tilde{g}'(0))^2]^{1/2}.$$

(6.26)

Heat transfer rate

Mathematically the rate of heat transfer is

$$Nu_x = \frac{R_0 q_w}{k_f(\hat{T}_f - \hat{T}_\infty)}\bigg|_{z=0},$$

(6.27)

in which wall heat flux q_w satisfies

$$q_w|_{z=0} = -k_f\frac{\partial \hat{T}}{\partial z}\bigg|_{z=0} = -k_f(\hat{T}_f - \hat{T}_\infty)(1+r^*)^\varsigma \left(\frac{\Omega R_0^2 \rho}{\mu}\right)^{\frac{1}{n+1}} \tilde{\theta}'(0).$$

(6.28)

Using Eq. (6.28) in Eq. (6.27) we have the following form

$$Nu_x Re^{\frac{-1}{n+1}} = -(1+r^*)^\varsigma \tilde{\theta}'(0).$$

(6.29)

Local Sherwood number satisfies

$$Sh_x = \frac{R_0 q_m}{D_B(C_f - C_\infty)}\bigg|_{z=0},$$

(6.30)

where q_m denotes the mass flux and

$$Sh_x \, Re^{\frac{-1}{n+1}} = -(1 + r^*)^\varsigma \phi'(0).$$

(6.31)

Entropy generation

Dimensional expression for entropy generation rate in terms of velocity, temperature and concentration is

$$S_G = \frac{k_f}{\hat{T}_f^2}\left(\frac{\partial \hat{T}}{\partial z}\right)^2 + \frac{\mu_{nf}}{\hat{T}_f}\Phi^* + \frac{RD_B}{C_f}(\nabla C)^2 + \frac{RD_B}{C_f}\left(\nabla C \cdot \nabla \hat{T}\right) + \frac{\sigma_f}{\hat{T}_f}B_0^2(\hat{u}^2 + \hat{v}^2),$$

(6.32)

where

$$\Phi = 2\left[\left(\frac{\partial \hat{u}}{\partial r}\right)^2 + \left(\frac{\partial \hat{w}}{\partial z}\right)^2 + \frac{1}{r^2}\left(\frac{\partial \hat{v}}{\partial \theta} + \hat{u}\right)^2\right] + \left[\frac{1}{r}\frac{\partial \hat{w}}{\partial \theta} + \frac{\partial \hat{v}}{\partial z}\right]^2 \\ + \left[\frac{\partial \hat{w}}{\partial r} + \frac{\partial \hat{u}}{\partial z}\right]^2 + \left[r\frac{\partial}{\partial r}\left(\frac{\hat{v}}{r}\right) + \frac{1}{r}\frac{\partial \hat{u}}{\partial \theta}\right]^2,$$

(6.33)

$$(\nabla C)^2 = \left(\frac{\partial C}{\partial r}, \frac{1}{r}\frac{\partial C}{\partial \theta}, \frac{\partial C}{\partial z}\right) \cdot \left(\frac{\partial C}{\partial r}, \frac{1}{r}\frac{\partial C}{\partial \theta}, \frac{\partial C}{\partial z}\right) \\ \nabla C \cdot \nabla \hat{T} = \left(\frac{\partial C}{\partial r}, \frac{1}{r}\frac{\partial C}{\partial \theta}, \frac{\partial C}{\partial z}\right) \cdot \left(\frac{\partial C}{\partial r}, \frac{1}{r}\frac{\partial C}{\partial \theta}, \frac{\partial C}{\partial z}\right).$$

(6.34)

In view of boundary layer assumptions, we can write

$$S_G = \underbrace{\frac{k_f}{\hat{T}_f^2}\left(\frac{\partial \hat{T}}{\partial z}\right)^2}_{\text{Thermal irreversibility}} + \underbrace{\frac{\mu_f}{\hat{T}_f}\left[\begin{array}{c} 2\left(\frac{\partial \hat{u}}{\partial r}\right)^2 + \frac{2}{r^2}(\hat{u})^2 + 2\left(\frac{\partial \hat{w}}{\partial z}\right)^2 \\ + \left[\frac{\partial \hat{v}}{\partial z}\right]^2 + \left[\frac{\partial \hat{u}}{\partial z}\right]^2 + \left[r\frac{\partial}{\partial r}\left(\frac{\hat{v}}{r}\right)\right]^2 \end{array}\right]}_{\text{Fluid friction irreversibility}} \\ \frac{RD_B}{C_f}\left(\left(\frac{\partial C}{\partial r}\right)^2 + \left(\frac{\partial C}{\partial z}\right)^2\right) + \frac{RD_B}{C_f}\left(\frac{\partial C}{\partial r}\frac{\partial \hat{T}}{\partial r} + \frac{\partial C}{\partial z}\frac{\partial \hat{T}}{\partial z}\right) \\ + \underbrace{\frac{\sigma_f}{\hat{T}_f}B_0^2(\hat{u}^2 + \hat{v}^2)}_{\text{Joule dissipation irreversibility}},$$

(6.35)

Dimensionless form of N_G is given as

$$
\left.
\begin{aligned}
N_G &= \tilde{\theta}'^2 \alpha_1 (Re)^{\frac{1-n}{1+n}} (1+r^*)^{2\varsigma} \\
&+ \frac{Br}{Re\left[\begin{array}{c} 2(\xi+\alpha)^2 \varepsilon^2 \varsigma^2 \tilde{f}'^2 + 4\tilde{f}^2 + 4\tilde{f}\tilde{f}'(\xi+\alpha)\varepsilon\varsigma \\ +2\tilde{h}'^2 + r^{*2}(Re)^{\frac{2}{1+n}}(1+r^*)^{2\varsigma}\tilde{g}'^2 + \\ r^{*2}(Re)^{\frac{2}{1+n}}(1+r^*)^{2\varsigma}\tilde{f}'^2 + (\xi+\alpha)^2\varepsilon^2\varsigma^2\tilde{g}'^2 \end{array}\right]} \\
&+ HaBrr^{*2}(\tilde{f}^2 + \tilde{g}^2) + \frac{\beta_1\alpha_2}{\alpha_1}\left((Re)^{\frac{1-n}{1+n}}(1+r^*)^{2\varsigma} + \frac{1}{Re}(\xi+\alpha)^2\varepsilon^2\varsigma^2\left(\alpha_1\tilde{\theta}'^2 + \alpha_2\phi'^2\right)\right)
\end{aligned}
\right\} \tag{6.36}
$$

$$
\left.
\begin{aligned}
\alpha_1 &= \frac{\hat{T}_f - \hat{T}_\infty}{\hat{T}_f} = \frac{\Delta T}{\hat{T}_f}, \alpha_2 = \frac{C_f - C_\infty}{C_f} \\
Br &= \frac{\mu_f \Omega^2 R_0^2}{k_f \Delta T}, N_G = \frac{\hat{T}_f S_G \nu_f}{k_f \Delta T \Omega}.
\end{aligned}
\right\} \tag{6.37}
$$

Here α_1 and α_2 are the dimensionless temperature difference and concentration parameters, Br Brinkman number and $N_G \left(= \frac{\hat{T}_f S_G \nu}{k_f \Delta T \Omega}\right)$ entropy generation rate.

Thermal irreversibility dominates when $Be \geq 0.6$. When $Be \leq 0.5$ the viscous effects dominate. For $Be = 0.5$ have equal effects. Similarly Bejan number (Be) is

$$
Be = \frac{Entropy\ generation\ due\ to\ heat\ transfer}{Total\ entropy\ generation}, \tag{6.38}
$$

$$
Be = \frac{\tilde{\theta}'^2 \alpha_1 (Re)^{\frac{1-n}{1+n}}(1+r^*)^{2\varsigma}}{\begin{array}{c} \tilde{\theta}'^2 \alpha_1 (Re)^{\frac{1-n}{1+n}}(1+r^*)^{2\varsigma} \\ + \frac{Br}{Re\left[\begin{array}{c} 2(\xi+\alpha)^2\varepsilon^2\varsigma^2\tilde{f}'^2 + 4\tilde{f}^2 + 4\tilde{f}\tilde{f}'(\xi+\alpha)\varepsilon\varsigma \\ +2\tilde{h}'^2 + r^{*2}(Re)^{\frac{2}{1+n}}(1+r^*)^{2\varsigma}\tilde{g}'^2 + \\ r^{*2}(Re)^{\frac{2}{1+n}}(1+r^*)^{2\varsigma}\tilde{f}'^2 + (\xi+\alpha)^2\varepsilon^2\varsigma^2\tilde{g}'^2 \end{array}\right]} \\ + HaBrr^{*2}(\tilde{f}^2+\tilde{g}^2) + \frac{\beta_1\alpha_2}{\alpha_1}\left((Re)^{\frac{1-n}{1+n}}(1+r^*)^{2\varsigma} + \frac{1}{Re}(\xi+\alpha)^2\varsigma^2\left(\alpha_1\tilde{\theta}'^2 + \alpha_2\phi'^2\right)\right) \end{array}}. \tag{6.39}
$$

Homotopy procedure

Initial guesses and corresponding linear operators are

$$
\tilde{h}_0(\xi) = 0, \tag{6.40}
$$

$$
\tilde{f}_0(\xi) = A\,exp(-\xi), \tag{6.41}
$$

$$\tilde{g}_0(\xi) = exp(-\xi), \tag{6.42}$$

$$\tilde{\theta}_0(\xi) = exp(-\xi), \tag{6.43}$$

$$\tilde{\phi}_0(\xi) = exp(-\xi), \tag{6.44}$$

$$L_{\tilde{h}} = \tilde{h}', L_{\tilde{f}} = \tilde{f}'' - \tilde{f}, L_{\tilde{g}} = \tilde{g}'' - \tilde{g}, L_{\tilde{\theta}} = \tilde{\theta}'' - \tilde{\theta}, L_{\phi} = \phi'' - \phi, \tag{6.45}$$

with

$$\left.\begin{array}{c} L_{\tilde{h}}[c_1] = 0, \\ L_{\tilde{f}}\left[c_2 e^{\xi} + c_3 e^{-\xi}\right] = 0, \\ L_{\tilde{g}}\left[c_4 e^{\xi} + c_5 e^{-\xi}\right] = 0, \\ L_{\tilde{\theta}}\left[c_6 e^{\xi} + c_7 e^{-\xi}\right] = 0, \\ L_{\phi}\left[c_8 e^{\xi} + c_9 e^{-\xi}\right] = 0, \end{array}\right\} \tag{6.46}$$

In which c_i $(i = 1 - 9)$ denote the constants.

Convergence analysis

Auxiliary variables $\hbar_{\tilde{h}}$, $\hbar_{\tilde{f}}$, $\hbar_{\tilde{g}}$, $\hbar_{\tilde{\theta}}$ and $\hbar_{\phi}$ give us the favor to control the convergence of given nonlinear problems. Fig. 2 shows the $\hbar$ -curves for velocity, temperature and concentration. Permissible ranges of auxiliary variables are $-1.6 \leq \hbar_{\tilde{h}} \leq -0.2$, $-1.5 \leq \hbar_{\tilde{f}} \leq -0.3$, $-1.6 \leq \hbar_{\tilde{g}} \leq -0.3$, $-4.0 \leq \hbar_{\tilde{\theta}} \leq -0.5$ and $-1.6 \leq \hbar_{\phi} \leq -0.6$. Table 6.1 indicates series solutions convergence of momentum as well as energy constraints for the given problem. Table 6.1 indicates that $\tilde{h}'(0)$, $\tilde{f}'(0)$, $\tilde{g}'(0)$, $\tilde{\theta}'(0)$ and $\phi'(0)$ converge at 11th, 15th, 19th, 25th and 20th orders respectively.
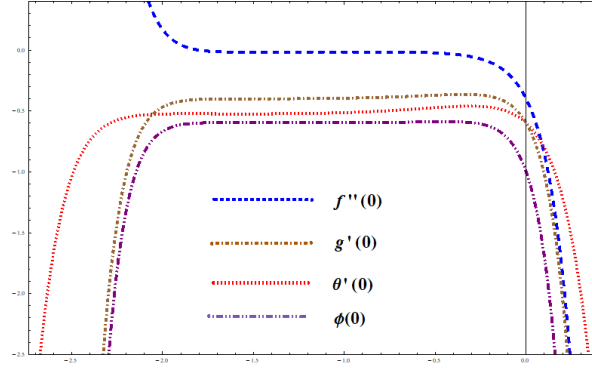
Fig 6.2 $\hbar - curves$

Table 6.1: Different order approximations for $\varsigma = 1$, $\varepsilon = 0.3$, $\alpha = 1.2$, $Re = 0.9$, $n = 0.5$, $r^* = 0.2$, $Ha = 0.7$, $A = 0.3$, $Pr = 1.9$, $Ec = 0.5$, and $\lambda = 0.4$

Order of approximations	$-\tilde{h}''(0)$	$\tilde{f}'(0)$	$-\tilde{g}'(0)$	$-\tilde{\theta}'(0)$	$-\phi'(0)$
1	0.009994	0.1610	0.8197	0.8295	1.55556
11	0.02034	0.2859	0.7965	0.5038	1.26243
15	0.02034	0.2857	0.7957	0.5233	1.25899
19	0.02034	0.2857	0.7980	0.5341	1.25894
25	0.02034	0.2857	0.7980	0.5350	1.25894
30	0.02034	0.2857	0.7980	0.5350	1.25894
35	0.02034	0.2857	0.7980	0.5350	1.25894
40	0.02034	0.2857	0.7980	0.5350	1.25894
50	0.02034	0.2857	0.7980	0.5350	1.25894

Discussion

Influence of various flow variables of rotating disk are displayed graphically. Figs. $(6.3 - 6.20)$ are sketched for results of different velocity components, temperature $\tilde{\theta}(\xi)$, skin friction $\left(C_{fx}Re^{\frac{n-1}{n+1}}\right)$ and Nusselt number $\left(Nu_xRe^{\frac{-1}{n+1}}\right)$. Figs. $(6.3a - 6.3c)$ display the physical characteristics of velocities $(\tilde{h}(\xi), \tilde{f}(\xi), \tilde{g}(\xi))$ for increasing magnetic parameter Ha. Since Hartman number mainly rely on Lorentz force, therefore an increase in Ha provides more Lorentz force which provides resistance which reduces the velocity. Impact of power law index n on

velocities $(\tilde{h}(\xi),\ \tilde{f}(\xi),\ \tilde{g}(\xi))$ is demonstrated in Figs. $(6.4a-6.4c)$. It is apparent from graphs that movement for liquid particles increases for larger n. Larger n decreases the viscosity of fluid and consequently the velocity of fluid is enhanced. Figs. $(6.5a-6.5c)$ clarify the impact of A on different components of velocity $(\tilde{h}(\xi),\ \tilde{f}(\xi),\ \tilde{g}(\xi))$. Here axial $(\tilde{h}(\xi))$ and radial $(\tilde{f}(\xi))$ components are larger for higher A. It is due to more stretching rate. Impacts regarding mixed convection parameter λ on velocity components are displayed by Figs. $(6.6a-6.6c)$. Magnitudes of axial and radial velocities are enhanced for larger λ while converse is observed for tangential component. For increasing values of λ the higher buoyancy force results an enhancement in axial and radial components of velocity. (see Figs. $6.6a$ and $6.6b$).

Magnetic parameter Ha influence on temperature $\tilde{\theta}(\xi)$ is indicated in Fig. 6.7. Here temperature enhances for larger Ha. Higher Lorentz force enhances the temperature. Figs. 8 discloses the effect of mixed convection λ on temperature distribution. Mixed convection λ is in direct relation to temperature field. Fig. 6.9 displayed the graph of temperature $\tilde{\theta}(\xi)$ for Eckert number Ec. Temperature curves enhances with higher Ec. Effect of Sc on concentration field is sketched in Fig. 6.10. Increasing values of Sc decreases concentration. Fig. 6.11 and 6.13 illustrate the impacts of N_T and N_B on temperature. Both Figs. show increasing behaviors due to more boundary layer thickness. Similarly Figs. 6.12 and 6. 14 are drawn to show the impacts of N_T and N_B on concentration. Fig. 6.12 illustrates that concentration increase for larger N_T. However it decays with Brownian motion parameter N_B.

Drag forces concerning Ha and λ parameters are observed via Figs. 6.15 and 6.16. Enhancement of surface drag force for larger Ha, and λ is observed. Figs. $(6.17-6.20)$ are displayed for impact of Eckert number Ec, magnetic parameter Ha, N_T and N_B on Nusselt number. Heat transfer decays for higher Ec, Ha, N_T and N_B.
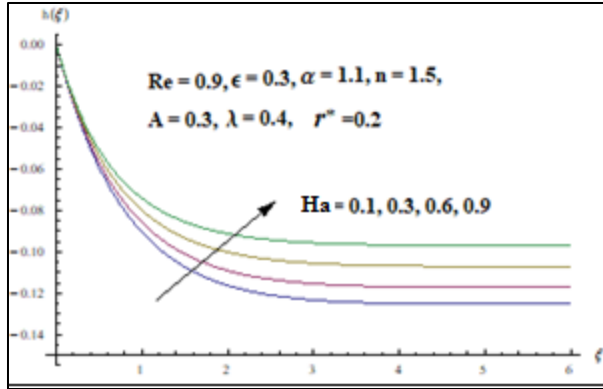
Fig. 6.3a: h(ξ) via Ha.
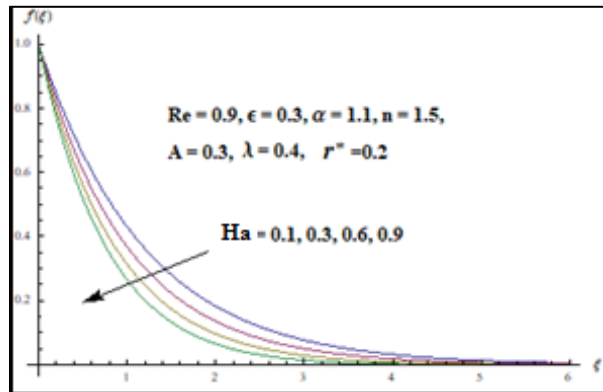
Fig. 6.3b: f(ξ) via Ha.
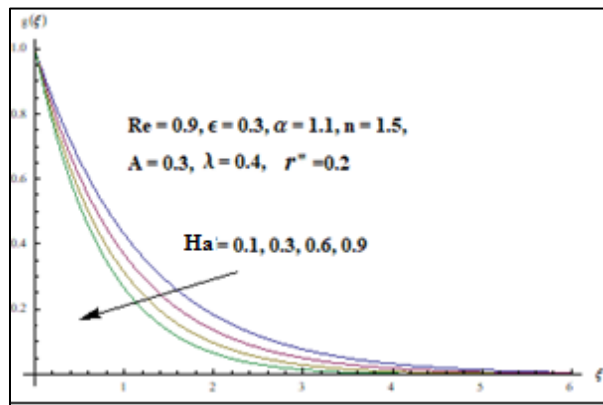
Fig. 6.3c: g(ξ) via Ha.
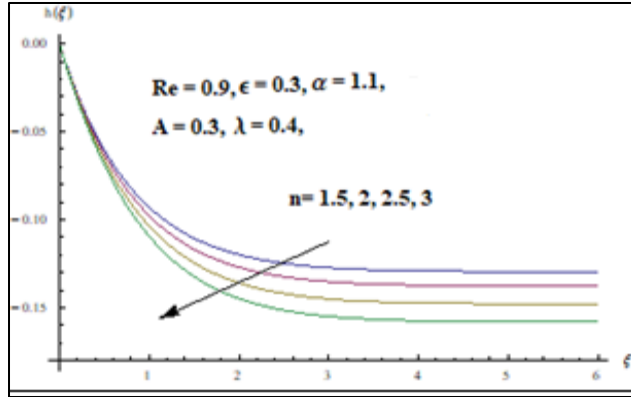
Fig. 6.4a: h(ξ) via n.
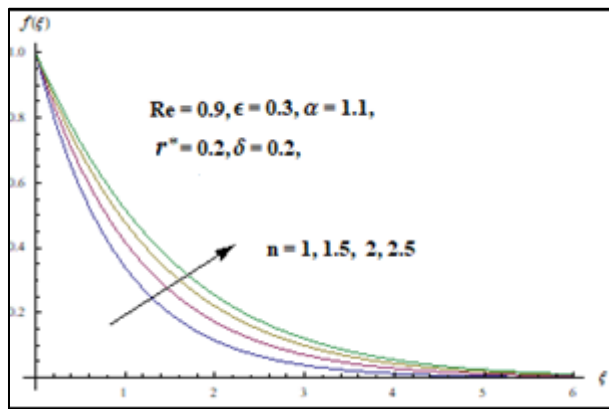
Fig. 6.4b: Impact of n on *f(ξ)*.
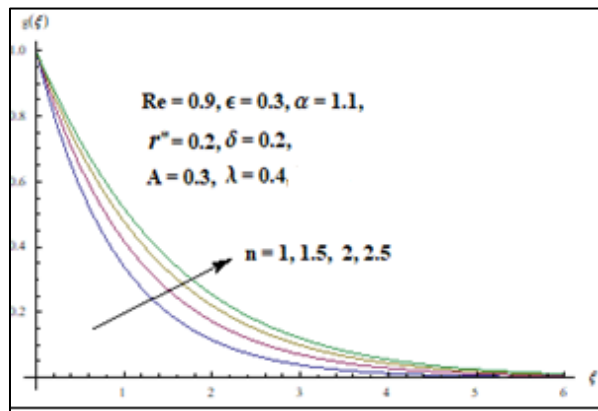
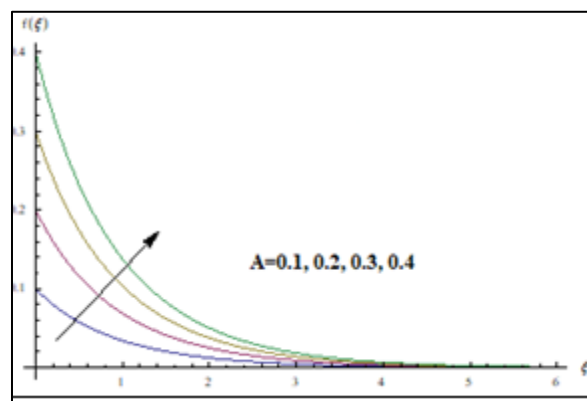Fig. 6.4c: Impact of n on g(ξ).
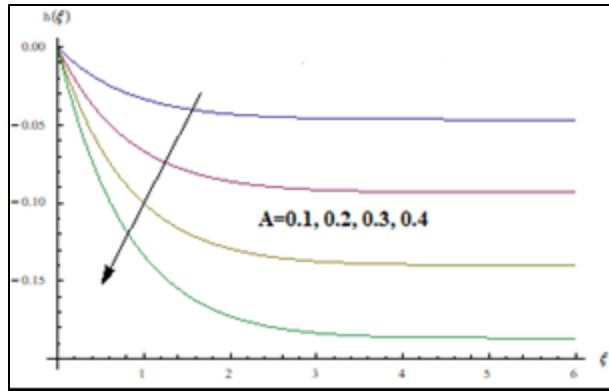
Fig. 6.5a: Impact of A on h(ξ).
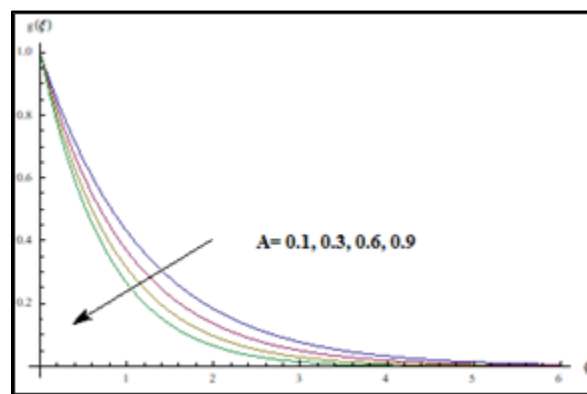

Fig. 6.5b: Impact of A on f(ξ).

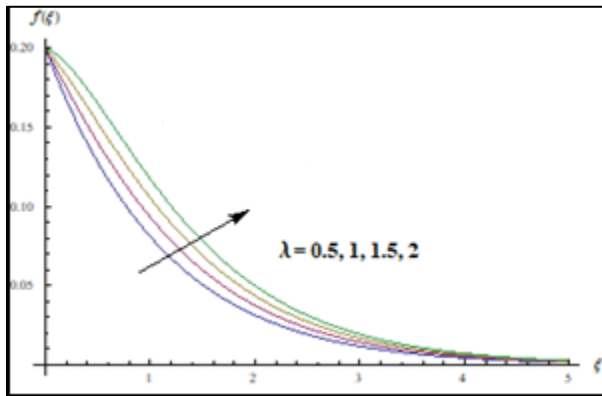Fig. 6.5c: Effect of A on $g(\xi)$.

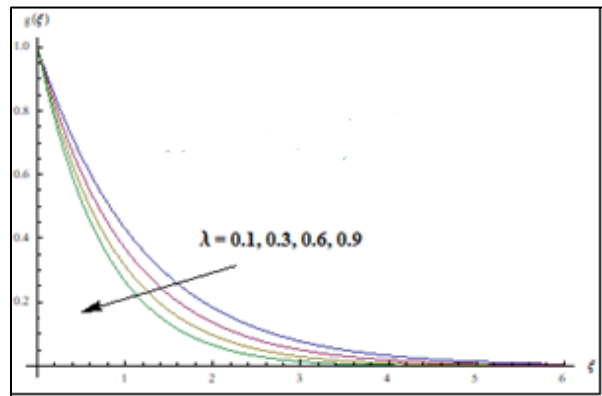Fig. 6.6a: Effect of λ on *h(ξ)*

Fig. 6.6b: *f(ξ)* via λ.

Fig. 6.6c: *g(ξ)* via λ.
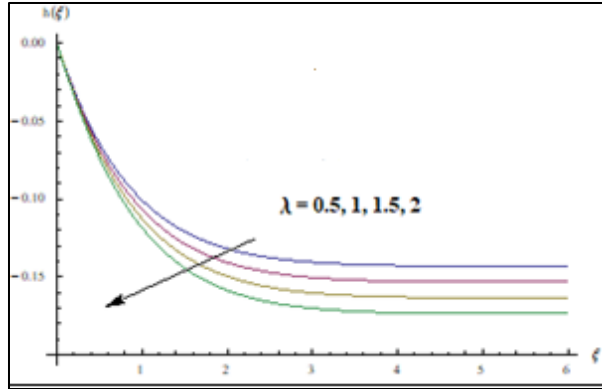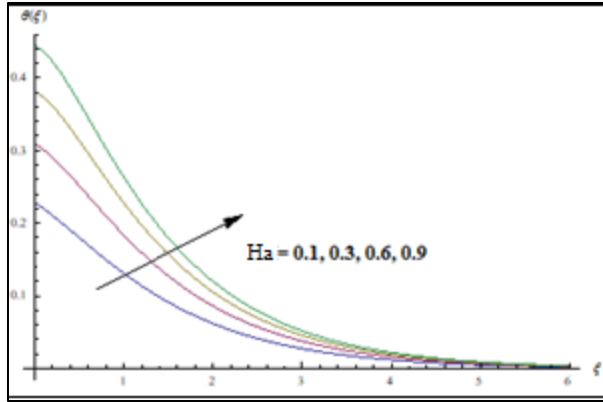
Fig. 6.7: Temperature $\theta(\xi)$ via Ha.
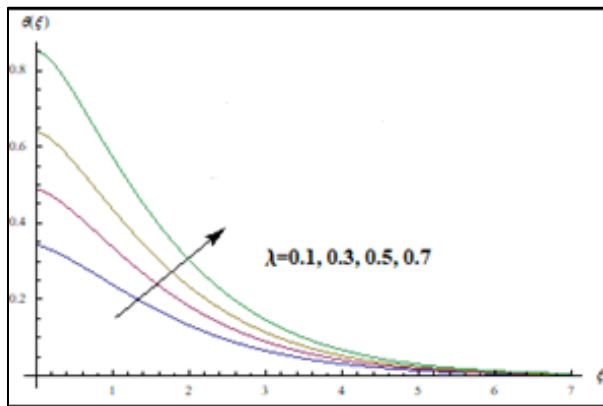
Fig. 6.8: Temperature $\theta(\xi)$ via λ.
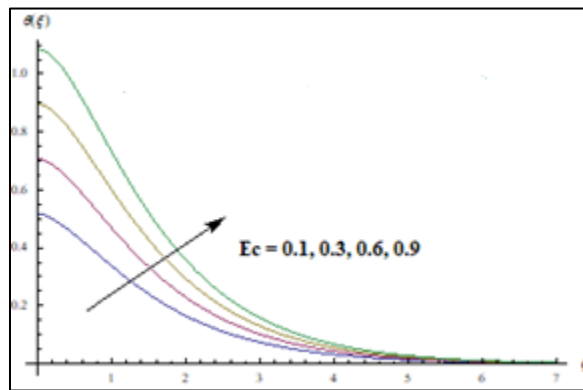
Fig. 6.9: Temperature $\theta(\xi)$ via Ec.

91
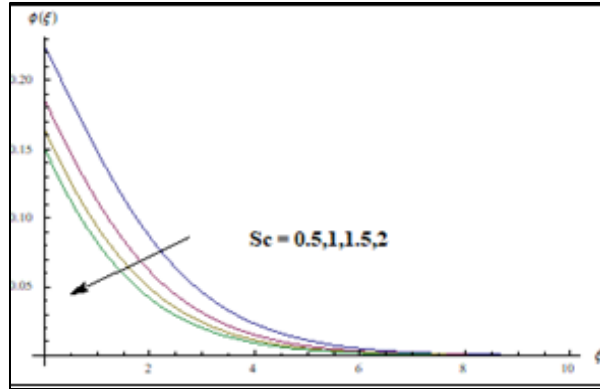
Fig. 6.10: Temperature $\phi\ (\xi)$ via Sc.
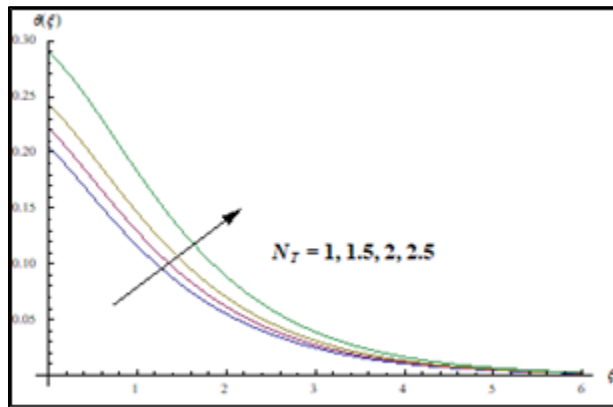
Fig. 6.11: Temperature $\theta(\xi)$ via N_T.
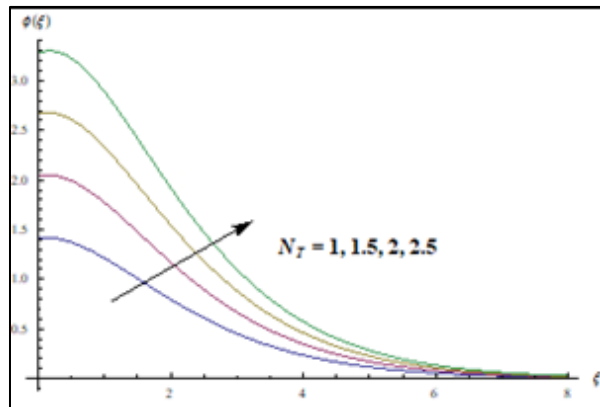
Fig. 6.12: Concentration $\phi\ (\xi)$ via N_T.
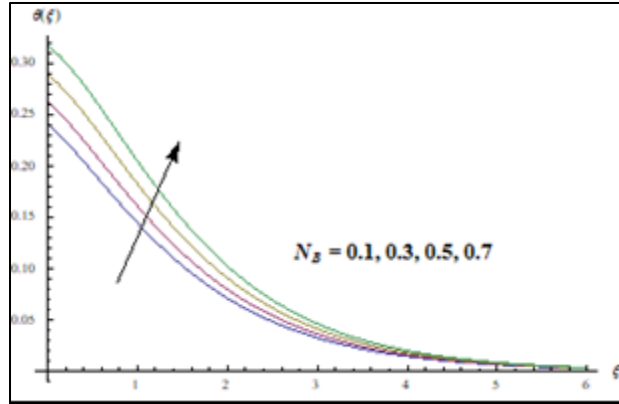
Fig. 6.13: Temperature $\theta(\xi)$ via N_B.
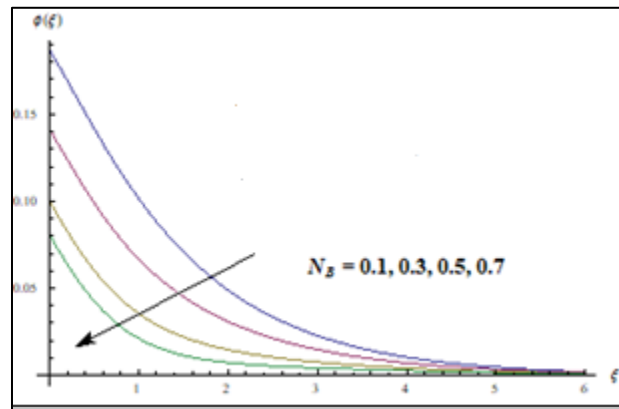
Fig. 6.14: Concentration $\phi(\xi)$ via N_B.
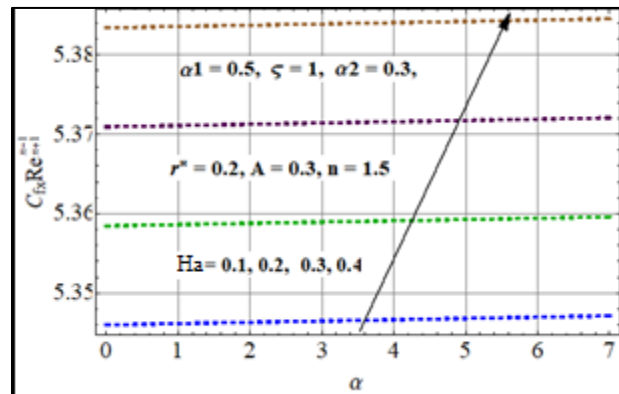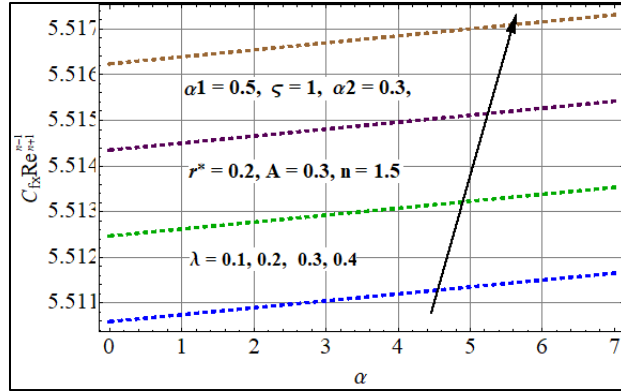

Fig. 6.15: Skin friction via Ha.

Fig. 6.16: Skin friction via λ.

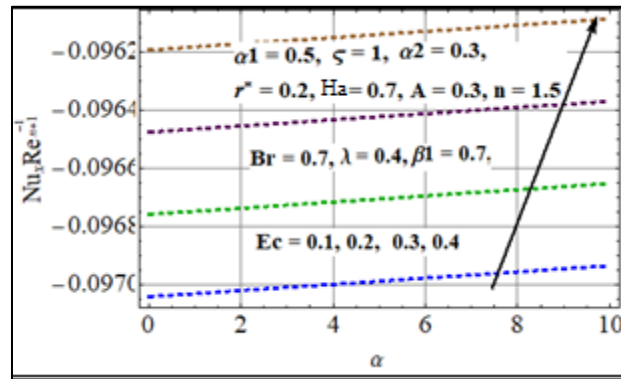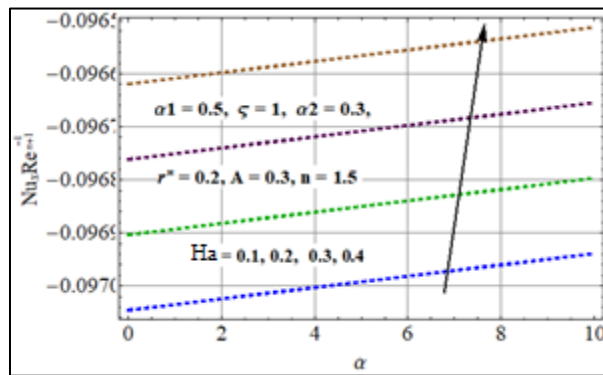Fig. 6.17: Nu via Ec.
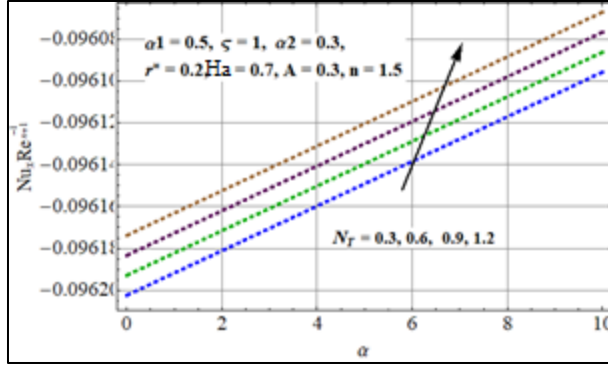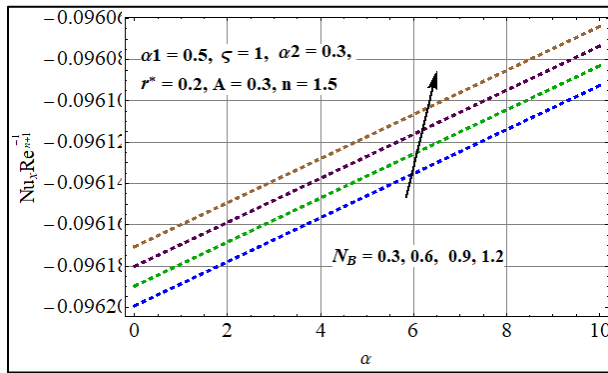

Fig. 6.18: Nu via Ha.

94

Fig. 6.19: Nu via N_T.

Fig. 6.20. Nu via N_B.

Entropy generation $(N_G(\xi))$ and Bejan number (Be)

Influences of dimensionless parameters α_1, Eckert number Ec, Brinkman number Br and Reynolds number Re on entropy generation rate $N_G(\xi)$ and Bejan number Be are analyzed in Figs. $(6.21 - 6.28)$.

Entropy and Bejan number for higher α_1 are exhibited graphically through Figs. 6.21 and 6.24. It is observed that $N_G(\xi)$ tends to zero far from the surface. For higher α_1 the effect of heat transfer is more dominating when compared with fluid friction effect as well as magnetic effect. Hence Be enhances. Figs. 6.23 and 6.24 are outlined to demonstrate outcomes of radiation parameter Ec on $N_G(\xi)$ and Be. Both increase for higher Ec due to increase in kinetic energy of system. Figs. 6.25 and 6.26 display entropy generation $N_G(\xi)$ and Bejan number Be for Brinkman number. Br is specifically identified close to surface of disk. Large amount of heat produced inside the system increases disturbance in the system. Fig. 6.26 demonstrates that Be decays for higher estimations of Br. Figs. 6.27 and 6.28 portrayed the impact of Re on $N_G(\xi)$ and Be. We noted that entropy

decreases while Bejan number increases for higher Re. For larger Re stream variance in the liquid improves so heat transfer increments and thus more disturbance is observed.
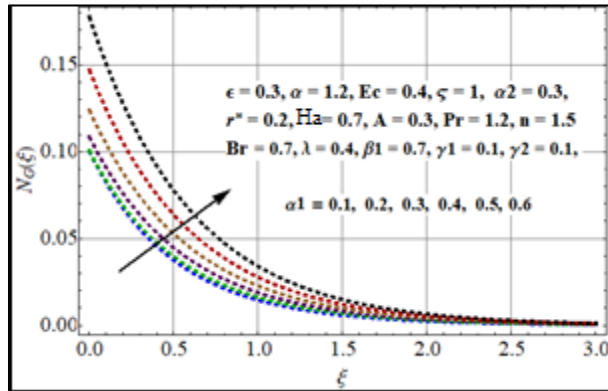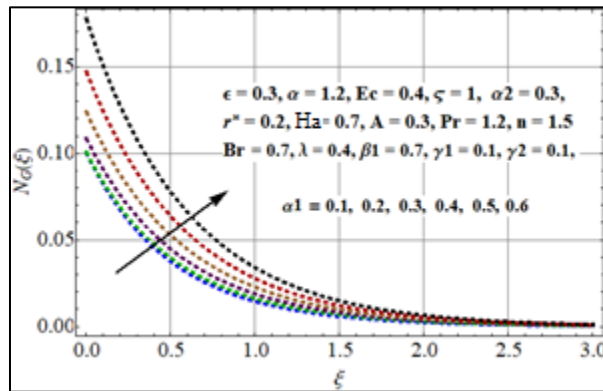

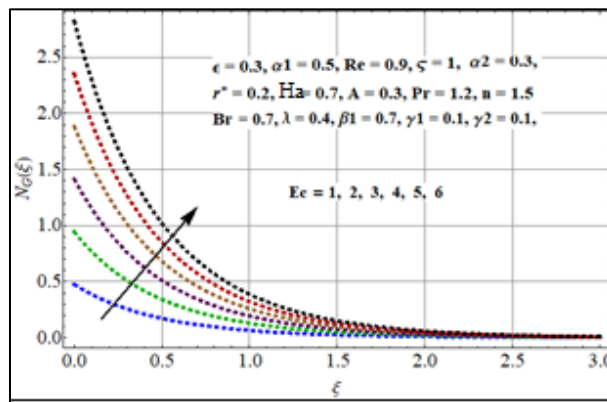Fig. 6.21 $N_G(\xi)$ via α_1.

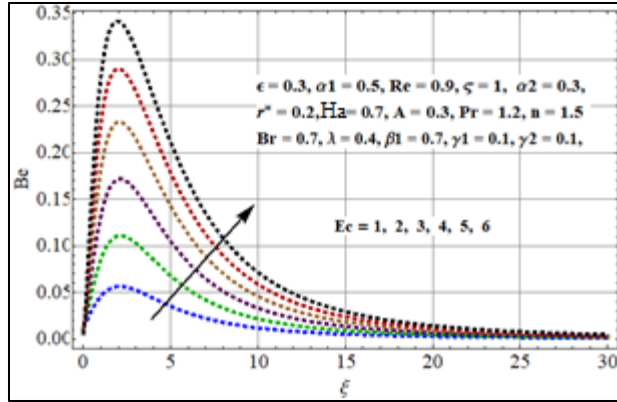Fig. 6.22: Be via α_1.

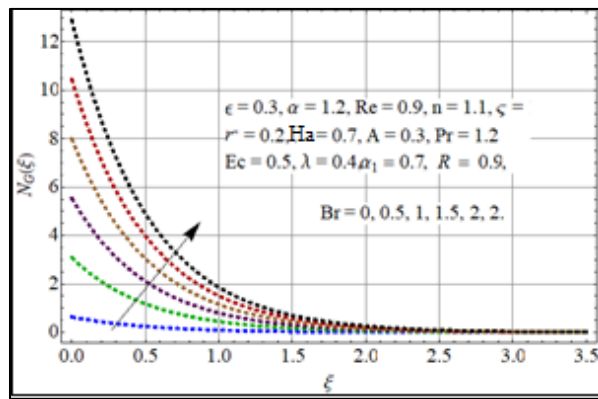Fig. 6.23: $N_G(\xi)$ via Ec.

Fig. 6.24: Be via Ec.
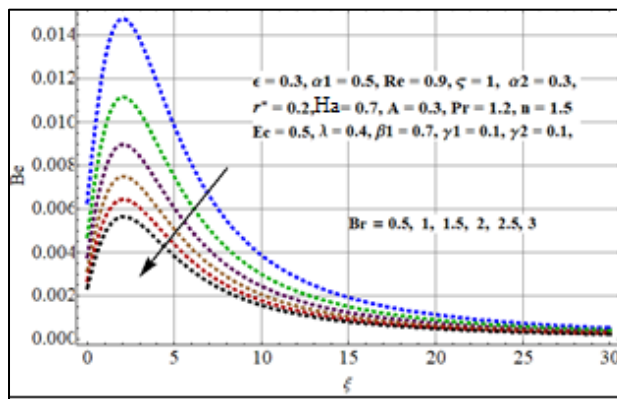

Fig. 6.25: $N_G(\xi)$ via Br.

Fig. 6.26: Be via Br.
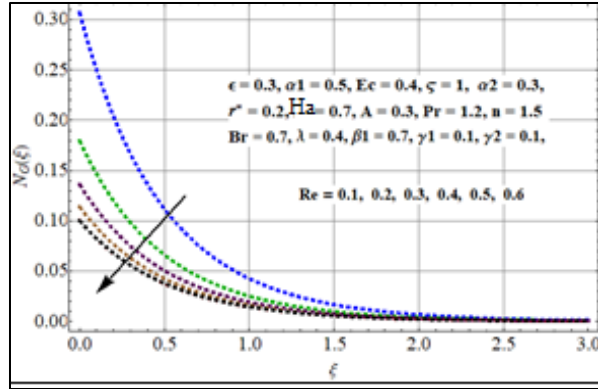
Fig. 6.27: $N_G(\xi)$ via Re.
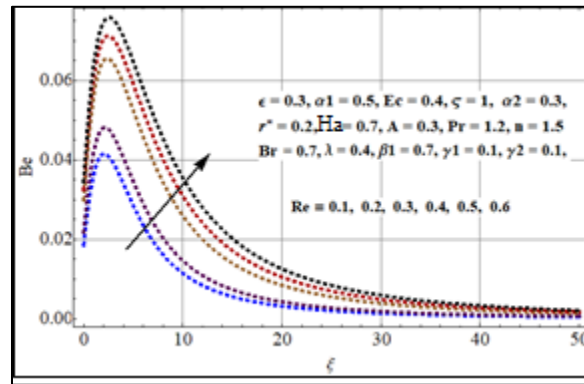
Fig. 6.28: Be via Re

Conclusions

Convective fluid flow caused by rotating disk is examined with viscous dissipation, convective conditions and Joule heating effects. Key points are summarized as:

- Magnitudes of velocity components increases for larger values of power law index of fluid
- Temperature $\tilde{\theta}(\xi)$ improves for larger Re, Ec and λ.
- Drag force increases for higher estimations of Ha.
- Magnitude of temperature gradient $Nu_x Re^{\frac{-1}{n+1}}$ is in inverse relation to Ec and Ha.
- Entropy generation rate $N_G(\xi)$ grows for higher Ec and Br while reverse behavior is observed for Re.
- Bejan number Be decreases with Br while it increases for Re.

Chapter 7

Dissipative convective flow of hybrid nanomaterials with entropy optimization

Introduction

Three-dimensional incompressible flow of hybrid nanofluid is presented by a stretchable surface of disk. Heat generation, radiation and viscous dissipation effects are considered. Computations are arranged for total entropy rate. Convective condition of heat transfer at the boundary is implemented. Outcomes of pertinent variables on the heat transfer irreversibility rate, porosity irreversibility rate, viscous dissipation irreversibility rate, Bejan number and total irreversibility rate are discussed. Special consideration is given to the engineering quantities like skin friction coefficient and heat transfer rate. It is concluded that entropy rate against radiation enhances.

Formulation

Here we have discussed three-dimensional dissipative hybrid nanofluid flow due to stretchable surface of disk. Disk at $z = 0$. is rotating with Ω (angular velocity) and stretching with rate a. Physical model of flow is presented in Fig. 7.1.
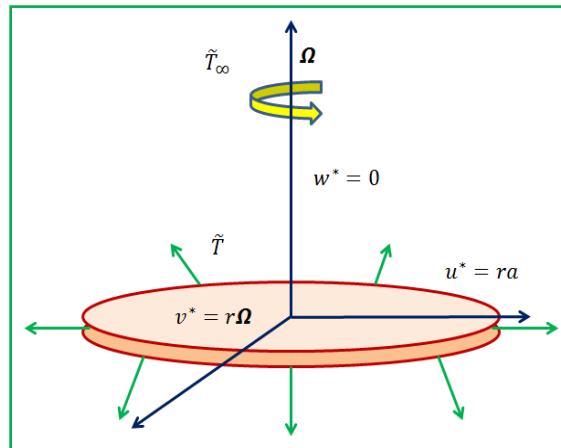

Fig. 7.1: Flow diagram

The governing equations are

$$\frac{\partial u^*}{\partial r} + \frac{u^*}{r} + \frac{\partial w^*}{\partial z} = 0, \tag{7.1}$$

$$u^* \frac{\partial u^*}{\partial r} - \frac{v^{*2}}{r} + w^* \frac{\partial u^*}{\partial z} = v_{hnf} \frac{\partial^2 u^*}{\partial z^2}, \tag{7.2}$$

$$u^* \frac{\partial v^*}{\partial r} + \frac{u^* v^*}{r} + w^* \frac{\partial v^*}{\partial z} = \nu_{hnf} \frac{\partial^2 v^*}{\partial z^2}, \tag{7.3}$$

$$(\rho c_p)_{hnf} \left(u^* \frac{\partial \tilde{T}}{\partial r} + w^* \frac{\partial \tilde{T}}{\partial z} \right) = k_{hnf} \frac{\partial^2 \tilde{T}}{\partial z^2} + \mu_{hnf} \left(\left(\frac{\partial u^*}{\partial z} \right)^2 + \left(\frac{\partial v^*}{\partial z} \right)^2 \right) + Q_0(\tilde{T} - \tilde{T}_\infty) \\ + \frac{16\sigma^* \tilde{T}_\infty^3}{3k^*} \frac{\partial^2 \tilde{T}}{\partial z^2}, \tag{7.4}$$

with boundary conditions

$$u^* = ra, v^* = r\Omega, w^* = 0, -k \frac{\partial \tilde{T}}{\partial z} = h_1(\tilde{T}_f - \tilde{T}) \text{ at } z = 0, \\ u^* = 0, v^* = 0, \tilde{T} = \tilde{T}_\infty \text{ at } z \to \infty, \tag{7.5}$$

in which x, y, z highlights the Cartesian coordinates, u^*, v^*, w^* the velocities components, ν_{hnf} the kinematic viscosity, σ_{hnf} the electrical conductivity, B_0 the magnetic field strength, ρ_{hnf} the density, $(\rho\beta)_{hnf}$ the thermal expansion coefficient, g the gravity, $\tilde{T}$ the temperature, $(\rho c_p)_{hnf}$ the specific heat capacity, Q_0 the heat generation, k_{hnf} the thermal conductivity, k^* the mean absorption coefficient, σ^* the Stefan-Boltzmann constant, μ_{hnf} the dynamic viscosity, $\tilde{T}_\infty$ the ambient temperature, a the dimensional constant and h_1 coefficient of heat transfer. In above expressions hnf denotes the hybrid nanofluid and nf the nanofluid.

Thermophysical characteristics of nanomaterial and hybrid nanofluid

The thermal properties of solid nanomaterials and hybrid nanofluid are defined as

$$\rho_{nf} = (1 - \phi)\rho_{bf} + \phi\rho_s, \tag{7.6}$$

$$\rho_{hnf} = \phi_{Al}\rho_{Al} + \phi_{cu}\rho_{cu} + \left(1 - \phi_{Al} - \phi_{cu}\right)\rho_{bf}, \tag{7.7}$$

$$(\rho c_p)_{hnf} = \left(1 - \phi_{Al} - \phi_{cu}\right)(\rho c_p)_{bf} + \phi_{Al}(\rho c_p)_{Al} + \phi_{cu}(\rho c_p)_{cu}. \tag{7.8}$$

The thermal conductivity of nanofluid $\left(k_{nf}\right)$ as well as hybrid nanofluid $\left(k_{hnf}\right)$ are

$$k_{nf} = \frac{(k_s + 2k_{bf}) - 2\phi(k_{bf} - k_s)}{(k_s + 2k_{bf}) + \phi(k_{bf} - k_s)} k_{bf}, \tag{7.9}$$

$$\frac{k_{hnf}}{k_{bf}} = \frac{\left(\frac{\phi_{Al} k_{Al} + \phi_{cu} k_{cu}}{\phi \cdot_{Al} + \varphi_{cu}} + 2k_{bf} + 2 \left(\phi_{Al} k_{Al} + \varphi_{cu} k_{cu} \right) - 2(\varphi_{Al} + \varphi_{cu})k_{bf} \right)}{\left(\frac{\varphi_{Al} k_{Al} + \varphi_{cu} k_{cu}}{\varphi_{Al} + \varphi_{cu}} + 2k_{bf} - (\varphi_{Al} k_{Al} + \varphi_{cu} k_{cu}) - (\varphi_{Al} + \varphi_{cu})k_{bf} \right)}. \tag{7.10}$$

Dynamic viscosity of hybrid nanofluid $\left(\mu_{hnf}\right)$ and nanofluid $\left(\mu_{nf}\right)$ are

$$\mu_{nf} = \frac{\mu_{bf}}{(1-\varphi)^{2.5}}, \tag{7.11}$$

$$\mu_{hnf} = \frac{\mu_{bf}}{(1-\varphi_{Al}-\varphi_{cu})^{2.5}}. \tag{7.12}$$

Considering the transformations

$$\left.\begin{array}{l} u^* = r\Omega f'(\eta), v^* = r\Omega g(\eta), w^* = (\nu_{bf}\Omega)^{\frac{1}{2}}h(\eta), \\[2mm] \theta = \dfrac{\hat{T}-\hat{T}_\infty}{\hat{T}_f-\hat{T}_\infty} \quad \eta = z\left(\dfrac{\Omega}{\nu_{bf}}\right)^{\frac{1}{2}}, \end{array}\right\} \tag{7.13}$$

one obtains

$$2f + h' = 0, \tag{7.14}$$

$$\frac{A_4}{(1-\varphi_{Al}-\varphi_{cu})^{2.5}} f'' - f^2 - hf' + g^2 = 0, \tag{7.15}$$

$$\frac{A_4}{(1-\varphi_{Al}-\varphi_{cu})^{2.5}} g'' - 2fg - hg' = 0, \tag{7.16}$$

$$A_2 \frac{1}{\text{Pr}}\theta''(A_5 + R_d) - h\theta' + \frac{EcA_2}{(1-\varphi_{Al}-\varphi_{cu})^{2.5}}(f''^2 + g'^2) + Q\theta A_2 = 0 \tag{7.17}$$

$$\left.\begin{array}{l} h(0) = 0, \ f(0) = A, \ g(0) = 1, \ \theta'(0) = -\beta_1(1-\theta(0)) \ \text{at } \eta = 0, \\[1mm] f \to 0, \ g \to 0, \ \theta \to 0 \ \text{ when } \eta \to \infty. \end{array}\right\} \tag{7.18}$$

Here $Ec\left(= \dfrac{r^2\Omega^2}{c_p(T_f-T_\infty)}\right)$ represents the Eckert number, $Pr\left(= \dfrac{(\rho c_p)_{bf}\nu_{bf}}{k_{bf}}\right)$ Prandtl number, $R_d =$

$\left(\dfrac{16\sigma^* T_\infty^3}{3k^* k_{bf}}\right)$ radiation parameter, $A\left(= \dfrac{a}{\Omega}\right)$ stretching parameter, β_1 Biot number and $Q\left(= \dfrac{Q_0}{(\rho c_p)_{bf}\Omega}\right)$

heat generation parameter. Mathematically A_1, A_2, A_3, A_4 and A_5 are:

$$A_1 = \left(1-\varphi_{Al}-\varphi_{cu} + \frac{(\rho\beta)_{Al}\varphi_{Al} + (\rho\beta)_{cu}\varphi_{cu}}{(\rho\beta)_{bf}}\right), \tag{7.19}$$

$$A_2 = \frac{1}{\left(1-\varphi_{Al}-\varphi_{cu} + \dfrac{(\rho c_p)_{Al}\varphi_{Al} + (\rho c_p)_{cu}\varphi_{cu}}{(\rho c_p)_{bf}}\right)}, \tag{7.20}$$

$$A_3 = \frac{\sigma_{hnf}}{\sigma_{bf}} = \frac{1 + 3\left(\dfrac{\sigma_{Al}\varphi_{Al} + \sigma_{cu}\varphi_{cu}}{\sigma_{bf}} - \varphi_{Al} - \varphi_{cu}\right)}{\left(\dfrac{\sigma_{Al} + \sigma_{cu}}{\sigma_{bf}} + 2\right) - \left(\dfrac{\sigma_{Al}\varphi_{Al} + \sigma_{cu}\varphi_{cu}}{\sigma_{bf}} - \varphi_{Al} - \varphi_{cu}\right)},$$ (7.21)

$$A_4 = \left(1 - \varphi_{Al} - \varphi_{cu} + \frac{\varphi_{Al}\rho_{Al} + \varphi_{cu}\rho_{cu}}{\rho_{bf}}\right),$$ (7.22)

$$A_5 = \frac{k_{hnf}}{k_{bf}} = \frac{\dfrac{k_{Al}\varphi_{Al} + k_{cu}\varphi_{cu}}{\varphi_{Al} + \varphi_{cu}} + 2k_{bf} - 2(\varphi_{Al} + \varphi_{cu})k_{bf} + 2(k_{Al}\varphi_{Al} + k_{cu}\varphi_{cu})}{\dfrac{k_{Al}\varphi_{Al} + k_{cu}\varphi_{cu}}{\varphi_{Al} + \varphi_{cu}} + 2k_{bf} - (\varphi_{Al} + \varphi_{cu})k_{bf} - (k_{Al}\varphi_{Al} + k_{cu}\varphi_{cu})}.$$ (7.23)

Entropy equation

Mathematically we can write

$$S_G = \underbrace{\frac{k_{bf}}{\tilde{T}_f^2}\left(\frac{k_{hnf}}{k_{bf}} + \frac{16\sigma^*\tilde{T}_\infty^3}{3k^*k_{bf}}\right)\left(\frac{\partial\tilde{T}}{\partial z}\right)^2}_{\text{heat transfer irreversibility}} + \underbrace{\frac{\mu_{hnf}}{\tilde{T}_f}\left[\left(\frac{\partial u^*}{\partial z}\right)^2 + \left(\frac{\partial v^*}{\partial z}\right)^2\right]}_{\text{viscous dissipation irreversibility}}. \left.\vphantom{\frac{1}{1}}\right\}$$ (7.24)

In view of Eq. (7.13), the dimensionless form of above expression yields

$$N_G = (A_5 + R_d)\alpha_1\theta'^2 + \frac{Br}{(1 - \varphi_{Al} - \varphi_{cu})^{2.5}}(f''^2 + g'^2),$$ (7.25)

where $\alpha_1\left(= \dfrac{\Delta T}{\tilde{T}_f}\right)$ depicts temperature ratio variable and $Br\left(= \dfrac{\mu_{bf}\Omega^2 r^2}{k_{bf}\Delta T}\right)$ the Brinkman number.

Mathematically Be is

$$Be = \frac{(A_5 + R_d)\alpha_1\theta'^2}{(A_5 + R_d)\alpha_1\theta'^2 + \dfrac{Br}{(1 - \varphi_{Al} - \varphi_{cu})^{2.5}}(f''^2 + g'^2) + A_3 HaBrf^2}.$$ (7.26)

Quantities of engineering interest

Surface drag force

We have

$$C_f = \frac{\sqrt{\tau_{zr}^2 + \tau_{z\theta}^2}}{\rho_{hnf}(\Omega r)^2},$$ (7.27)

where τ_{zr} and $\tau_{z\theta}$ satisfy the following relation

$$\tau_{zr} = \mu_{hnf} \frac{\partial \hat{u}}{\partial z}\Big|_{z=0} = \frac{1}{(1 - \varphi_{Al} - \varphi_{cu})^{2.5}} \left(\frac{\Omega}{v}\right)^{\frac{1}{2}} rf''(0),$$

$$\tau_{z\theta} = \mu_{hnf} \frac{\partial \hat{v}}{\partial z}\Big|_{z=0} = \frac{1}{(1 - \varphi_{Al} - \varphi_{cu})^{2.5}} \left(\frac{\Omega}{v}\right)^{\frac{1}{2}} rg'(0).$$

(7.28)

The total stress τ_w is represented by

$$\tau_w = \sqrt{\tau_{zr}^2 + \tau_{z\theta}^2}.$$

(7.29)

Invoking Eq. (7.28) in Eq. (7.27) we can write

$$C_{fx} Re^{\frac{1}{n+1}} = [(f''(0))^2 + (g'(0))^2]^{1/2}.$$

(7.30)

Heat transfer rate

Mathematically

$$Nu_x = \left(\frac{rq_w}{k_{bf}(\tilde{T}_f - \tilde{T}_\infty)}\right)_{z=0},$$

(7.31)

where q_w is defined as

$$q_w = -\left(k_{hnf} \frac{\partial \tilde{T}}{\partial z}\right)_{z=0} - \left(\frac{16\sigma^* \tilde{T}_\infty^3}{3k^*} \frac{\partial \tilde{T}}{\partial z}\right)_{z=0}.$$

(7.32)

From Eqs. (7.31) and (7.32), one arrives at

$$Nu_x Re^{\frac{-1}{n+1}} = -\left(\frac{k_{hnf}}{k_{bf}} + R_d\right)\theta'(0).$$

(7.33)

In the above expressions τ_{zr}, $\tau_{z\theta}$, C_f, τ_w, $Re^{\frac{1}{n+1}}$, Nu_x and q_w denote shear stress components in radial and tangential direction, skin friction coefficient, total shear stress, Reynolds number, Nusselt number and wall heat flux.

Results and analysis

Here results are presented through Built-in-Shooting method. The influences of pertinent variables on three-dimensional hybrid nanomaterial flow by rotating stretchable disk are scrutinized through various plots. Figs. 7.2-7.15 are plotted for the impacts of different parameters like stretching parameter, Eckert number, Biot number, radiation parameter, heat source/sink parameter on velocity components i.e., $(h(\xi))$, $(f(\xi))$ and $(g(\xi))$, $\theta(\xi)$ temperature, entropy generation, $Nu_x Re_x^{-0.5}$ Nusselt number and Bejan number. Effect of stretching variable $(A =$

$0.1, 0.3, 0.6, 0.9, 1.2, 1.5)$ on velocities $h(\xi)$ and $f(\xi)$ is given in Figs. 7.2 and 7.3. It is clear from plots that both velocity components enhance versus larger stretching variable. Physically for higher γ_1 the stretching rate enhances due to which velocity components become higher.

Fig. 7.4 identifies the impact of Eckert number $(Ec = 0.0, 0.2, 0.4, 0.6, 0.8, 1.0)$ on $\theta(\xi)$. An increase in temperature field for rising values of Ec is noted. In fact such increase is conversion of huge amount of mechanical energy into heat energy caused by the internal frictions of the molecules. Effect of $(\beta_1 = 0.1, 0.2, 0.4, 0.6, 0.8, 1.0)$ on $\theta(\xi)$ is displayed in Fig. 7.5. It is clear from this plot that movement of material particles enhances for Biot number. Physically it is due to decay in viscosity of liquid and thus fluid temperature increases. Fig. 7.6 is made to study how radiation parameter affects the thermal field. Increasing behavior of thermal field is noticed in Fig. 7.7 for larger heat source parameter.

Figs. 7.8 and 7.9 are sketched to examine the heat transfer rate against Eckert number, radiation parameter and Biot number. Here heat transfer rate (Nusselt number) decreases with increase in Eckert number while it enhances via higher Biot number.

Entropy generation rate

Figs. 7.10 and 7.11 are sketched to study how radiation parameter affects the entropy rate and Bejan number. Here we can see that both $N_G(\xi)$ and Be increase against larger radiation parameter. Physically more heat is generated in the working fluid in the presence of larger radiative parameter. Figs. 7.12 and 7.13 are drawn to show the behavior of Brinkman number on $N_G(\xi)$ and Be. Physically the Brinkman number shows relation of heat conduction through viscous dissipation from disk surface to heat transport through molecular conduction. Production of heat inside the layers enhances the entropy and disorderliness in the system (see Fig. 7.12). Fig. 7.13 highlights that Be declines with Br. Figs. 7.14 and 7.15 are drawn to portray the impact of stretching variable on $N_G(\xi)$ and Be. An increase in entropy generation for larger values of A is noticed. Physically for increasing stretching variable more disturbances in the liquid particles is noted so heat transfer upsurges and thus entropy enhances. Moreover Be number increases for higher A (see Fig. 7.15).
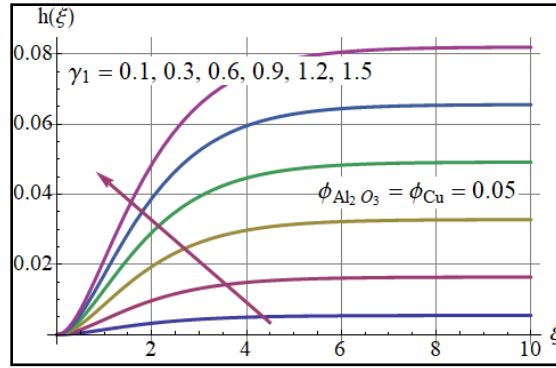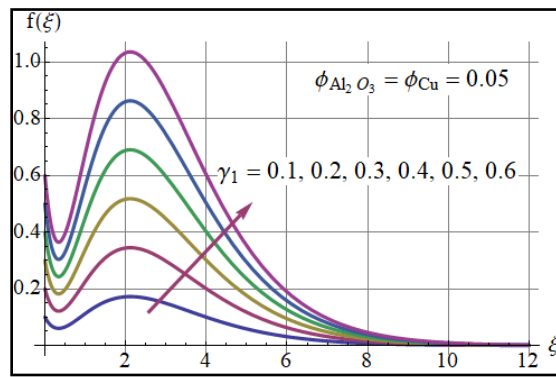
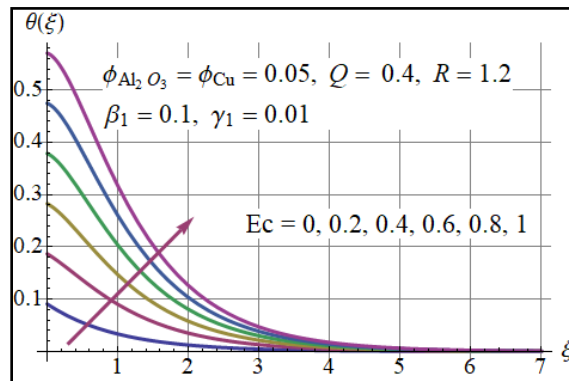*Fig*. 7.2: γ_1 *against* $h(\xi)$.

Fig. 7.3: γ_1 *against* $f(\xi)$

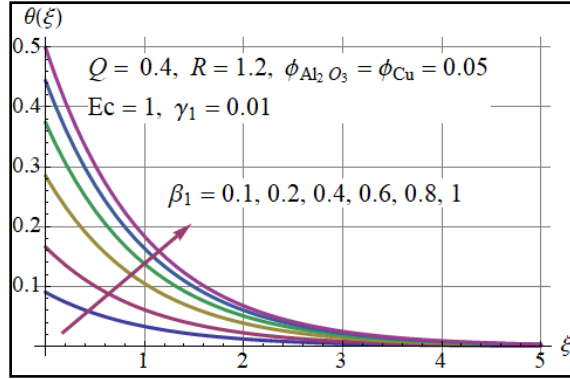*Fig*. 7.4: Ec *against* $\theta(\xi)$.
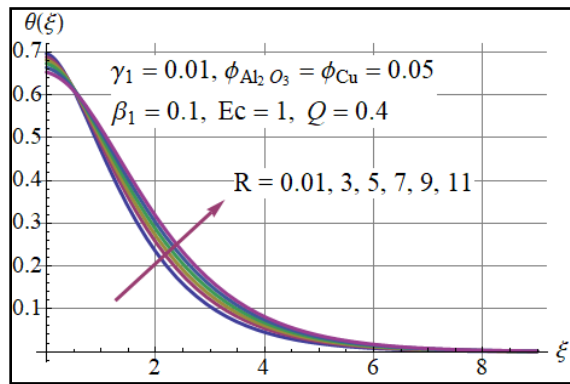
Fig. 7.5: β_1 against $\theta(\xi)$.

Fig. 7.6: R against $\theta(\xi)$

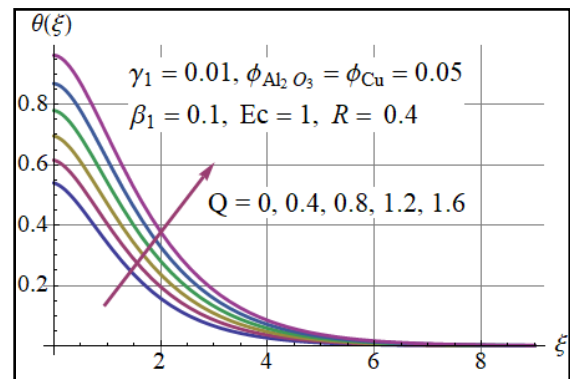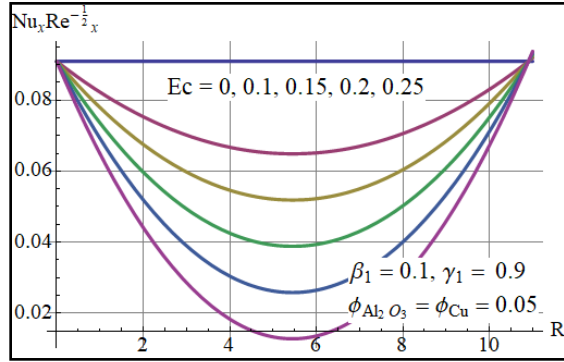*Fig. 7.7: Q against $\theta(\xi)$*
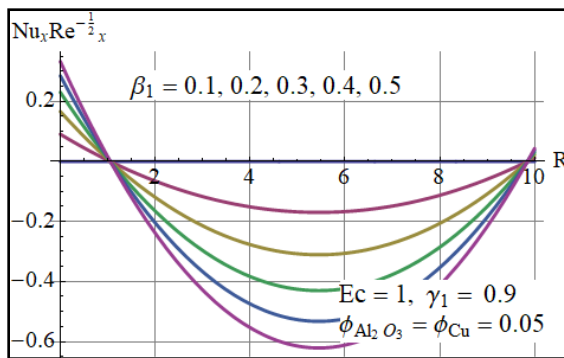
Fig. 7.8: *Heat transfer via Ec and R.*

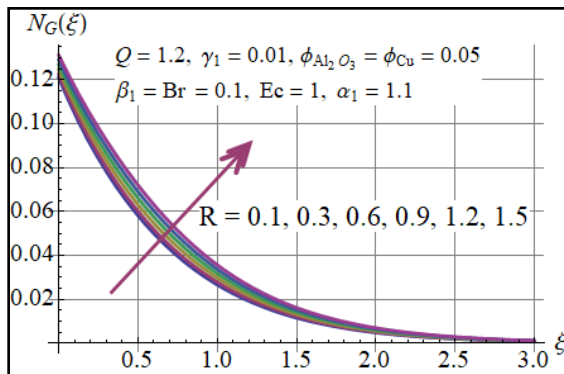Fig. 7.9: *Heat transfer via β_1 and R.*
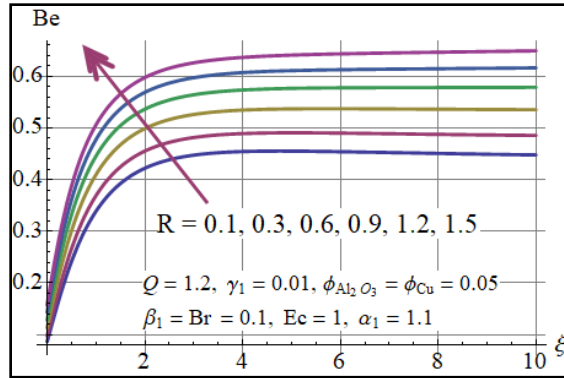

Fig. 7.10: $N_G(\xi)$ *versus R.*

Fig. 7.11: $Be(\xi)$ versus R
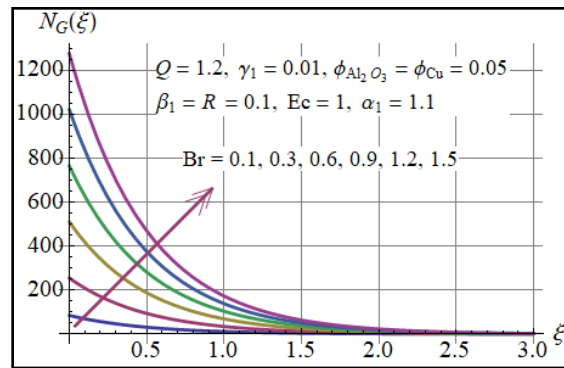

Fig. 7.12: $N_G(\xi)$ versus Br
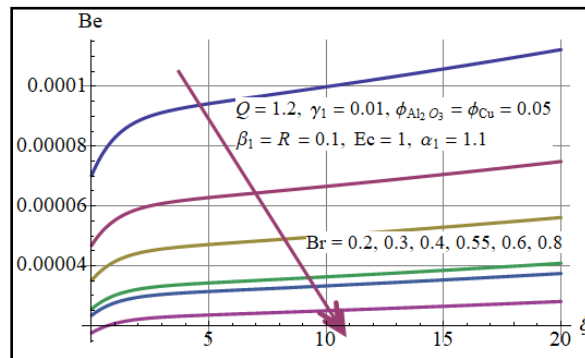
Fig. 7.13: $Be(\xi)$ versus Br

108
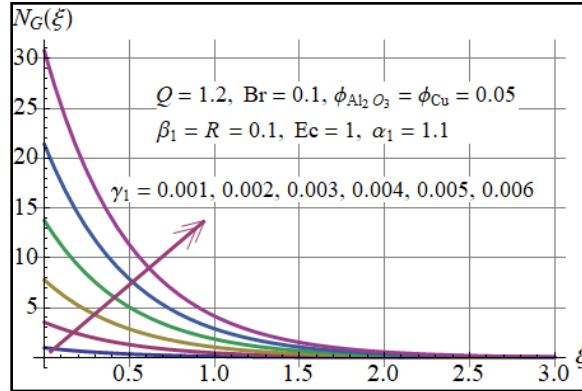
Fig. 7.14: $N_G(\xi)$ versus γ_1

Fig. 7.15: $Be(\xi)$ versus γ_1
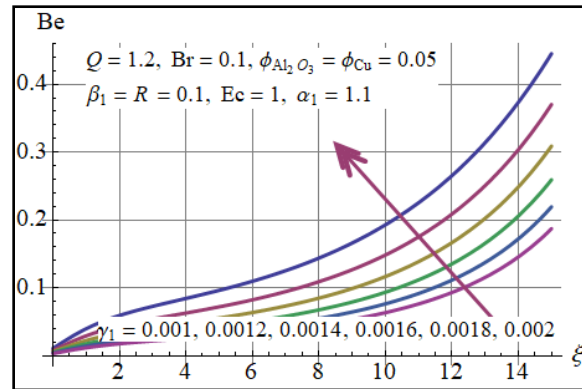
Conclusions

The remarkable results are listed as follows:

- Velocity components increase versus stretching variable.
- Temperature field increases for Eckert number and radiation parameter.
- $Nu_x Re_x^{-0.5}$ declines against Eckert and Biot numbers.
- $N_G(\xi)$ upsurges for higher estimations of Ec and Br.
- Be decreases with Br while it enhances with radiation parameter.

Chapter 8

Entropy analysis in magnetohydrodynamic Hybrid nanofluid flow due to a rotating disk

Introduction

The salient features of three-dimensional magnetohydrodynamic hybrid nanofluid flow by a rotating disk have been investigated in this chapter. Velocity with mixed convection and magnetic properties has been anlayzed for radial, tangential and axial directions. Entropy rate and Bejan number are key points to be discussed. Effects for total irreversibilities are calculated. Low Reynolds number and boundary layer approximations are used to formulate relevant systems. Transformation procedure yield nonlinear system of ordinary differential equations. Such resultant systems are numerically solved by ND solve method. Nusselt and Sherwood number are addressed.

Formulation

We examined MHD steady three-dimensional flow of hybrid nanofluid due to a rotating stretchable disk. The stretched disk at $z = 0$ rotates with a angular speed Ω. H_0 is value of uniform magnetic field and flow description is in Fig. (8.1). Heat properties are studied with Joule heating and dissipation effects. Boundary layer expressions are:
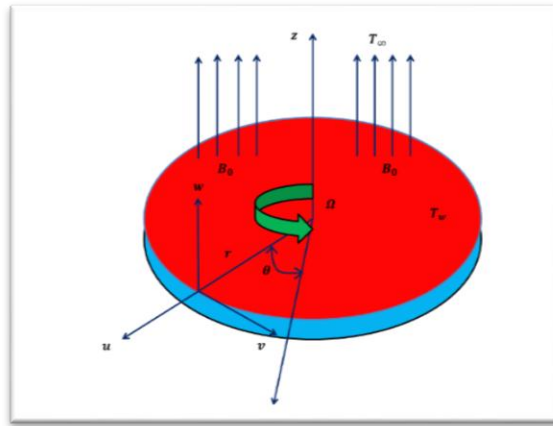

Fig. 8.1 Flow configuration.

$$\frac{\partial \tilde{u}}{\partial r} + \frac{\partial \tilde{w}}{\partial z} + \frac{\hat{u}}{r} = 0, \tag{8.1}$$

$$\tilde{u}\frac{\partial \tilde{u}}{\partial r} + \tilde{w}\frac{\partial \tilde{u}}{\partial z} - \frac{\tilde{v}^2}{r} = \frac{\mu_{hnf}}{\rho_{hnf}}\frac{\partial^2 \tilde{u}}{\partial z^2} - \frac{\sigma_{hnf}}{\rho_{hnf}}B_0^2\tilde{u} + g\left\{\lambda_1(\tilde{T} - \tilde{T}_\infty) + \lambda_2(\tilde{T} - \tilde{T}_\infty)^2\right\}, \tag{8.2}$$

$$\tilde{u}\frac{\partial \tilde{v}}{\partial r} + \tilde{w}\frac{\partial \tilde{v}}{\partial z} + \frac{\tilde{u}\tilde{v}}{r} = \nu\frac{\partial^2 \tilde{v}}{\partial z^2} - \frac{\sigma_{hnf}}{\rho_{hnf}}B_0^2\tilde{v}, \tag{8.3}$$

$$\left(\tilde{u}\frac{\partial \tilde{T}}{\partial r} + \hat{w}\frac{\partial \tilde{T}}{\partial z}\right) = \frac{k_f}{(\rho c_p)_{hnf}}\frac{\partial^2 \tilde{T}}{\partial z^2} + \frac{\sigma_{hnf}}{(\rho c_p)_{hnf}}B_0^2(\tilde{u}^2 + \tilde{v}^2) + \frac{\mu_{hnf}}{(\rho c_p)_{hnf}}\left(\left(\frac{\partial \tilde{u}}{\partial z}\right)^2 + \left(\frac{\partial \tilde{u}}{\partial z}\right)^2\right), \tag{8.4}$$

$$\tilde{u}\frac{\partial C}{\partial r} + \tilde{w}\frac{\partial C}{\partial z} = \frac{D_T}{T_\infty}\frac{\partial^2 \tilde{T}}{\partial z^2} + D_B\frac{\partial^2 C}{\partial z^2}, \tag{8.5}$$

with

$$\left.\begin{array}{l}\tilde{u} = cr, \tilde{v} = r\Omega, \tilde{w} = 0, \tilde{T} = \tilde{T}_w, C = C_w \text{ at } z = 0,\\ \tilde{u} = 0, \tilde{v} = 0, \tilde{T} = \tilde{T}_\infty, C = C_\infty \text{ at } z \to \infty,\end{array}\right\} \tag{8.6}$$

where u, v, w represent the velocities in radial, tangential and axial directions respectively σ° Stefan-Boltzman constant, c dimensional constant, ρ_f density, μ_f absolute viscosity of fluid , k_f thermal conductivity, σ_f electrical conductivity, ν_f kinematic viscosity, C concentration, $\hat{T}$ ambient fluid temperature, C ambient concentration and c_{pf} heat capacitance.

Quantities of engineering interest

Mathematically the equation for drag force is given as

$$C_f = \frac{-2\sqrt{\tau_{zr}^2 + \tau_{z\theta}^2}}{\rho_f(\Omega r)^2}, \tag{8.7}$$

where τ_{zr} and $\tau_{z\theta}$ show the radial and tangential stress components respectively. These are

$$C_{fr}\,Re = -2\frac{A_1}{A_2 A^2}(\tilde{f}''(0))^2, \tag{8.8}$$

$$C_{f\theta}\,Re = -2\frac{A_1}{A_2}(\tilde{g}'(0))^2. \tag{8.9}$$

Total stress τ_w is given by

$$\tau_w = \sqrt{\tau_{zr}^2 + \tau_{z\theta}^2}. \tag{8.10}$$

Equations $(8.8 - 8.10)$ yield

$$C_{fr} \, Re = -2\frac{A_1}{A_2}\left[\frac{1}{A^2}(\tilde{f}''(0))^2 + (\tilde{g}'(0))^2\right]. \tag{8.11}$$

Heat transfer rate

Heat transfer rate in dimensional form is

$$Nu_x = \left.\frac{cq_w}{k_{nf}(\hat{T}_w - \hat{T}_\infty)}\right|_{z=0}, \tag{8.12}$$

where q_w the wall heat flux is

$$q_w|_{z=0} = -\left.k_f\frac{\partial \hat{T}}{\partial z}\right|_{z=0}. \tag{8.13}$$

Putting Eq. (8.13) in Eq. (8.12) we get

$$Nu_x \, Re^{\frac{-1}{n+1}} = -\tilde{\theta}'(0). \tag{8.14}$$

Similarly the local Sherwood number is

$$Sh_x = \left.\frac{R_0 q_m}{D_B(C_f - C_\infty)}\right|_{z=0}, \tag{8.15}$$

in which the mass flux q_m satisfies

$$Sh_x \, Re^{\frac{-1}{n+1}} = -\varphi'(0). \tag{8.16}$$

Entropy

Entropy generation is given as

$$S_G = \frac{k_{hnf}}{\tilde{T}_\infty^2}\left(\frac{\partial \tilde{T}}{\partial z}\right)^2 + \frac{\mu_{nf}}{\tilde{T}_\infty}\Phi^* + \frac{\sigma_f}{\tilde{T}_\infty}B_0^2(\hat{u}^2 + \hat{v}^2), \tag{8.17}$$

where

$$\Phi^* = \left(\frac{\partial \hat{u}}{\partial z}\right)^2 + \left(\frac{\partial \hat{v}}{\partial z}\right)^2. \tag{8.18}$$

We can write

$$
S_G = \underbrace{\frac{k_{hnf}}{\tilde{T}_\infty^2}\left(\frac{\partial \tilde{T}}{\partial z}\right)^2}_{\text{Thermal irreversibility}} + \underbrace{\frac{\mu_{nf}}{\tilde{T}_\infty}\left[\left(\frac{\partial \hat{u}}{\partial z}\right)^2 + \left(\frac{\partial \hat{v}}{\partial z}\right)^2\right]}_{\text{Fluid friction irreversibility}} \left.\begin{array}{c} \\ \\ \\ \\ \\ \end{array}\right\}
$$
$$
+ \underbrace{\frac{\sigma_f}{\tilde{T}_\infty}B_0^2(\tilde{u}^2 + \tilde{v}^2)}_{\text{Joule dissipation irreversibility}}.
$$

(8.19)

In nondimensional form the entropy generation E_g has the following expression

$$
\left.\begin{array}{c}
E_g = A_4\tilde{\theta}'^2 + \dfrac{A_1\,Pr\,E\,c}{\tilde{\theta}_w}\left[\tilde{f}''^2 + \tilde{g}'^2\right] \\[2ex]
+ \dfrac{A_3 Ha\,Pr\,E\,cRe}{\tilde{\theta}_w\left[\tilde{f}'^2 + \tilde{g}^2\right]}
\end{array}\right\},
$$

(8.20)

$$
\tilde{\theta}_w = \frac{\hat{T}_w - \hat{T}_\infty}{\hat{T}_\infty} = \frac{\Delta T}{\hat{T}_\infty}, A_1 = \frac{\mu_{hnf}}{\mu_f}, A_3 = \frac{\sigma_{hnf}}{\sigma_f}, A_4 = \frac{k_{hnf}}{k_f}.
$$

Here T_c is the temperature difference parameter, A_1, A_3, A_4 the dimensionless parameters and E_g entropy generation rate.

Heat transfer irreversibility dominates when $Be \gg 0.5$. For $Be \ll 0.5$ the viscous effects are dominant while both are equal for $Be = 0.5$. Bejan number (Be) is given as

$$
\mathrm{Be} = \frac{\text{Thermal entropy}}{\text{Total entropy}},
$$

(8.22)

or

$$Be = \left. \frac{A_4 \tilde{\theta}'^2}{E_g = A_4 \tilde{\theta}'^2 + \dfrac{A_1 \, Pr \, E \, c}{\tilde{\theta}_w}\left[\tilde{f}''^2 + \tilde{g}'^2\right] + \dfrac{A_3 Ha \, Pr \, E \, cRe}{\tilde{\theta}_w \left[\tilde{f}'^2 + \tilde{g}^2\right]}} \right\} . \qquad (8.23)$$

Discussion

Influences of pertinent parameters on MHD hybrid nanofluid flow due to rotating disk are presented graphically. Figs. ($8.2 - 8.12$) are shown for velocity $\tilde{f}'(\xi)$, temperature $\tilde{\theta}(\xi)$, skin friction $C_{fx} Re^{(1/2)}$ and Nusselt number $N_{ux} Re^{-(1/2)}$. Fig. 2 depicts the impact of A on radial component of velocity $\tilde{f}'(\xi)$. Here velocity is enhanced for higher A. The reason for it is the increase in stretching rate of disk. Velocity profile shows more increase in case of hybrid nanoparticles when compared with simple nanoparticles. Influence of mixed convection parameters λ_1 and λ_2 on radial component of velocity is shown via Figs. (8.3) and (8.4). Velocity is enhanced for higher values of λ_1 and λ_2. Since convection parameter shows the ratio between buoyancy and inertial forces so more buoyancy force is observed for larger convection parameter. It increases the velocity. Influences of Re on velocity components are given in Figs. (8.5-8.7). It is obvious from the graphs that movement of liquid particles decreases for higher Re. Physically it is due to higher viscous forces of the fluid which provides internal friction to the fluid particles and consequently velocity components in axial, tangential and radial directions decrease. Fig. 8.8 portrays outcomes of Eckert number Ec on temperature $\tilde{\theta}(\xi)$. An enhancement in temperature for higher values of Ec is noted. Conversion of mechanical energy into heat energy during the frictions of the molecules is the main reason for an increase in temperature of system. Influence of m (shape parameter) on temperature profile is given in Fig. (8.9). Different shaped nanoparticles e.g. brick, spherical, platelets and cylindrical were considered. In case of hybrid nanoparticles, the platelets are seen more efficient for heat transfer rate. Influence of Re on temperature profile is given through Fig. (8.10). For higher estimations of Re, the fluid particles speed up, which causes more collision between the particles. It produces internal heat in system and thus temperature profile increases. The contribution of both nanoparticles in the hybrid nanofluid for higher thermal properties is taken at different percentages as shown in Fig. (8.11). By taking equal amount of

both particles there is less efficiency. Taking 70% Al_2O_3 and 30% of Cu gives better results than any other quantity as shown in Fig. (8.11).

Drag forces (presented in Tables. 8.3 and 8.4) are showing the impacts of different parameters on skin friction components. Surface drag force is decreased for larger mixed convection parameters λ_1, λ_2 and stretching parameter A. Table. 8.5 portrays the influence of Re and Ec on Nusselt number. Heat transfer rate increases with and Ec.
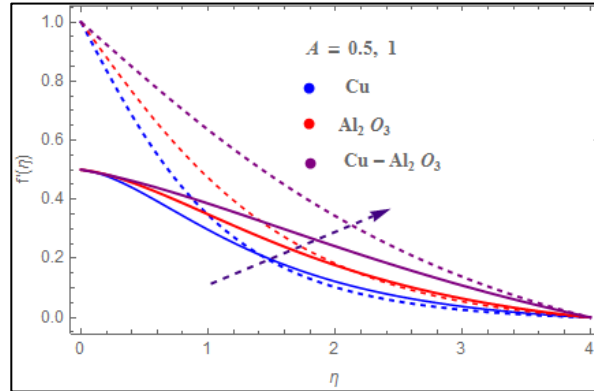
Fig.8.2 $f'(\eta)$ via A.
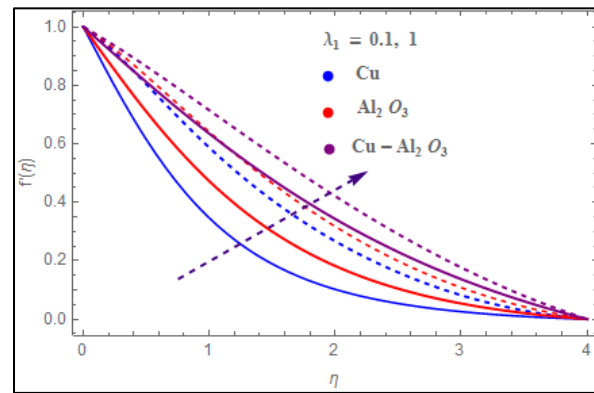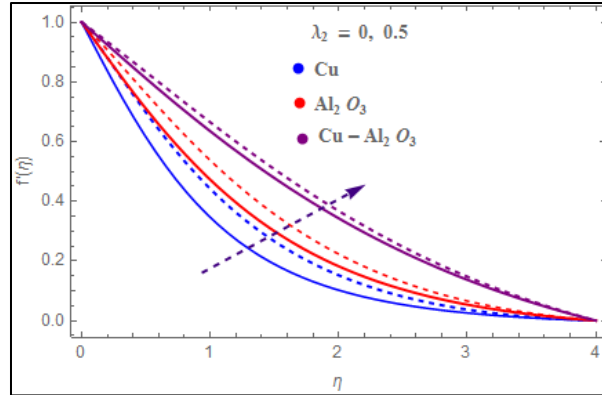

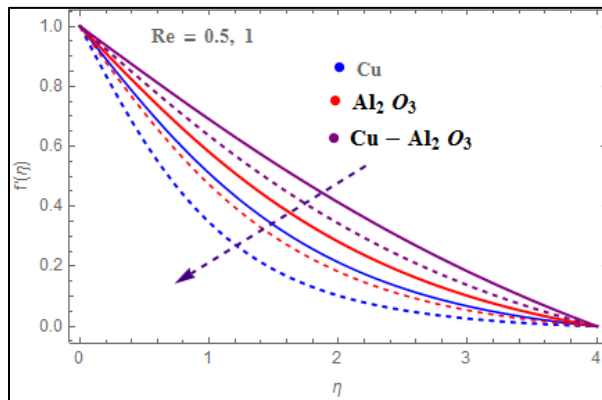Fig.8.3 $f'(\eta)$ via λ_1

Fig.8.4 $f'(\eta)$ via λ_2.

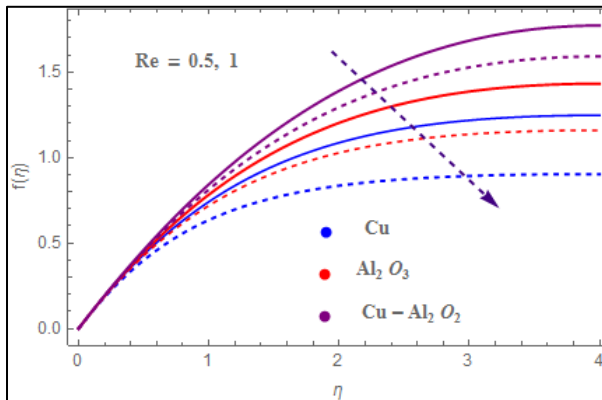Fig.8.5 $f'(\eta)$ via Re

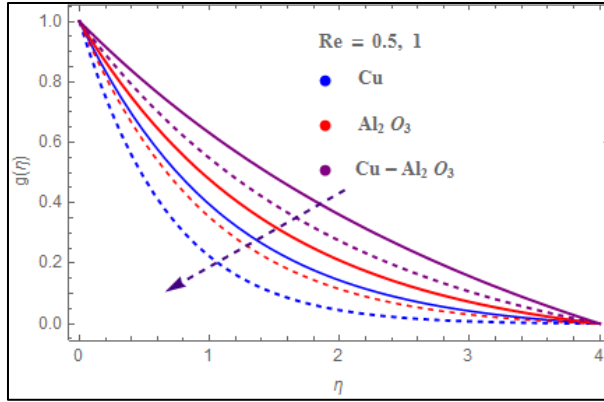Fig. 8.6 $f(\eta)$ via Re.
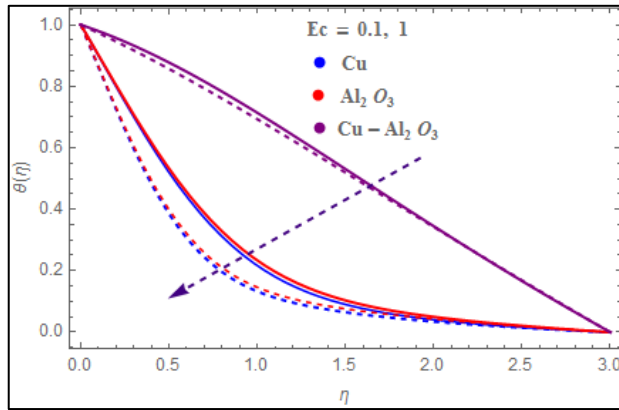
Fig.8.7 $g(\eta)$ via Re
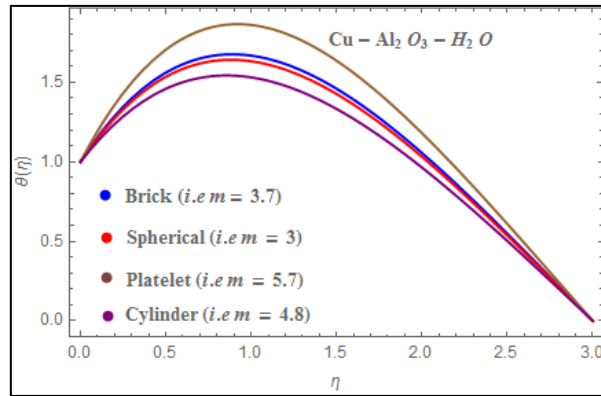

Fig. 8.8 $\theta(\eta)$ via Ec
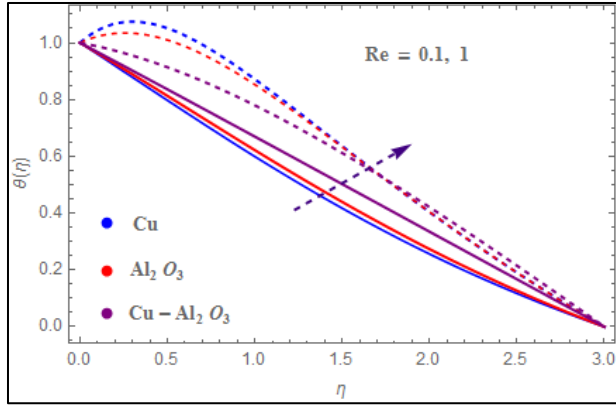

Fig. 8.9 $\theta(\eta)$ via m.
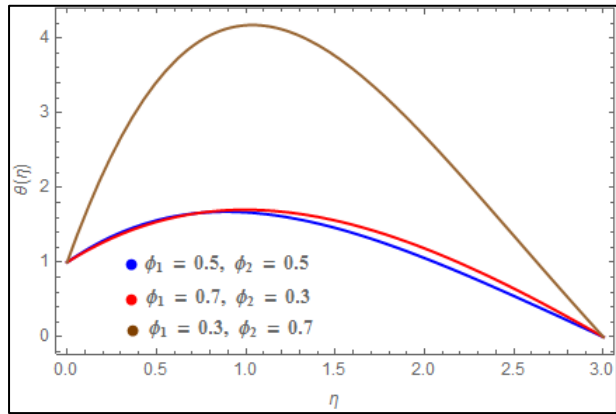
Fig.8.10 $\theta(\eta)$ via Re.

Fig.8.11 $\theta(\eta)$ via different concentrations
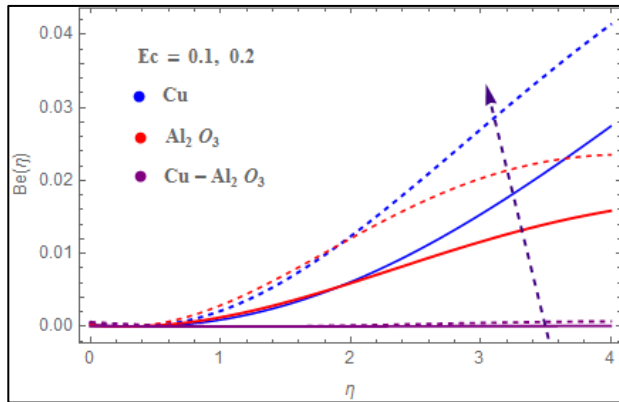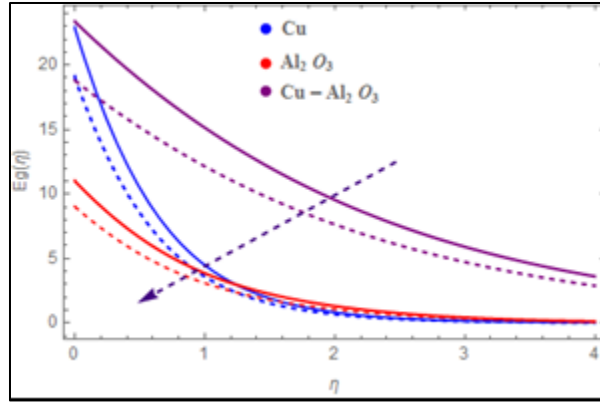

Fig. 8.13 $Be(\eta)$ via Ec.
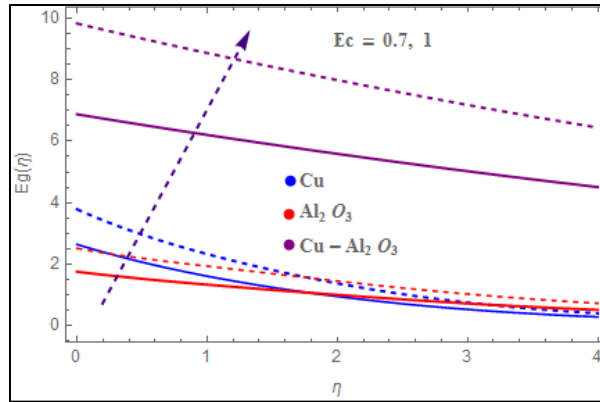
Fig. 8.14 $Eg(\eta)$ via $\tilde{\theta}_w$
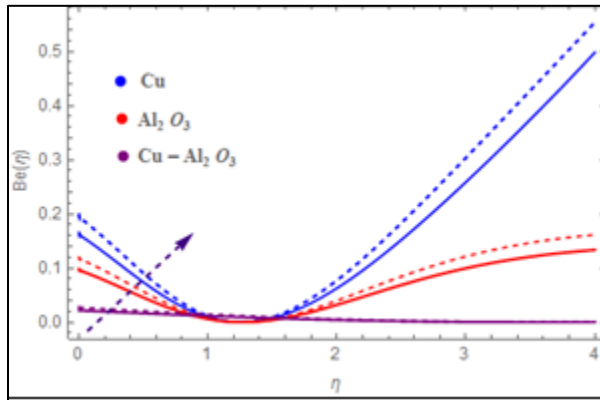

Fig.8.14 $Eg(\eta)$ via Ec

Fig. 8.15 $Be(\eta)$ via $\tilde{\theta}_w$

Entropy generation rate $(N_G(\xi))$

The influences of Ec and temperature difference parameter on $N_G(\xi)$ and Be are shown through Figs. $(8.12 - 8.15)$. Behavior of Ec number on entropy and Bejan number is sketched graphically

119

in Figs. (8.12) and (8.13). Since Ec is related to kinetic energy of system, so by increasing Ec more kinetic energy is produced inside the system and thus entropy increases. Effect of thermal irreversibilities is more than fluid friction and magnetic irreversibilities. So Bejan number increase for higher values of Ec as shown in Fig (8.13). Effect of temperature ratio parameter for entropy E_g and Bejan number Be is given in Figs. (8.14) and (8.15). The main reason for entropy of the system to decrease is lower temperature difference. Less heat is transferred to the system and so less entropy is observed. Yet the effect of thermal irreversibilities is dominates than the total irreversibilities. Hence larger values of temperature ratio parameter increases the Bejan number.

Conclusions

MHD radiative flow of hybrid nanofluid due to a rotating stretchable disk is analyzed with Joule heating, mixed convection and dissipation effects. The obtained results are:

- Velocity components are higher for stretching and mixed convection parameters.
- Temperature $\tilde{\theta}(\xi)$ is an increasing function of Ec.
- Drag force in radial direction decreases for larger A, λ_1, λ_2 and Re.
- Temperature gradient $Nu_x Re^{\frac{-1}{n+1}}$ increases for higher Ec.
- Entropy enhances for larger values of Ec.
- Bejan number Be increases for Ec and temperature ratio parameter.

Chapter 9

Entropy minimization in flow of non-Newtonian nanofluid with activation energy and binary chemical reaction.

Abstract: Our motivation here is to analyze the radiative mixed convective flow of Casson nanofluid over a stretching surface. The properties of heat transfer with nonlinear thermal radiation, viscous dissipation and heat generation/absorption are analyzed. Total entropy is first calculated and then shown graphically for different involved parameters. Velocity is studied with uniform magnetic field and nonlinear mixed convection. Brownian diffusion, activation energy and thermophoresis effects are considered. Governing equations are converted from partial differential equations into their corresponding ordinary ones using appropriate transformations. ND solve technique is utilized to solve these equations. Main outcomes are presented graphically.

Mathematical description

Here flow of MHD mixed convective Casson nanofluid with entropy minimization and Bejan number has been investigated. Non-linear thermal radiation, mixed convection, activation energy and viscous dissipation are examined. Sheet is stretched with a stretching rate a. Joule heating and convective boundary conditions for heat transfer are considered T_w and C_w are the values of wall temperature and wall concentration respectively (see Fig. 9.1).
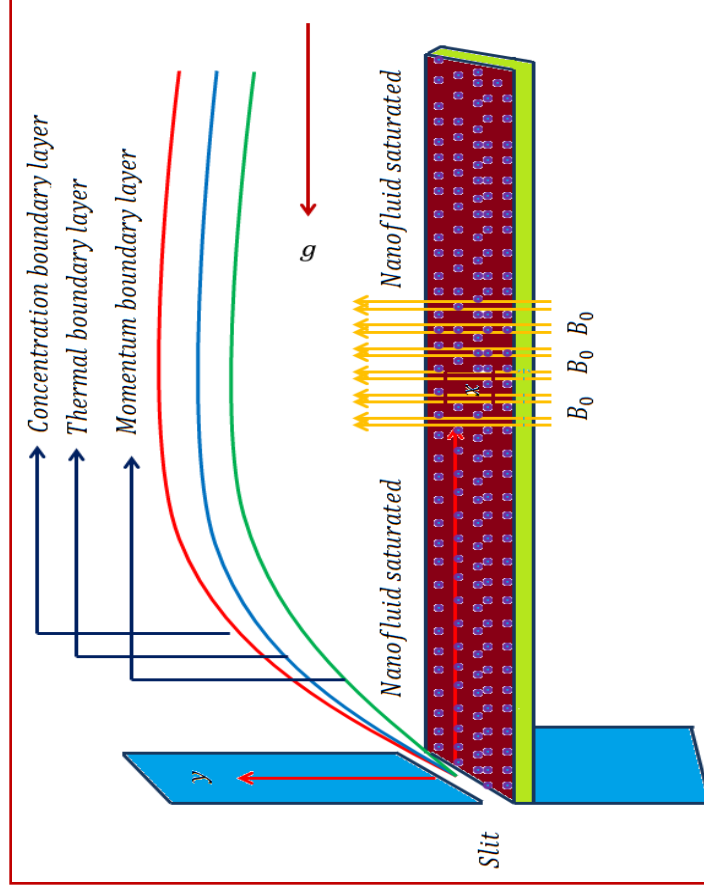
$Fig. 9.1: Flow\ diagram$

Magnetic field is applied in normal direction to the sheet. Governing equations are:

$$\frac{\partial u}{\partial x} + \frac{\partial v}{\partial y} = 0,\tag{9.1}$$

$$\left.\begin{aligned}u\frac{\partial u}{\partial x} + v\frac{\partial u}{\partial y} &= \mu\left(1+\frac{1}{\beta}\right)\left(\frac{\partial^2 u}{\partial y^2}\right) + u_e\frac{du_e}{dx} - \frac{\sigma B_0^2}{\rho}(u - u_e)\\ &+ g(\lambda_1(T - T_\infty) + \lambda_2(T - T_\infty)^2) + g(\lambda_3(C - C_\infty) + \lambda_4(C - C_\infty)^2),\end{aligned}\right\}\tag{9.2}$$

$$\left.\begin{aligned}u\frac{\partial T}{\partial x} + v\frac{\partial T}{\partial y} &= \alpha\frac{\partial^2 T}{\partial y^2} + \frac{1}{\rho c_p}\frac{\partial q_r}{\partial y} + \tau\left(D_B\frac{\partial T}{\partial y}\frac{\partial C}{\partial y} + \frac{D_T}{T_\infty}\left(\frac{\partial T}{\partial y}\right)^2\right) + \frac{\mu}{\rho c_p}\left(1+\frac{1}{\beta}\right)\left(\frac{\partial u}{\partial y}\right)^2\\ &+ \frac{\sigma}{\rho c_p}B_0^2 u^2 + \frac{Q^*}{\rho c_p}(T - T_\infty),\end{aligned}\right\}\tag{9.3}$$

$$u\frac{\partial C}{\partial x} + v\frac{\partial C}{\partial y} = \frac{D_T}{T_\infty}\frac{\partial^2 T}{\partial y^2} + D_B\frac{\partial^2 C}{\partial y^2} - k_r^2(C - C_\infty)\left(\frac{T}{T_\infty}\right)^n exp\left[\frac{-E_a}{\kappa T}\right],\tag{9.4}$$

$$\left.\begin{aligned}u = u_w = ax, v = 0, -k\frac{\partial T}{\partial y} = h_f\left(T_f - T\right), C = C_w, \text{ at } y = 0,\\ u = u_e = cx, T \to T_\infty, C \to C_\infty \text{ when } y \to \infty,\end{aligned}\right\}\tag{9.5}$$

where ρ denotes the density, u, v the velocity components, B_0 the strength of magnetic field, x, y the Cartesian coordinates, μ the dynamic viscosity, u_e the free stream velocity, β the Casson

122

parameter or material parameter, g the gravity acceleration, T the temperature, σ the electrical conductivity, α the thermal diffusivity, c_p the specific heat capacity, q_r the radiative flux coefficient, D_B the diffusion coefficient, Q^* the heat generation coefficient, C the concentration, D_T the thermophoretic coefficient, λ_1 and λ_2 the coefficient of linear and nonlinear thermal expansion, T_∞ the ambient temperature, λ_3 and λ_4 the coefficient of linear and nonlinear concentration expansion, C_∞ the ambient concentration, k_r^2 the coefficient of chemical reaction, n the fitted rate constant, T_f the fluid or surface temperature, h_f the coefficient of convective heat transport, C_w the surface concentration, κ the Boltzmann constant, E_a the coefficient of activation energy, ν the kinematic viscosity and τ the ratio of base fluid and nanoparticles heat capacities. Mathematically q_r is addressed as:

$$q_r = -\frac{16\sigma^*}{3k^*}\left[3T^2\left(\frac{\partial T}{\partial y}\right)^2 + T^3\frac{\partial^2 T}{\partial y^2}\right], \tag{9.6}$$

where σ^* symbolizes the Stefan-Boltzmann coefficient and k^* signifies the absorption coefficient. Transformations for the given flow problem are:

$$\left.\begin{array}{l} \eta = \sqrt{\frac{a}{\nu}}y, u = axf'(\eta), v = -\sqrt{a\nu}f(\eta), \\[2mm] \theta = \frac{T-T_\infty}{T_f-T_\infty}, \phi = \frac{C-C_\infty}{C_f-C_\infty}. \end{array}\right\} \tag{9.7}$$

Condition of incompressibility is identically satisfied and Eqs. (9.2-9.5) yield

$$\left.\begin{array}{l} \left(1+\frac{1}{\beta}\right)f''' - f'^2 + ff'' - Ha(f'-A) + A^2 \\[2mm] +\lambda\theta(1+\beta_t^*\theta) + \phi\lambda N^*(1+\beta_c^*\phi) = 0, \end{array}\right\} \tag{9.8}$$

$$\left.\begin{array}{l} \frac{1}{Pr}\theta'' + \frac{4}{3}R_d(\theta(\theta_w-1)+1)^2(3\theta'^2(\theta_w-1)+\theta(\theta_w-1)+1)\theta'' \\[2mm] +\gamma\theta + Nt\theta'^2 + Nb\theta'\varphi' + f\theta' + HaEcf'^2 + Ec\left(1+\frac{1}{\beta}\right)f''^2 = 0, \end{array}\right\} \tag{9.9}$$

$$\frac{1}{Sc}\varphi'' + \frac{1}{Sc}\left(\frac{Nt}{Nb}\right)\theta'' + f\varphi' + \sigma_1(\alpha_1\theta+1)^m \exp\left[\frac{-\Gamma}{1+\alpha_1\theta}\right] = 0, \tag{9.10}$$

$$\left.\begin{array}{l} f(0) = 0, \quad f'(0) = 1, \quad f'(\infty) = A, \\[2mm] \theta'(0) = -\beta_t\big(1-\theta(0)\big), \quad \phi(0) = 1, \\[2mm] \theta(\infty) = 0, \quad \phi(\infty) = 0. \end{array}\right\} \tag{9.11}$$

The dimensionless variables are addressed as

$$Ha = \frac{\sigma B_0^2}{\rho a}, Pr = \frac{\rho c_p \nu}{k}, A = \frac{c}{a}, \theta_w = \frac{T_w}{T_\infty}, \Gamma = \frac{E_a}{\kappa T_\infty}, R_d = \frac{16\sigma^* T_\infty^3}{3kk^*},$$

$$\beta_t^* = \frac{\lambda_3(T_w - T_\infty)}{\lambda_1}, \quad \beta_c^* = \frac{\lambda_4(C_w - C_\infty)}{\lambda_3}, \quad \lambda = \frac{Gr_x}{Re_x^2}, Ec = \frac{a^2 x^2}{c_p(T_w - T_\infty)}, \gamma = \frac{Q_0}{a\rho c_p},$$

$$Gr_x = \frac{g\lambda_1(T_w - T_\infty)x^3}{\nu^2}, Gr^* = \frac{g\lambda_3(C_w - C_\infty)x^3}{\nu^2}, Nt = \frac{\tau D_T(T_f - T_\infty)}{T_\infty \nu}, Nb = \frac{\tau D_B(C_f - C_\infty)}{\nu},$$

$$N^* = \frac{Gr_x^*}{Gr_x} = \frac{\lambda_3(C_w - C_\infty)}{\lambda_1(T_w - T_\infty)}, \quad Sc = \frac{\nu}{D_B}, \quad \sigma_1 = \frac{k_r^2}{a}, \beta_t = \frac{h_f}{k}\sqrt{\frac{\nu}{a}}, \quad \alpha_1 = \frac{T_f - T_\infty}{T_\infty}.$$

(9.12)

where Ha denotes the magnetic parameter, Pr the Prandtl number, A the stretching parameter, θ_w the temperature difference parameter, β_t^*, β_c^* the nonlinear mixed convections for temperature and concentration, λ the mixed convection variable, Γ the activation energy parameter, R_d the radiation parameter, λ_1 the thermal buoyancy parameter, Re_x the local Reynold number, λ_2 the ratio of thermal to concentration buoyancy, Gr_x^*, Gr_x the concentration and temperature respectively, Ec the Eckert number, γ the heat generation parameter, Nb Brownian diffusion parameter, N^* ratio of concentration to buoyancy forces, Sc the Schmidt number, Nt the thermophoresis constant, σ_1 the chemical reaction parameter, β_t the Biot number and α_1 the ratio of temperature parameter.

Physical quantities

Mathematical equations for drag force, heat and mass transfer rates are:

$$C_f = \frac{2\tau_w}{\rho u_w^2}, \tag{9.13}$$

$$Nu_x = \frac{xq_w}{k(T_w - T_\infty)}\bigg|_{y=0}, \tag{9.14}$$

$$Sh_x = \frac{xq_m}{D_B(C_w - C_\infty)}\bigg|_{y=0}, \tag{9.15}$$

where τ_w, q_w are q_m are defined

$$\tau_w = \mu\left(1 + \frac{1}{\beta}\right)\frac{\partial u}{\partial y}\bigg|_{y=0}, \tag{9.16}$$

$$q_w = -k\left(\frac{\partial T}{\partial y}\right)_{y=0} + q_r, \tag{9.17}$$

$$q_m = -D_B\frac{\partial C}{\partial y}\bigg|_{y=0}. \tag{9.18}$$

Finally, we have

$$\frac{1}{2}C_{fx}Re^{0.5} = \left(1 + \frac{1}{\beta}\right)f''(0), \tag{9.19}$$

$$Re^{-0.5}Nu_x = -\left(1 + \frac{4}{3}R_d(1 + (\theta_w - 1)\theta(0))^3\right)\theta'(0), \tag{9.20}$$

$$Sh_x \, Re^{-0.5} = -\phi'(0). \tag{9.21}$$

Entropy generation

Entropy is shown as

$$
\begin{aligned}
S_G = \frac{k}{T_\infty^2}\left(1 + \frac{16\sigma^* T^3}{3kk^*}\right)\left(\frac{\partial T}{\partial y}\right)^2 + \frac{\mu}{T_\infty}\left(1 + \frac{1}{\beta}\right)\left(\frac{\partial u}{\partial y}\right)^2 + \frac{\sigma B_0^2}{T_\infty}u^2 \\
+ \frac{RD}{T_\infty}\left(\frac{\partial C}{\partial y}\frac{\partial T}{\partial y}\right) + \frac{RD}{C_\infty}\left(\frac{\partial C}{\partial y}\right)^2,
\end{aligned}
\tag{9.22}
$$

The dimensionless form is

$$
\begin{aligned}
N_G = (1 + R_d(\theta(\theta_w - 1) + 1)^3 \theta'^2 \alpha_1^* \\
+ \left(1 + \frac{1}{\beta}\right) Br f''^2 + HaBr f'^2 + \frac{\alpha_2^*}{\alpha_1^*} L\phi'^2 + L\theta'\phi',
\end{aligned}
\tag{9.23}
$$

where the dimensionless parameters are defined as

$$
\begin{aligned}
\alpha_1^* = \frac{\Delta T}{T_\infty}, \qquad N_G = \frac{S_G T_\infty \nu}{k \Delta T a}, \qquad Br = \frac{\mu u_w^2}{k \Delta T} \\
L = \frac{RD(C_f - C_\infty)}{C_\infty}, \qquad \alpha_2^* = \frac{\Delta C}{C_\infty}.
\end{aligned}
\tag{9.24}
$$

Note that $Br, \alpha_1^*, \alpha_2^*, N_G$ and L denote respectively the Brinkman number, nondimensional temperature ratio variable, concentration ratio variable, entropy generation rate and diffusive variable.

Mathematically Bejan number is

$$Be = \frac{entropy\ due\ to\ heat\ and\ mass\ transfers}{Total\ entropy\ generation}, \tag{9.25}$$

Solution technique

ND Solve is a numerical solver of differential equations. With the help of ND Solve technique we can handle various ODE's system as well as some specific PDE's system. For general ODE's system having number of equation n .i.e $(q_1, q_2, q_3, \ldots q_n)$, number of dependent variable n (i.e $u_1, u_2, u_3, \ldots u_n$), independent variable x and conditions according to the order system of ODE's. By ND Solve technique this system can be handled as

$NDSolve[\{q_1, q_2, q_3, \ldots q_n, \text{ boundary conditions}\}, \{u_1, u_2, u_3, \ldots u_n\}, \{x, x_{\min}, x_{\max}\}].$

Discussion

This section elaborates the detail of involved variables on velocity profile, temperature and

concentration fields.

Velocity

Fig. 9.2 shows the influence of N^* on velocity. More fluid motion is noted for higher values of N^* and therefore velocity is increased. Velocity field versus magnetic field is portrayed in Fig. 9.3. Since more Lorentz force is for increasing values of Ha, therefore fluid motion is opposed. Hence velocity decreases as seen in Fig. 9.3. Velocity is showing an increasing behavior for nonlinear mixed convection thermal variable in Fig. 9.4. Physically, temperature difference between the liquid particles increases which is the reason for the fluid velocity enhancement. Fig. 9.5 sketches the effect of nonlinear mixed variable subject to concentration on velocity. Here velocity field boosts up subject to larger nonlinear mixed convection variable subject to concentration. Fig. 9.6 displays the behavior of β on velocity distribution. For larger β, relaxation time is increased which reduces velocity of the fluid. Fig. 9.7 portrayed the impact of A on velocity distribution. Increasing trend is observed around stagnation point. No boundary layer exists when both sheet/wall and free stream velocity are same.
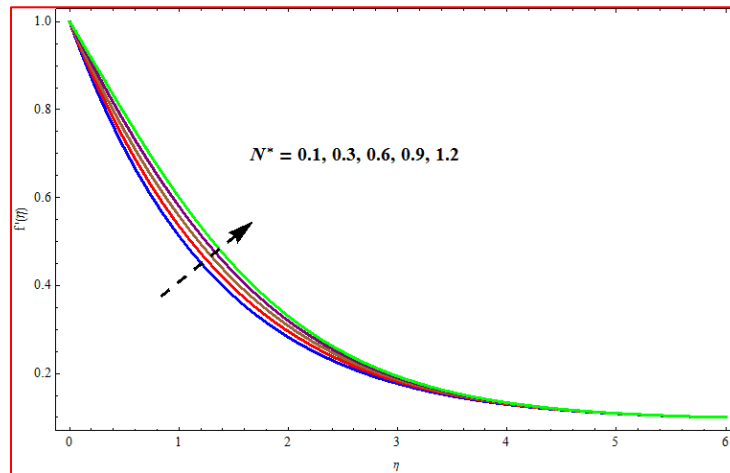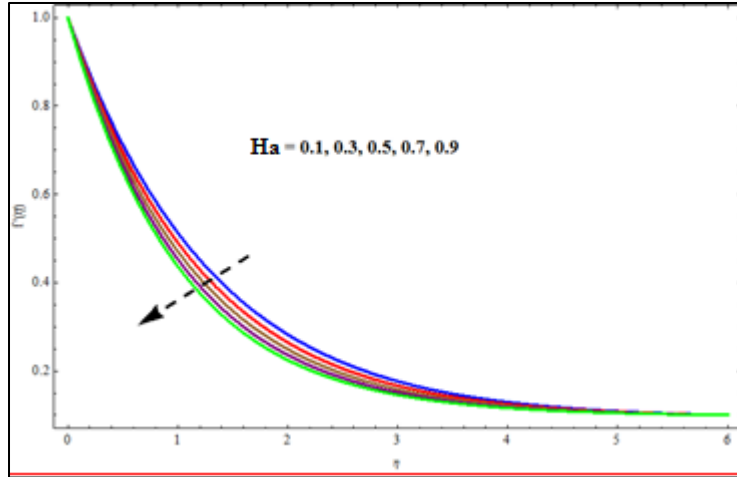

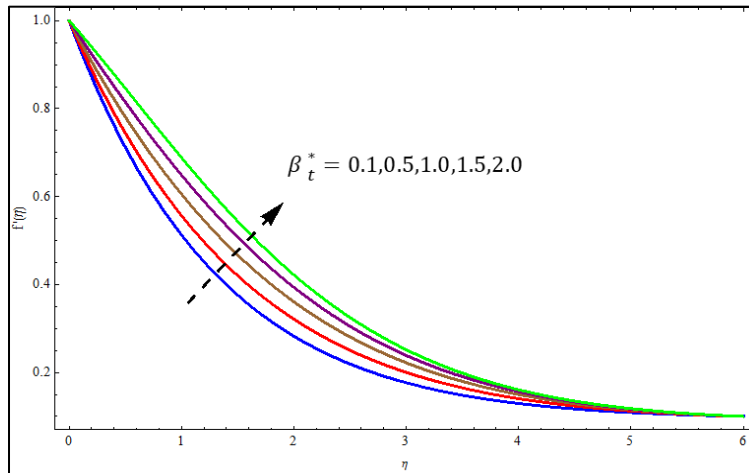$Fig. 9.2: f'(\eta)\ versus\ N^*.$

126

Fig. 9.3: $f'(\eta)$ *versus Ha.*

Fig. 9.4: $f'(\eta)$ *versus* β_t^*.
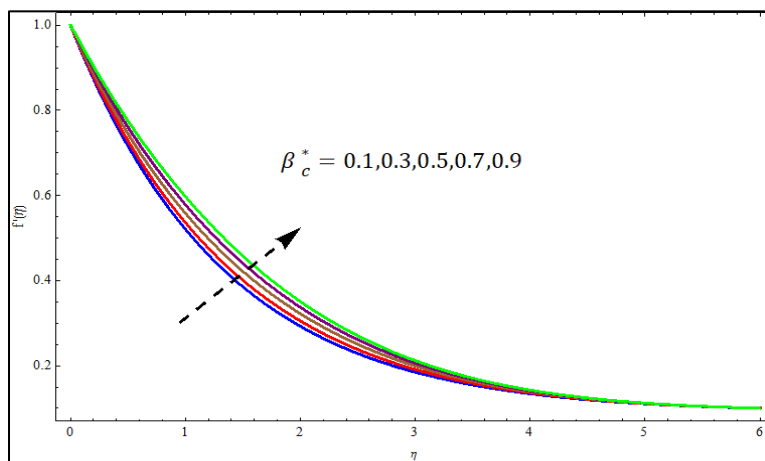
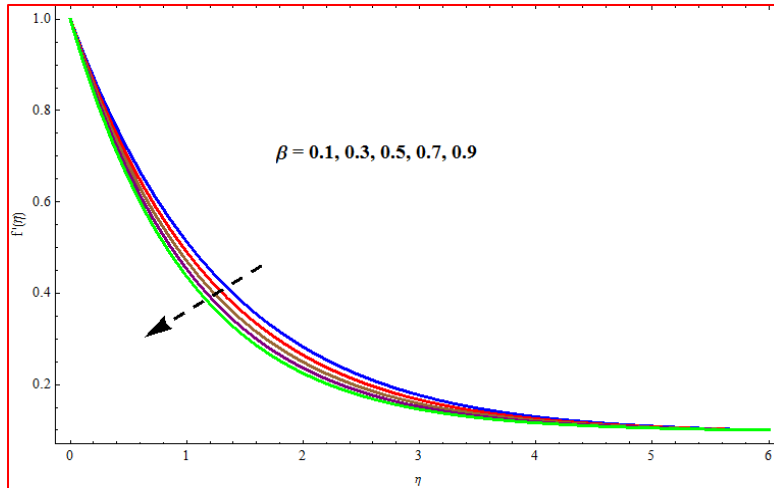*Fig.* 9.5: $f'(\eta)$ *versus* β_c^*.
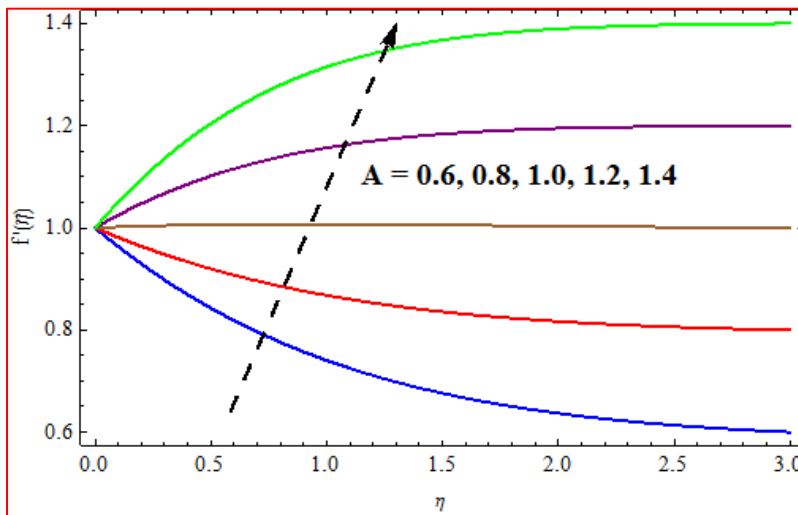
Fig. 9.6: $f'(\eta)$ *versus* β.

Fig. 9.7: $f'(\eta)$ *versus* A.

Temperature

Behaviors of different involved parameters such as thermophoresis parameter N_t, temperature ratio parameter θ_w, Brownian motion Nb, Eckert number Ec, Prandtl Pr and radiation parameter R_d on temperature are shown though Figs. 9.8-9.13. For larger N_t, motion of particles from hot to cold region increases which enhances temperature as given in Fig. 9.8. Similarly Brownian motion parameter N_b is responsible for enhancement in thermophoresis force, thus temperature rises (See Fig. 9.9). Increasing behavior is noted for larger values of temperature difference parameter and consequently it rises the temperature (see Fig. 9.10). Effect of Pr number on temperature is given in Fig. 9.11. Temperature decreases for higher Pr. Fig. 9.12 displays the temperature distribution

128

via Eckert number Ec. The internal friction between the layers result in the conversion of mechanical into thermal energy. Consequently, temperature of the system rises. Similarly more temperature distribution is observed for R_d. (See Fig. 9.13). Fig. 9.14 is presented to portray the influence of γ on temperature. Since more heat is provided which increases the temperature.
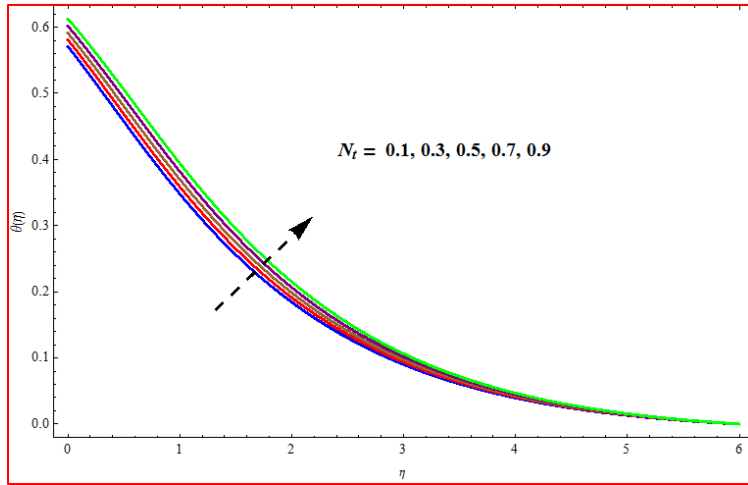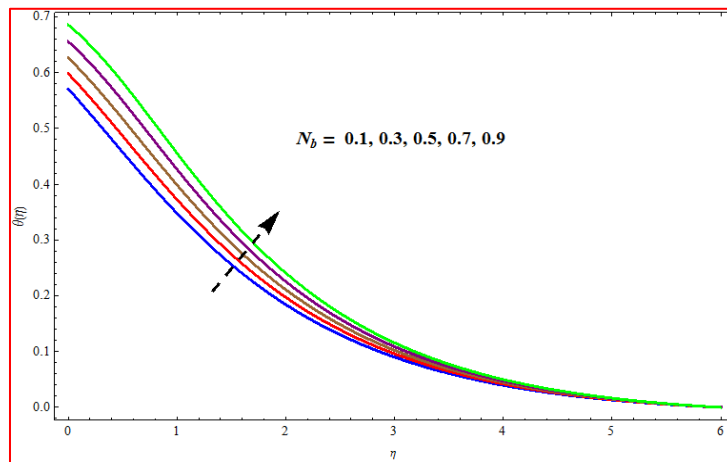

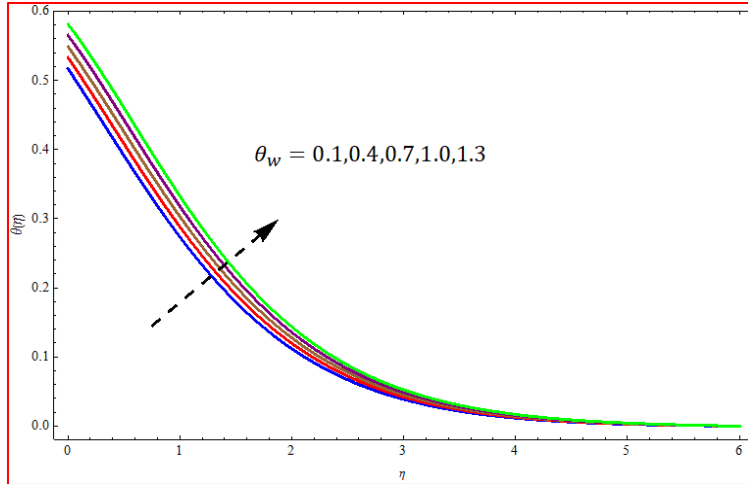$Fig. 9.8: \theta(\eta) \; versus \; N_t.$

$Fig. 9.9: \theta(\eta) \; versus \; N_b.$

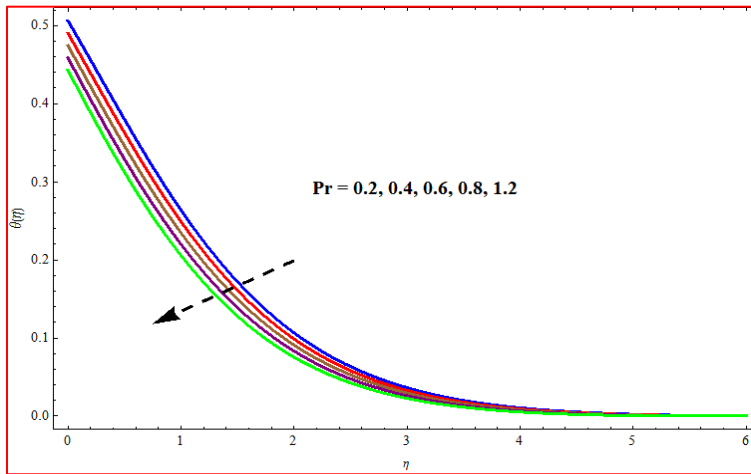*Fig.* 9.10: $\theta(\eta)$ *versus* θ_w.

Fig. 9.11: $\theta(\eta)$ *versus Pr*.

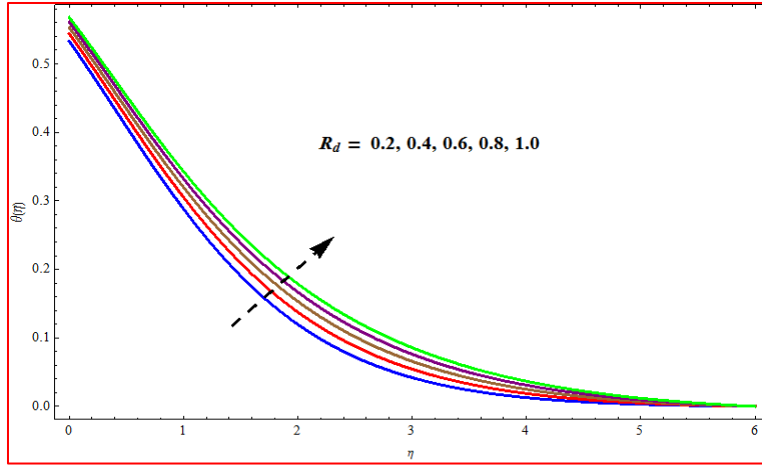*Fig.* 9.12: $\theta(\eta)$ *versus Ec*.

130
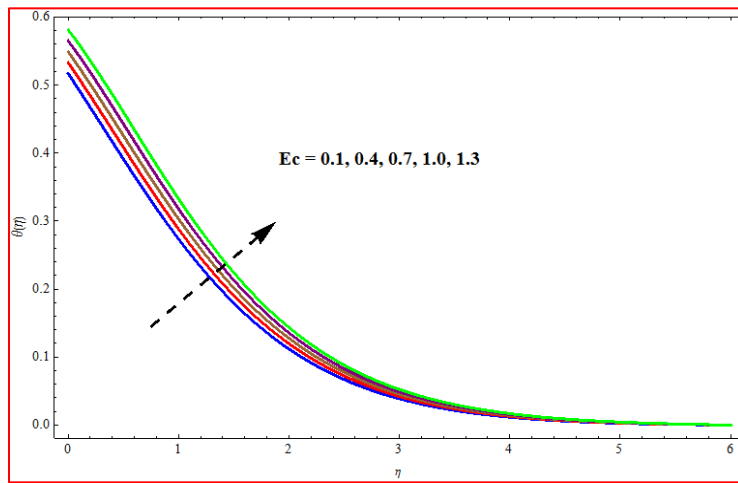
Fig. 9.13: $\theta(\eta)$ *versus* R_d.
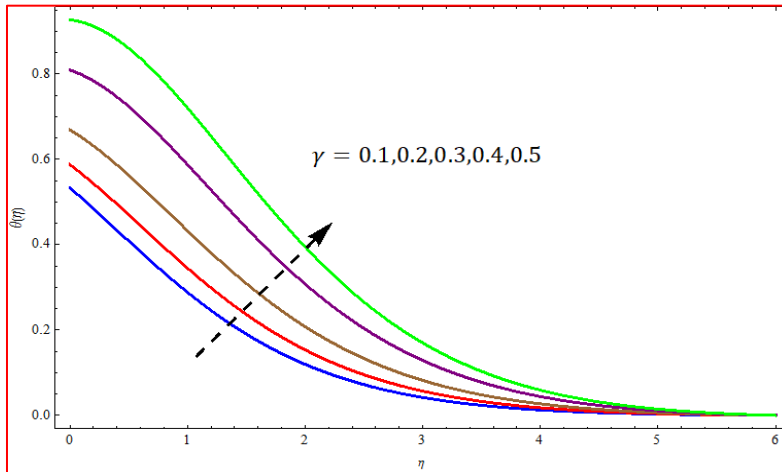
Fig. 9.14: $\theta(\eta)$ *versus* γ.

Concentration

Figs. 9.15-9.18 portray the influence of chemical reaction σ_1, thermophoresis N_t, Brownian motion N_b, Schmidt number Sc and activation energy Γ on concentration. Effect of chemical reaction on concentration field is shown in Fig. 9.15. It is noticed that concentration decreases for larger σ_1. For increasing σ_1 the destruction increases. Hence concentration decreases. Fig. 9.16 shows the impact of Schmidt number Sc on concentration field. Larger Sc results into decay of mass diffusion as well as its boundary layer. The effect of N_t on concentration profile is drawn through Fig. 9.17. Concentration increases for larger N_t. Effect of activation energy on concentration profile is shown in Fig. 9.18. Larger activation energy decays the Arrhenius function and it increases the productive chemical reaction. Thus concentration of the nanoparticles increases.
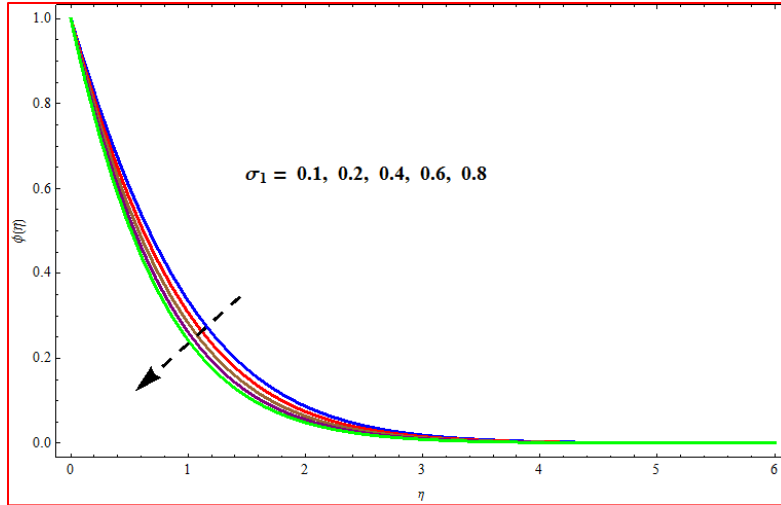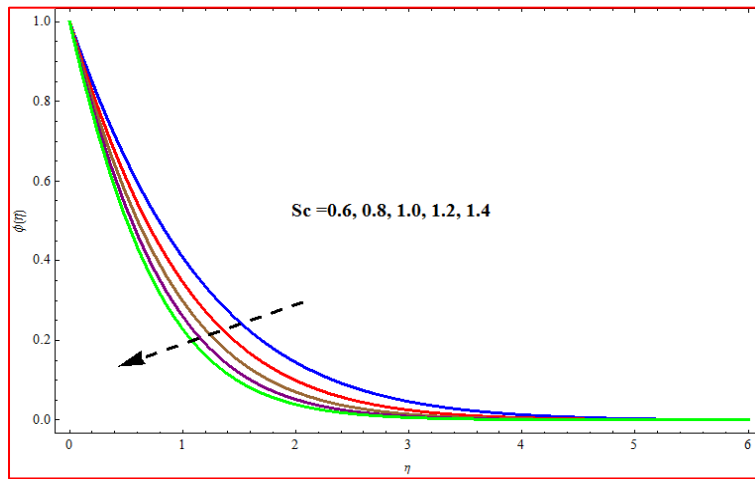
Fig. 9.15: $\phi(\eta)$ versus σ_1.
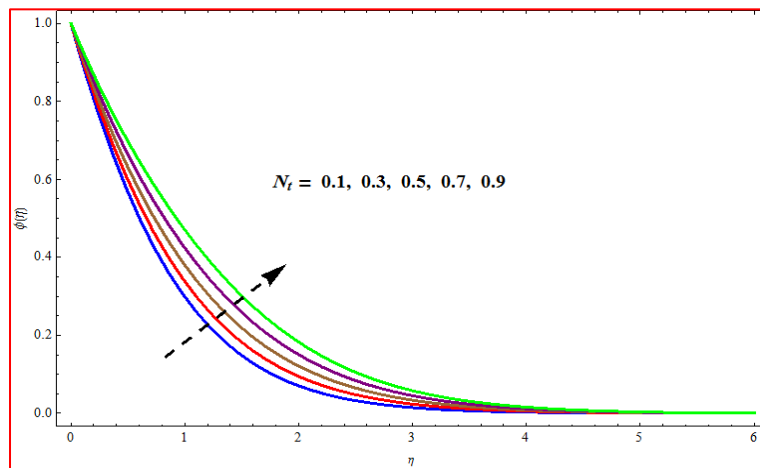

Fig. 9.16: $\phi(\eta)$ versus Sc.

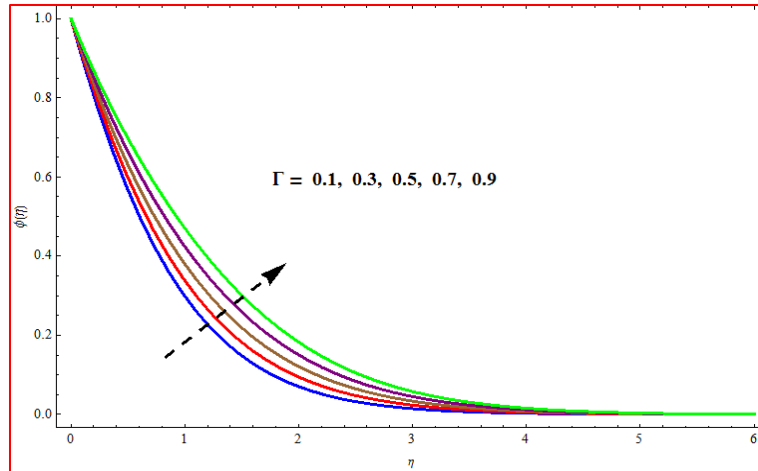Fig. 9.17: $\phi(\eta)$ versus N_t.

$Fig. 9.18: \phi(\eta) \ versus \ \Gamma.$

Entropy

This section describes in detail the quantities of engineering interests such as entropy optimization and Bejan number through different involved parameters. Figs. 9.19-9.32 are displayed for such purpose. Behaviors of β on N_G and Be are shown via Figs. 9.19 and 9.20. Higher β requires more relaxation time which is responsible for losing more heat. That is why entropy of the system declines (see Fig. 9.19). However for Bejan number the opposite trend is seen in Fig. 9.20. Here heat and mass transfer irreversibilities are dominating the viscous irreversibility and thus Be number increases. Behaviors of Brinkman number on N_G and Be are represented in Figs. 9.21 and 9.22. Here contrast impact is noticed for larger Brinkman number on both entropy and Bejan number. In Fig. 9.21 entropy increases while in Fig. 9.22 Bejan number decreases. Brinkman number Br always increases the entropy generation due to the heat conducting towards the fluid. (see Fig. 9.21). While opposite is the case for Bejan number. (See Fig. 9.22). Larger Hartmann number resists the fluid motion which enhances the entropy as given in Fig. 9.23. However increasing behavior is observed for Bejan number (see Fig. 9.24). Figs. 9.25 and 9.26 are sketched for the graphical interpretation of radiation parameter on both entropy and Bejan number. Clearly both entropy and well as Bejan number monotonically boosts up against larger radiation parameter. Figs. 9.27 and 9.28 highlight the salient features of Re on entropy as well as Bejan number. Clearly, both show inverse behavior against larger Re. Behavior of σ_1 on N_G and Be is displayed in Figs. 9.29 and 9.30. For higher σ_1, an enhancement in k_r is observed which results an increase in entropy generation. While Bejan number decays against reaction parameter (see Fig. 9.30). Influences of

diffusion parameter L on N_G and Be are shown through Figs. 9.31 and 9.32. Both increase for larger L due to more disturbance produced in the system and thus entropy enhances.
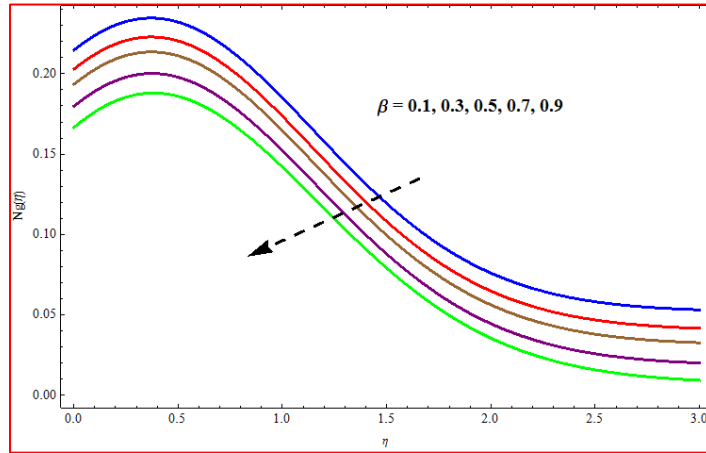
$Fig. 9.19: Ng(\eta) \; versus \; \beta.$
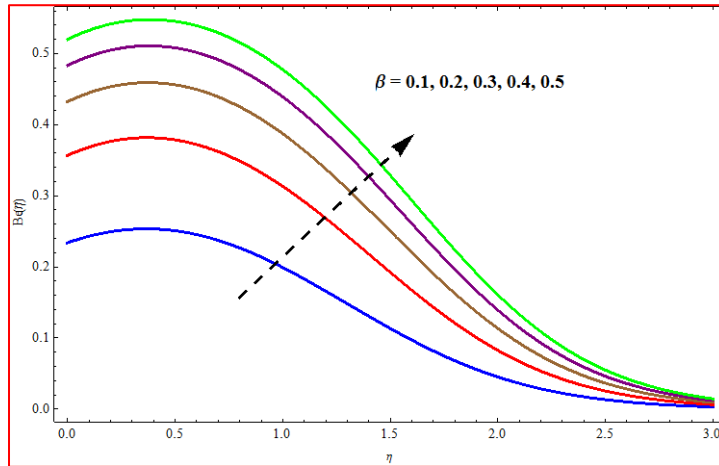
$Fig. 9.20: Be(\eta) \; versus \; \beta.$
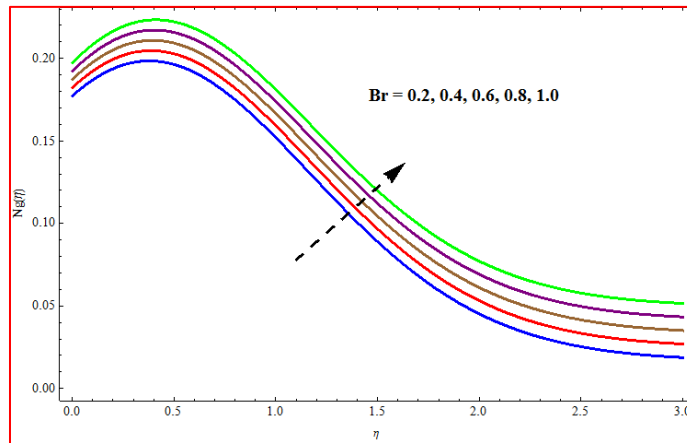
$Fig. 9.21: Ng(\eta) \; versus \; Br.$

$Fig. 9.22: Be(\eta) \ versus \ Br.$

$Fig. 9.23: Ng(\eta) \ versus \ Ha.$
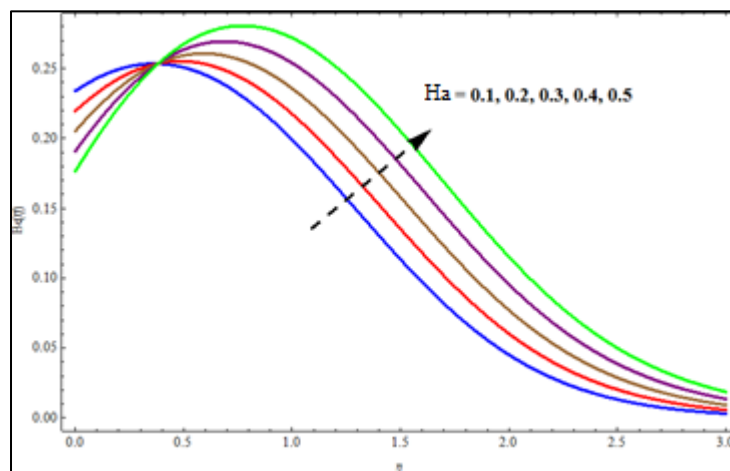
$Fig. 9.24: Be(\eta) \ versus \ Ha.$
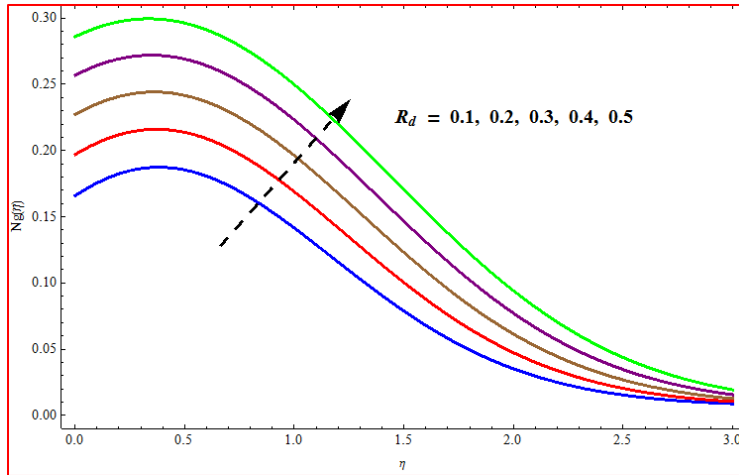
Fig. 9.25: $Ng(\eta)$ *versus* R_d.
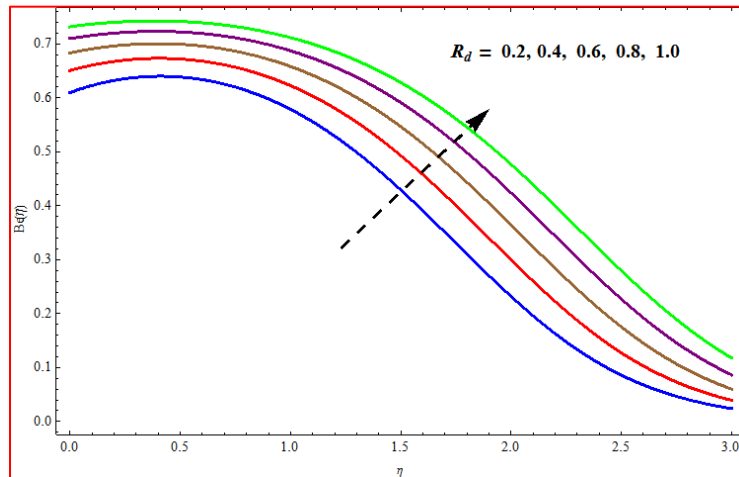
Fig. 9.26: $Be(\eta)$ *versus* R_d.

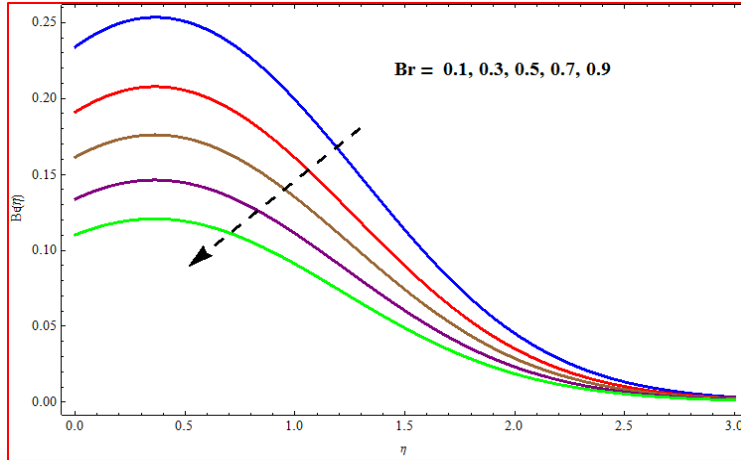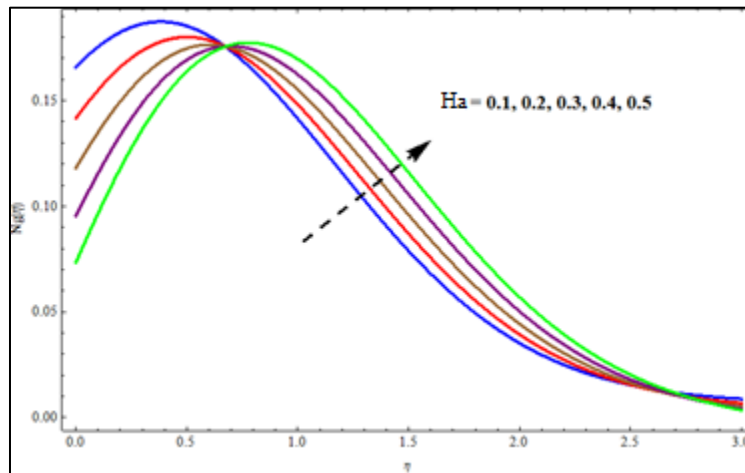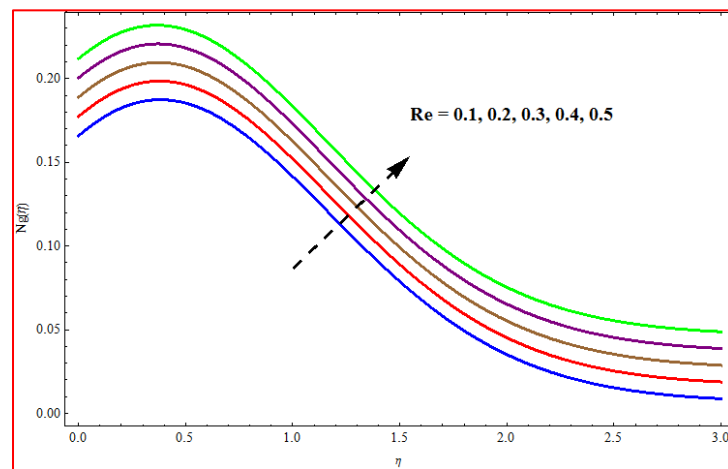*Fig.* 9.27: $Ng(\eta)$ *versus* Re.
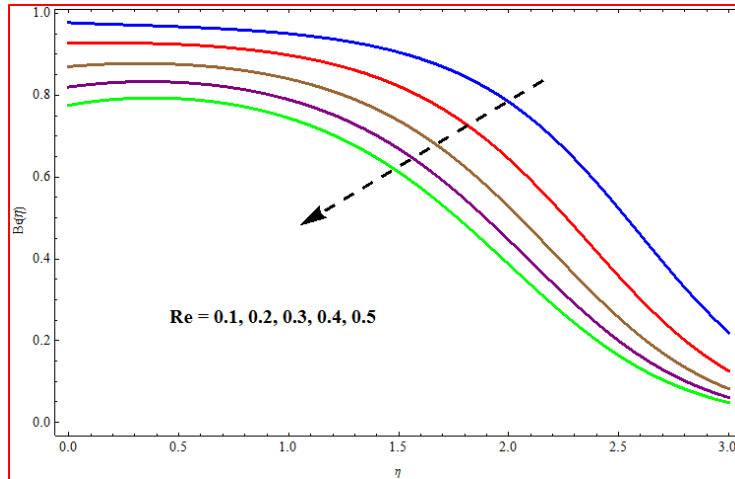
$Fig. 9.28: Be(\eta) \; versus \; Re.$
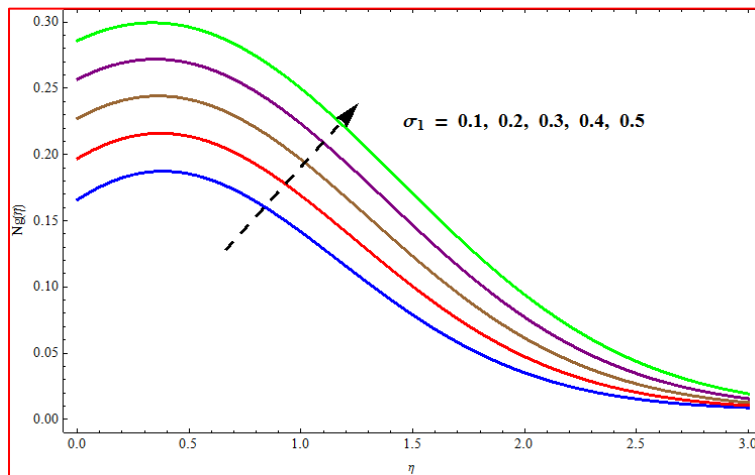
$Fig. 9.29: Ng(\eta) \; versus \; \sigma_1.$
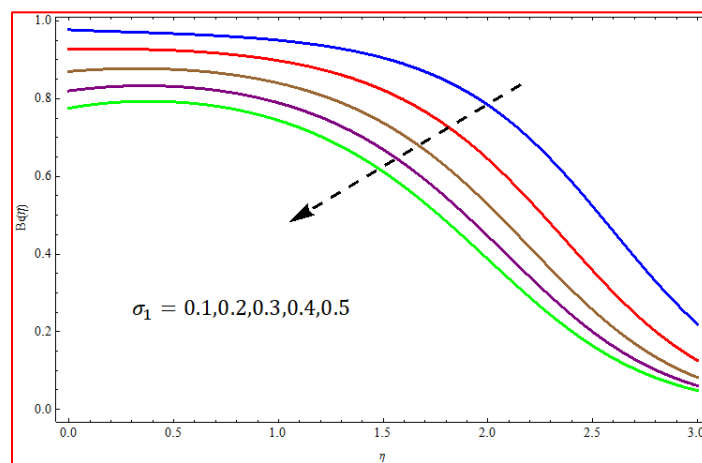
$Fig. 9.30: Be(\eta) \; versus \; \sigma_1.$
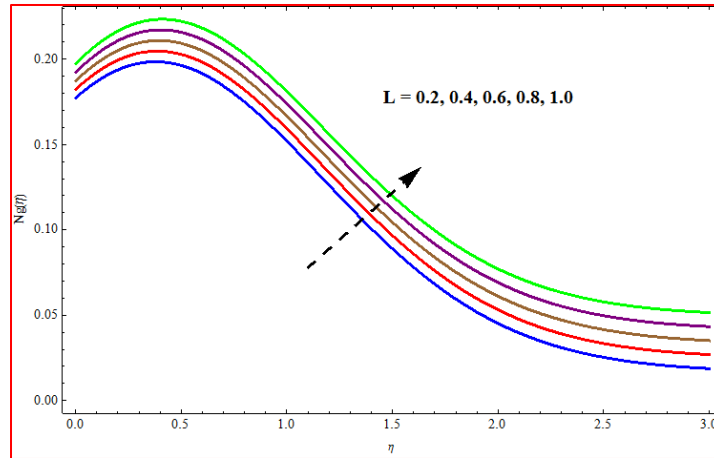
Fig. 9.31: $Ng(\eta)$ *versus L.*
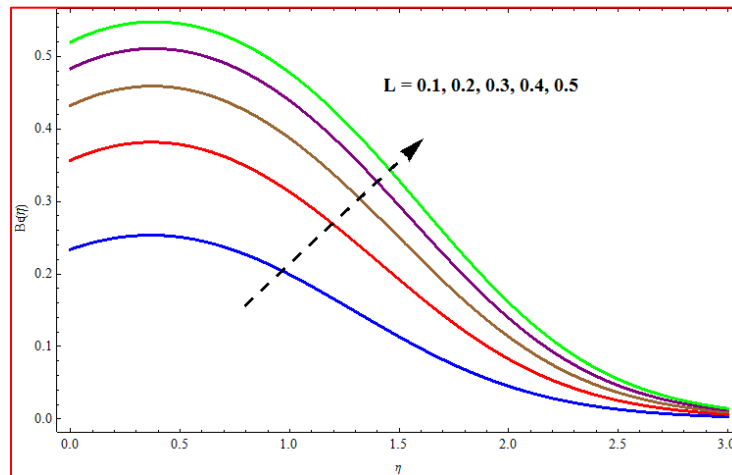
Fig. 9.32: $Be(\eta)$ *versus L.*

Concluding remarks

Here nonlinear radiative and mixed convective flow of Casson fluid is discussed. Heat generation, activation energy and magnetic effects are calculated. Key points are:

- Velocity of the liquid particles enhances versus N^* while it declines against magnetic parameter.
- Thermal field is more prominent against larger Eckert number, Brownian motion and thermophoresis variables.
- Concentration field declines against reaction variable.
- Entropy and Bejan number show inverse impact against material parameter.

References

1. L.J. Crane, Flow past a stretching plate, Zeitschrift Für Angewandte Mathematik und Physik (ZAMP), 21 (4) (1970) 645-647.

2. B.K. Dutta, P. Roy and A.S. Gupta, Temperature field in flow over a stretching sheet with uniform heat flux, Int. Commun. Heat Mass Transfer, 12 (1) (1985) 89-94.

3. M.I. Char, Heat transfer of a continuous, stretching surface with suction or blowing, J. Math Anal. Appl., 135 (2) (1988) 568-580.

4. P.S. Gupta and A.S. Gupta, Heat and mass transfer on a stretching sheet with suction or blowing, Can. J. Chem. Eng., 55 (6) (1977) 744-746.

5. S. Nadeem, R.U. Haq and Z.H. Khan. Heat transfer analysis of water-based nanofluid over an exponentially stretching sheet, Alexandria Eng. J., 53 (1) (2014) 219-224.

6. S. Mukhopadhy, Slip effects on MHD boundary layer flow over an exponentially stretching sheet with suction/blowing and thermal radiation, Ain Shams Eng. J., 4 (3) (2013) 485-491

7. Y. Zhang, M. Zhang and Y. Bai, Unsteady flow and heat transfer of power-law nanofluid thin film over a stretching sheet with variable magnetic field and power-law velocity slip effect, J. Taiwan Inst. Chem. Eng., 70 (2017) 104-110.

8. A. Majeed, A. Zeeshan and R. Ellahi, Unsteady ferromagnetic liquid flow and heat transfer analysis over a stretching sheet with the effect of dipole and prescribed heat flux, J. Mol. Liq., 223 (2016) 528-533

9. D. Pal and P. Saha, Influence of nonlinear thermal radiation and variable viscosity on hydromagnetic heat and mass transfer in a thin liquid film over an unsteady stretching surface, Int. J. Mech. Sci., 119 (2016) 208-216.

10. P. Weidman and M.R. Turner, Stagnation-point flows with stretching surfaces: a unified formulation and new results, Eur. J. Mech. B-Fluids, 61 (2017) 144-153.

11. A.W. Sisko, The flow of lubricating greases, Ind. Eng. Chem. Res., 50 (1958) 1789-1792.

12. A. Shaheen and M. I. Asjad, Peristaltic flow of a Sisko fluid over a convectively heated surface with viscous dissipation, J. Phys. Chem. Solid., 122 (2018) 210-217.

13. R. Malik, M. Khan and M. Mushtaq, Cattaneo-Christov heat flux model for Sisko fluid flow past a permeable non-linearly stretching cylinder, J. Mol. Liq., 222 (2016) 430-434.

14. O.D. Makinde, Effects of viscous dissipation and Newtonian heating on boundary-layer flow of nanofluids over a flat plate. Int. J. Numer. Meth. Heat & Fluid Flow, 23 (2013)1291-1303.

15. T Hayat, M. Khan, M. Waqas, T. Yasmeen and A. Alsaedi, Viscous dissipation effect in flow of magneto-nanofluid with variable properties. J. Mol. Liq., 222 (2016).47-54.

16. T. Hayat, M. Sajid and I. Pop, Three-dimensional flow over a stretching surface in a viscoelastic fluid, Nonlinear Anal: Real World Appl., 9, (2008) 1811-1822.

17. Z. Abbas, Y. Wang, T. Hayat and M. Oberlack, Mixed convection in the stagnation-point flow of a Maxwell fluid towards a vertical stretching surface, Nonlinear Anal: Real World Appl., 11 (2010) 3218-3228,

18. T. Hayat, T. Javed and Z. Abbas, MHD flow of a micropolar fluid near a stagnation-point towards a non-linear stretching surface, Nonlinear Anal: Real World Appl., 10 (2009) 1514-1526.

19. A. Mushtaq, M. Mustafa, T. Hayat and A. Alsaedi, Numerical study for rotating flow of nanofluids caused by an exponentially stretching sheet, Adv. Powder Techol., 27 (2016) 2223-2231.

20. T Hayat, M. I. Khan, S. Qayyum, A. Alsaedi and M. I. Khan, New thermodynamics of entropy generation minimization with nonlinear thermal radiation and nanomaterials, Phys. Lett. A, 382 (2018) 749-760.

21. M.I. Khan, T. Hayat, M.I. Khan, M. Waqas and A. Alsaedi, Numerical simulation of hydromagnetic mixed convective radiative slip flow with variable fluid properties: A mathematical model for entropy generation, J. Phys. Chem. Solids, 125 (2019) 153-164.

22. B. C. Rout and S. R. Mishra,, Thermal energy transport on MHD nanofluid flow over a stretching surface: A comparative study, Eng. Sci. Tech., an Inter. J., 21 (2018) 60-69.

23. M. Rashid, M.I. Khan, T. Hayat, M.I. Khan and A. Alsaedi, Entropy generation in flow of ferromagnetic liquid with nonlinear radiation and slip condition, J. Mol. Liq., 276 (2019) 441-452.

24. J. V. R. Reddy, V. S and N. Sandeep, Thermophoresis and Brownian motion effects on unsteady MHD nanofluid flow over a slendering stretching surface with slip effects, Alexandria Eng. J., 57 (2018) 2465-2473.

25. S. Qayyum, M.I. Khan, T. Hayat, A. Alsaedi and M. Tamoor, Entropy generation in dissipative flow of Williamson fluid between two rotating disks, Int. J. Heat Mass Transfer., 127 (2018) 933-942.

26. J. Gu, B. Yin, S, Fu, M. Feng, Z. Zhang, H. Dong, F. Gao and Y. S. Zhao, Surface tension driven aggregation of organic nanowires via lab in a droplet, Nanoscale, 10 (2018) 11006-11012.

27. T. Hayat, T. Nasir, M.I. Khan and A. Alsaedi, Non-Darcy flow of water-based single (SWCNTs) and multiple (MWCNTs) walls carbon nanotubes with multiple slip conditions due to rotating disk, Results Phys., 9 (2018) 390-399.

28. J. Gu, J. Wu, C. Jin, X. Sun, B. Yin, G. C. Zhang, B. Wen and F. Gao, Solvent engineering for high conversion yields of layered raw materials into large-scale freestanding hybrid perovskite nanowires, Nanoscale, 10 (2018) 17722-17729.

29. A. Alsaedi, M. I. Khan and T. Hayat, Recent progresses about statistical declaration and probable error for surface drag force of chemically reactive squeezing flow with temperature dependent thermal conductivity, J. Theor. Comput. Chem., 16 (2017) 1750064.

30. M.I. Khan, S. Ullah, T. Hayat, M. Waqas, M.I. Khan and A. Alsaedi, Salient aspects of entropy generation optimization in mixed convection nanomaterial flow, Int. J. Heat and Mass Transfer., 126 (2018) 1337-1346.

31. S. U. S. Choi, Enhancing thermal conductivity of fluids with nanoparticles, In: D. A. Siginer and H. P. Wang, Eds., Developments and applications of non-Newtonian flows, ASME, New York, 66 (1995) 99-105.

32. D. Wen, G. Lin, S. Vafaei and K. Zhang, Review of nanofluids for heat transfer applications, Particuology, 7 (2009) 141-150.

33. R. Saidur, K.Y. Leong and H.A. Mohammad, A review on applications and challenges of nanofluids, Renewable Sustainable Energy Rev., 15 (2011) 1646-1668.

34. L. Godson, B. Raja, D.M. Lal and S. Wongwises, Enhancement of heat transfer using nanofluids-an overview, Renewable Sustainable Energy Rev., 14 (2010) 629-641.

35. M.H. Esfe, S. Saedodin, O. Mahian and S. Wongwises, Heat transfer characteristics and pressure drop of COOH-functionalized DWCNTs/water nanofluid in turbulent flow at low concentrations, Int. J. Heat Mass Transfer, 73 (2014) 186-194.

36. T. Yiamsawasd, A.S. Dalkilic and S. Wongwises, Measurement of the thermal conductivity of titania and alumina nanofluids, Thermochim. Acta, 545 (2012) 48-56.

37. L. Godson, B. Raja, D.M. Lal and S. Wongwises, Experimental investigation on the thermal conductivity and viscosity of silver-deionized water nanofluid, Exp. Heat Transfer, 23 (2010) 317--332.

38. L.G. Asirvatham, R. Nimmagadda and S. Wongwises, Heat transfer performance of screen mesh wick heat pipes using silver-water nanofluid, Int. J. Heat Mass Transfer, 60 (2013) 201-209.

39. L. Godson, D.M. Lal and S. Wongwises, Measurement of thermo physical properties of metallic nanofluids for high temperature applications, Nanoscale Microscale Thermophys. Eng., 14 (2010) 152-173.

40. N. Ahammed, L.G. Asirvatham, J. Titus, J.R. Bose and S. Wongwises, Measurement of thermal conductivity of graphene-water nanofluid at below and above ambient temperatures, Int. Commun. Heat Mass Transfer, 70 (2016) 66-74.

41. T. Hayat, M. Z. Kiyani, I. Ahmad, M. I. Khan and A. Alsaedi, Stagnation point flow of viscoelastic nanomaterial over a stretched surface, Results Phys., 9 (2018) 518-526.

42. M. I. Khan, F. Shah, T. Hayat and A. Alsaedi, Transportation of CNTs based nanomaterial flow confined between two coaxially rotating disks with entropy generation, Physica A: Stat. Mech. Appl., 527 (2019) 121-154,

43. T. Hayat, I. Ullah, A. Alsaedi and M. Farooq, MHD flow of Powell-Eyring nanofluid over a non-linear stretching sheet with variable thickness, Results Phys., 7 (2017) 189-196.

44. A. Rauf, M.K. Siddiq, F.M. Abbasi, M.A. Meraj, M. Ashraf and S.A. Shehzad, Influence of convective conditions on three dimensional mixed convective hydromagnetic boundary layer flow of Casson nanofluid, J. Magn. Magn. Mater., 416 (2016), 200-207

45. T. Hayat, S. Ullah, M. I. Khan, A. Alsaedi and Q. M. Z. Zia, Non-Darcy flow of water-based carbon nanotubes with nonlinear radiation and heat generation/absorption, Results Phys., 8 (2018) 473-480.

46. M. Farooq, M. I. Khan, M. Waqas, T. Hayat and M. I. Khan, MHD stagnation point flow of viscoelastic nanofluid with non-linear radiation effects, J. Mol. Liq., 221 (2016) 1097-1103.

47. M. Sheikholeslami, Numerical approach for MHD Al2O3-water nanofluid transportation inside a permeable medium using innovative computer method, Comput. Meth. Appl. Mech Eng., 344 (2019) 306-318.

48. S. Dogonchi and D. D. Ganji, Impact of Cattaneo--Christov heat flux on MHD nanofluid flow and heat transfer between parallel plates considering thermal radiation effect, J. Taiwan Inst. Chem. Eng., 80 (2017) 52-63.

49. G.B. Kim, J.M. Hyun, and H.S. Kwak, Transient buoyant convection of a power law non-Newtonian fluid in an enclosure Int. J. Heat Mass Transfer., 46 (2003).3605-3617

50. M. Lamsaadi, M. Naimi, M. Hasnaoui and M. Mamou, Natural convection in a vertical rectangular cavity filled with a non- Newtonian Power law Fluid and subjected to a horizontal temperature gradient, Numer. Heat Transfer, Part A, 49 (2006) 969-990.

51. O. Turan, A. Sachdeva, N. Chakraborty and R.J. Poole, Laminar natural convection of power-law fluids in a square enclosure with differentially heated side walls subjected to constant temperatures, J. non-Newton. Fluid Mech., 166 (2011) 1049-1063.

52. L. Khezzar, D. Siginer and I. Vinogradov, Natural convection of power law fluids in inclined cavities, Int. J. Therm. Sci., 53 (2012) 8-17

53. M.H. Matin, I. Pop, and S. Khanchezar, Natural convection of power-law fluid between two-square eccentric duct annuli, J. non-Newton. Fluid Mech., 197 (2013) 11-23.

54. A. Bejan, Entropy generation through heat and fluid flow, Wiley, New York (1982)

55. M. I. Khan, S. Qayyum, T. Hayat, M. I. Khan and A. Alsaedi, Entropy optimization in flow of Williamson nanofluid in the presence of chemical reaction and Joule heating, Int. J. Heat Mass Transfer, 133 (2019) 959-967.

56. T. Hayat, L. Sajjad, M. I. Khan, M. I. Khan and A. Alsaedi, Salient aspects of thermo-diffusion and diffusion thermo on unsteady dissipative flow with entropy generation, J. Mol. Liq., 282 (2019) 557-565.

57. M.M. Sheikholeslami, Gorji-Bandpy and D.D. Ganji, Numerical investigation of MHD effects on Al2O3 water nanofluid flow and heat transfer in a semi-annulus enclosure using LBM Energy, 60 (2013) 501-510.

58. M. H. Matin, and A. K. Waqar, Entropy generation analysis of heat and mass transfer in mixed electrokinetically and pressure driven flow through a slit microchannel, Energy 56 (2013) 207-217.

59. J. Escandón, O. Bautista and F. Méndez, Entropy generation in purely electroosmotic flows of non-Newtonian fluids in a microchannel, Energy, 55 (2013) 486-496.

60. G. Ibáñez, A. López, J. Pantoja, J. Moreira and J. A. Reyes, Optimum slip flow based on the minimization of entropy generation in parallel plate microchannels, Energy 50 (2013) 143-149

61. M. Khan, E. Naheed, C. Fetecau and T. Hayat, Exact solutions of starting flows for second grade fluid in a porous medium, Inter. J. Non Linear. Mech., 43 (2008) 868-879.

62. T. Hayat, Z. Hussain, B. Ahmed and A. Alsaedi, Base fluids with CNTs as nanoparticles through non-Darcy porous medium in convectively heated flow: A comparative study, Adv. Powder Technol., 28 (2017) 1855-1865.

63. M.G. Reddy, K.V. Reddy and O.D. Makinde, Hydromagnetic peristaltic motion of a reacting and radiating couple stress fluid in an inclined asymmetric channel filled with a porous medium, Alexendria Eng J., 55 (2016) 1841-1853.

64. Z. Shafique, M. Mustafa and A. Mushtaq, Boundary layer flow of Maxwell fluid in rotating frame with binary chemical reaction and activation energy, Results Phys., 6 (2016) 627-633

65. A. Zeeshan, N. Shehzad and R. Ellahi, Analysis of activation energy in Couette-Poiseuille flow of nanofluid in the presence of chemical reaction and convective boundary conditions, Results Phys., 8 (2018).502-512.

66. M. Ijaz and M. Ayub, Activation energy and dual stratification effects for Walter-B fluid flow in view of Cattaneo-Christov double diffusion, Heliyon, 5 (2019) e01815

67. T. Hayat, A. A Khan, F. Bibi, and S. Farooq, Activation energy and non-Darcy resistance in magneto peristalsis of Jeffrey material, J. Phys. Chem. Solids, 129 (2019) 155-161.

68. S. Liao, Notes on the homotopy analysis method. Some definitions and theorems, Commun. Nonlinear Sci. Numer. Simul., 14(2009) 983-997.